Synthesis and photophysical properties of novel porphyrin dendrimers containing organoiron complexes

by

Mosa Halal Alsehli

A THESIS SUBMITTED IN PARTIAL FULFILLMENT
OF THE REQUIREMENTS FOR THE DEGREE OF

MASTER OF SCIENCE

in

The College of Graduate Studies
(Chemistry)

THE UNIVERSITY OF BRITISH COLUMBIA
(Okanagan)

July 2011

Abstract

Dendritic porphyrins and metalloporphyrins are of great interest for their applications in many fields such as light-energy conversion, photodynamic therapy (PDT), third-order non-linear optical materials, organic light-emitting diode (OLED) devices, fluorescence switches, and molecular wires. The synthesis and preliminary photophysical properties of novel porphyrin and metalloporphyrin dendrimers containing cationic η^6-chloroarene-η^5-cyclopentadienyliron(II) complexes functionalized with naphthalene and capped with ferrocene are described. The incorporation of cationic η^6-chloroarene-η^5-cyclopentadienyliron moieties can enhance solubility and facilitate nucleophilic aromatic substitution and addition reactions due to the intense electron-withdrawing ability of the iron center.

Divergent approaches were employed to give highly symmetrical branched materials. The preparation of these dendrimers was achieved via metal-mediated nucleophilic aromatic substitutions and Steglich esterifications. These dendrimers and their precursors were characterized through nuclear magnetic resonance spectroscopy, infrared spectroscopy, and ultraviolet-visible and fluorescence spectroscopy.

Table of contents

Abstract…. iii

Table of contents iii

List of tables vii

List of figures viii

List of schemes xi

List of abbreviations xiii

Acknowledgements xvi

Chapter 1. Introduction 1

1.1 Porphyrins 1

1.2 Photophysical and electronic properties of free-base porphyrins and metalloporphyrins 7

1.2.1 Fundamental concepts of photophysical processes 7

1.2.2 Absorption spectra of free-base porphyrins and metalloporphyrins 9

1.2.2.1 Gouterman four-orbital mode 10

1.2.2.2 Substituent effects on *meso*-substituted porphyrin absorption spectra 13

1.2.3 Emission spectra of the free-base porphyrin and metalloporphyrin 14

1.3 The synthesis of tetraphenylporphyrins and their metal analogues 16

1.4 Porphyrin dendrimers 19

1.4.1 Synthetic strategies and structural variation 19

1.5 Applications 24

1.6 The chemistry of ferrocene 26

1.7 Organoiron complexes based on cyclopentadienyliron cations 27

1.7.1 The synthesis and chemistry of the η^6-haloarene-η^5-cyclopentadienyliron(II) hexafluorophosphate complex with carboxylic groups 32

1.8 Steglich esterification of bimetallic carboxylic acid complex 33

Chapter 2. Synthesis of porphyrin dendrimers containing organoiron complexes 36

2.1 Synthesis of free-base porphyrin 2.1, nickel 2.2a and Zinc 2.2b Porphyrins 36

2.1.1 Absorption spectroscopy of free-base porphyrin 2.1, nickel complex 2.2a, and zinc complex 2.2b 42

2.1.2 Fluorescence spectroscopy of free-base porphyrin 2.1 and Zn-porphyrin 2.2b 43

2.2 Porphyrin dendrimers containing cationic organoiron moieties 44

2.3 Synthesis of porphyrins and metalloporphyrins containing η^6- monochlorobenzene η^5-cyclopentadienyliron complexes 45

2.3.1 Absorption spectroscopy of complexes 2.3a-c 50

2.3.2 Fluorescence spectroscopy of free-base 2.3a and Zn-porphyrin complex 2.3c 52

2.4 Syntheses of porphyrins and metalloporphyrins containing η^6-dichlorobenzene-η^5-cyclopentadienyliron complexes 54

2.4.1 Absorption spectroscopy of compounds 2.4a-c 59

2.4.2 Fluorescence spectroscopy of free-base porphyrin 2.4a and Zn-porphyrin 2.4c 61

2.5 Synthesis of porphyrins and metalloporphyrins containing naphthalene 63

2.5.1 Absorption spectroscopy of complexes 2.7a and 2.7c 68

2.5.2 Fluorescence spectroscopy of free-base porphyrin 2.7a and Zn-porphyrin 2.7c 69

2.6 Synthesis of free-base porphyrin and metalloporphyrin dendrimers containing neutral and cationic organoiron species 70

2.6.1 Absorption spectroscopy of compounds 2.9a and 2.9c 74

2.6.2 Fluorescence spectroscopy of free-base porphyrin dendrimer 2.9a and Zn-porphyrin dendrimer 2.9c 76

2.6.3 Absorption spectroscopy of porphyrin compounds 2.10a and 2.11a 87

2.6.4 Fluorescence spectroscopy of free-base porphyrin dendrimers 2.10a and 2.11a 88

Chapter 3. Experimental 90

3.1 Materials 90

3.2 Characterization 90

3.3 Synthetic methodology 90

3.3.1 Synthesis of 5,10,15,20-tetrakis(4-hydroxyphenyl) porphyrin 2.1 90

3.3.2 Synthesis of T(P-OH)PPNi 2.2a and T(P-OH)PPZn 2.2b 91

3.3.3 Synthesis of 2.3a-c 91

3.3.4 Synthesis of 2.4a-c 92

3.3.5 Synthesis of 2.6a-c 93

3.3.6 Synthesis of 2.7a and 2.7c 93

3.3.7 Synthesis of 2.9a-c 94

3.3.8 Synthesis of 2.9d 95

3.3.9 Synthesis of 2.10a and 2.10c 95

3.3.10 Synthesis of 2.11a 96

Chapter 4. Conclusions and future work 97

References 99

List of tables

Table 1-1: Absorption maxima of H_2PP and ZnPP in benzene at room temperature…….12

Table 2-1: UV-visible data of compounds **2.1**, **2.2a**, and **2.2b** in DMF (1.5 x 10^{-5} M).. ...43

Table 2-2: Fluorescence data of compounds **2.1** and **2.2b** in DMF (1.5 x 10^{-5}M)…… ….44

Table 2.3: UV-visible data of compounds **2.3a-c** in DMF (1.5 x 10^{-5} M)……..52

Table 2.4: Fluorescence data of compounds **2.3a** and **2.3c** in DMF (1.5 x 10^{-5} M)……...52

Table 2-5: UV-visible data of compounds **2.4a-c** in DMF (1.5 x 10^{-5} M)……..60

Table 2-6: Fluorescence data of compounds **2.4a** and **2.4c** in DMF (1.5 x 10^{-5} M)……...61

Table 2-7: UV-visible data of compounds **2.7a** and **2.7c** in DMF (1.5 x 10^{-5} M)…….….68

Table 2-8: Fluorescence data of compounds **2.7a** and **2.7c**.in DMF (1.5 x 10^{-5} M)…....70

Table 2-9: UV-visible data of compounds **2.9a** and **2.9c** in DMF (1.5 x 10^{-5} M)…….....75

Table 2-10: Fluorescence data of compounds **2.9a** and **2.9c** in DMF (1.5 x 10^{-5} M)……..77

Table 2-11: UV-visible data of compounds **2.10a** and **2.11a** in DMF (1.5 x 10^{-5} M)….....88

Table 2-12: Fluorescence data of compounds **2.10a** and **2.11a** in DMF (1.5 x 10^{-5} M)…..89

List of figures

Figure 1-1: Examples of porphyrin derivatives that occur in nature 1

Figure 1-2: Porphyrin macrocycle 2

Figure 1-3: Biologically active systems containing the porphyrin core structure 4

Figure 1-4: Electromagnetic spectrum, with the visible light region enlarged 8

Figure 1-5: Electronic orbitals of an organic molecule showing the ground state (S_0) and the first excited singlet state (S_1) 9

Figure 1-6: Porphine MOs showing the symmetry notations of porphine HOMOs and LUMOs; Gouterman's orbital re-labeling is shown in parentheses[19,22] 10

Figure 1-7: The changes induced in the orbitals upon introducing a metal or hydrogen atoms to the center of the macrocyclic porphyrin 12

Figure 1-8: UV-vis absorption of a) free-base tetraphenylporphyrin (H_2TPP) and b) zinc tetraphenylporphyrin in benzene (the Q band intensities are expanded 20 times from the actual intensities). Reprinted with permission from *J. Phys. Chem. A* 2002, *106*, 9837- 9844 and *J. Phys. Chem. A*. 2002, *106*, 9845-9854.[24,25] 13

Figure 1-9: Decay scheme for singlet and triplet relaxation; the radiationless processes are shown as wavy lines and the radiation processes are shown by straight lines 15

Figure 1-10: Absorption (solid line) and fluorescence (dashed lines) spectra of H_2TPP (left) and ZnTPP (right) in benzene. Reprinted with permission from *J. Phys. Chem. A*. 2002, *106*, 9837-9844 and *J. Phys. Chem. A*. 2002, *106*, 9845-9854.[24,25] 16

Figure 1-11: Structural classification of porphyrin dendrimers as reported thus far; symbol "P" denotes a porphyrin unit. (O = generic atom) 20

Figure 1-12: Structural classification of porphyrin dendrimers 20

Figure 1-13: Porphyrin unit integrated into the center of poly(benzyl ether) dendrimer[40] 22

Figure 1-14: Dendrimer with arms attached to both pyrrole-β and *meso*-positions[45] 23

Figure 1-15: Comparison of 400 MHz ^{1}H NMR spectrum of dichlorobenzene 1.3 (spectrum 2) and complex 1.5 (spectrum 1) 30

Figure 2-1: 400 MHz ^{1}H NMR spectrum of free-base porphyrin **2.1** 37

Figure 2-2: 101 MHz ^{13}C NMR spectrum of free-base porphyrin **2.1** 38

Figure 2-3: HSQC spectrum of free-base porphyrin **2.1** 39

Figure 2-4: 400 MHz ^{1}H NMR spectrum of **2.2a**, T(P-OH)PPNi 41

Figure 2-5: 101 MHz ^{13}C NMR spectrum of **2.2a**, T(P-OH)PPNi 42

Figure 2-6: Absorption spectra of compounds **2.1**, **2.2a**, and **2.2b** in DMF 43

Figure 2-7: Fluorescence spectra of free-base porphyrin **2.1** and Zn-porphyrin **2.2b** 44

Figure 2-8: 400 MHz ^{1}H NMR spectrum of free-base porphyrin **2.3a** 47

Figure 2-9: 101 MHz ^{13}C NMR spectrum of free-base porphyrin **2.3a** 48

Figure 2-10: HSQC spectrum of porphyrin **2.3a** 49

Figure 2-11: Absorption spectra of compounds **2.3a-c** in DMF 51

Figure 2-12: Fluorescence spectra of free-base porphyrin **2.3a** excited at different wavelengths 53

Figure 2-13: Fluorescence spectra of Zn-porphyrin **2.3c** excited at different wavelengths 53

Figure 2-14: 400 MHz ^{1}H NMR spectrum of porphyrin complex **2.4b** 54

Figure 2-15: 101 MHz ^{13}C NMR spectrum of metalloporphyrin **2.4b** 57

Figure 2-16: COSY spectrum of metalloporphyrin **2.4b** 58

Figure 2-17: HSQC spectrum of metalloporphyrin **2.4b** 59

Figure 2-18: Absorption spectra of compounds **2.4a-c** in DMF 60

Figure 2-19: Fluorescence spectra of free-base porphyrin **2.4a** excited at different wavelengths 62

Figure 2-20: Fluorescence spectra of Zn-porphyrin **2.4c** excited at different wavelengths 62

Figure 2-21: 400 MHz ^{1}H NMR spectrum of porphyrin dendrimer **2.6a** 65

Figure 2-22: 400 MHz ^{1}H NMR spectrum of porphyrin dendrimer **2.7a** 66

Figure 2-23: Absorption spectra of compounds **2.7a** and **2.7c** in DMF 68

Figure 2-24: Fluorescence spectra of free-base porphyrin **2.7a** and zinc porphyrin dendrimer **2.7c** 69

Figure 2-25: 400 MHz ^{1}H NMR spectrum of metalloporphyrin dendrimer **2.9b** 72

Figure 2-26: 101 MHz ^{13}C NMR spectrum of metalloporphyrin dendrimer **2.9b** 73

Figure 2-27: HSQC spectrum of metalloporphyrin dendrimer **2.9b** 74

Figure 2-28: Absorption spectra of compounds **2.9a** and **2.9c** in DMF 75

Figure 2-29: Fluorescence spectra of compounds **2.9a** and **2.9c** 76

Figure 2-30: 400 MHz ^{1}H NMR spectrum of porphyrin **2.9d** 79

Figure 2-31: Absorption of 2.9a and demetalated porphyrin **2.9d** in DMF 80

Figure 2-32: Fluorescence spectra of porphyrin dendrimers **2.9a** and **2.9d** 80

Figure 2-33: 400 MHz ^{1}H NMR spectrum of ferrocene-capped metalloporphyrin dendrimer **2.10c** 81

Figure 2-34: 400 MHz ^{1}H NMR spectrum of free-base porphyrin dendrimer **2.11a** containing twelve metallic moieties 85

Figure 2-35: HSQC spectrum of metalloporphyrin dendrimer **2.11a** 87

Figure 2-36: Absorption spectra of compounds **2.10a** and **2.11a** in DMF 88

Figure 2-37: Fluorescence spectra of compounds **2.10a** and **2.11a** 89

List of schemes

Scheme 1-1: 18-π electron pathways, which make up the aromatic character of the porphyrin ring system 3

Scheme 1-2: N-H tautomerism in porphyrins[14] 6

Scheme 1-3: Synthesis of tetraphenylporphyrin (TPP) 17

Scheme 1-4: Lindsey's method of synthesis of TPP 18

Scheme 1-5: The synthetic routes towards porphyrin dendrimers 21

Scheme 1-6: Ligand exchange reaction of ferrocene 27

Scheme 1-7: Proposed mechanism for the ligand exchange of ferrocene[79] 28

Scheme 1-8: Metal-mediated nucleophilic reaction of an η^6-dichloroarene-η^5-cyclopentadienyliron(II) hexafluorophosphate complex[79] 28

Scheme 1-9: Potentials for the oxidation states determined by cyclic voltammetry of (i) ferrocene and (ii) η^6-hexamethylbenzene-η^5-cyclopentadienyliron(II); potentials are given versus a saturated calomel reference electrode[89] 31

Scheme 1-10: Mechanism of the photolytic cleavage of the cationic cyclopentadienyliron moiety. X^- is a counter ion such as PF_6^- 32

Scheme 1-11: Synthesis of the monometallic acid complex[102] 33

Scheme 1-12: Synthesis of bimetallic carboxylic acid complex 1.7[102] 33

Scheme 1-13: A simplified Steglich esterification[103] 34

Scheme 1-14: Mechanism of the Steglich esterification using DCC/DMAP conditions 35

Scheme 2-1: Synthesis of 5,10,15,20-tetrakis(4-hydroxyphenyl) porphyrin 36

Scheme 2-2: Synthesis of 5,10,15,20-tetrakis(4-hydroxyphenyl) porphyrin metal complexes 40

Scheme 2-3: Synthesis of free-base porphyrin and metalloporphyrins 2.3a-c 46

Scheme 2-4: Synthesis of free-base porphyrin 2.4a and metalloporphyrins 2.4b and 2.4c ... 56

Scheme 2-5: Synthesis of free-base porphyrin 2.6a and metalloporphyrin dendrimers 2.6b and 2.6c 64

Scheme 2-6: Synthesis of free-base porphyrin 2.7a and metalloporphyrins 2.7c 67

Scheme 2-7: Synthesis of tetrahydroxy-functionalized free-base porphyrin and metalloporphyrin dendrimers 2.9a-c 71

Scheme 2-8: Synthesis of free-base porphyrin dendrimer 2.9d 78

Scheme 2-9: Synthesis of ferrocene-capped free-base porphyrin and metalloporphyrin dendrimers 2.10a and 2.10c..... 83

Scheme 2-10: Synthesis of free-base porphyrin dendrimer 2.11a with twelve metallic moieties 86

List of abbreviations

Ar	aryl
*Ar	complexed aryl
br	broad
^{13}C	carbon-13
conc.	concentrated
°C	degrees Celsius
Cp	cyclopentadienyl ring
*Cp	functionalized cyclopentadienyl ring of ferrocene-1-carboxylic acid
δ	chemical shift
d	doublet
dd	doublet of doublets
d	deuterium
DCC	N,N'-dicyclohexylcarbodiimide ($C_{13}H_{22}N_2$)
DCM	dichloromethane
DCU	N,N'-dicyclohexylurea ($C_{13}H_{24}N_2O$)
DMAP	4-dimethylaminopyridine ($(CH_3)_2NC_5H_4N$)
DMF	N,N-dimethylformamide
DMSO	dimethylsulfoxide
eq.	equivalents
Et	ethyl
FTIR	Fourier transform infrared
g	grams
HMBC	heteronuclear multiple bond coherence

HSQC	heteronuclear single quantum coherence
HOMO	highest occupied molecular orbital
H_2PP	free-base phenylporphyrin
H_2TPP	free-base tetraphenylporphyrin
^1H	proton
h	hours
Hz	Hertz (s^{-1})
H_2P	unsubstituted porphyrin macrocycle
IR	infrared spectroscopy
J	coupling constant (in spectroscopy; Hz)
L	litre (10^{-3} m^{-3})
LOMO	lowest occupied molecular orbital
M	molar ($mol \cdot L^{-1}$)
m	multiplet
Me	methyl
min	minutes
mL	millilitre (10^{-3} L)
mmol	millimole (10^{-3} mole)
mol	mole ($6.022 \cdot 10^{-23}$ particles)
nm	nanometer
NMR	nuclear magnetic resonance
o	ortho
p	para
ppm	parts per million

q	quartet
RBF	round bottom flask
s	singlet
t	triplet
THF	tetrahydrofuran
T(P-OH)PPH_2	5,10,15,20-tetrakis(4-hydroxyphenyl) porphyrin
T(P-OH)PPZn	5,10,15,20-tetrakis(4-hydroxyphenyl) porphyrin zinc complex
T(P-OH)PPNi	5,10,15,20-tetrakis(4-hydroxyphenyl) porphyrin nickel complex
UV	ultraviolet
UV-vis	ultraviolet-visible
λ_{max}	maximum wavelength
λ_{em}	emission wavelength
ZnPP	zinc phenylporphyrin
ZnTPP	zinc tetraphenylporphyrin

Acknowledgements

I would like to thank my supervisor, Dr. Alaa Abd-El-Aziz, for all of his inspiration, encouragement and support, without whom this research would not have been possible.

I would like to acknowledge the members of my committee, Dr. Shipley and Dr. Neeland, for their constant support and in NMR spectroscopy. Also, I would like to thank Dr. Jack and Dr. Smith for their assistance.

I will take this opportunity to thank all past and current members of the Abd-El-Aziz research group for useful discussions, support, and friendship. Thank you to Inan Kucukkaya and Jessica Pilfold for their help in editing the thesis. Many thanks are due to Taibah University, which financed my studies at UBC Okanagan.

I am at a total loss of words in expressing the depth of my emotion for my parents, sisters, and brothers for their constant support and inspiration. Last but not least, I am thankful to all my friends here in Canada and back home for making me feel comfortable during the most difficult and trying moments of my life.

Chapter 1. Introduction

1.1 Porphyrins

The word porphyrin is derived from the Greek *porphura*, meaning purple, as all the porphyrins are intensely coloured**.** Porphyrins and metalloporphyrins display photophysical, photochemical, and electrochemical properties. They play essential roles in biological activities such as photosynthesis. Their applications are in many fields such as light-energy conversion,[1] photodynamic therapy (PDT),[2] third-order non-linear optical materials,[3] fluorescence switches[4], and molecular wires.[5] Porphyrins that occur naturally play an important role in life-sustaining biochemical reactions, and comprise a major class of molecules with many important biological representatives including chlorophylls, hemes, peroxidases, bacteriochlorophyll, myoglbins, and cytochromes (Figure 1-1). Therefore, much research has been performed to establish substantial understanding of the structure-function relationship in these natural porphyrins.

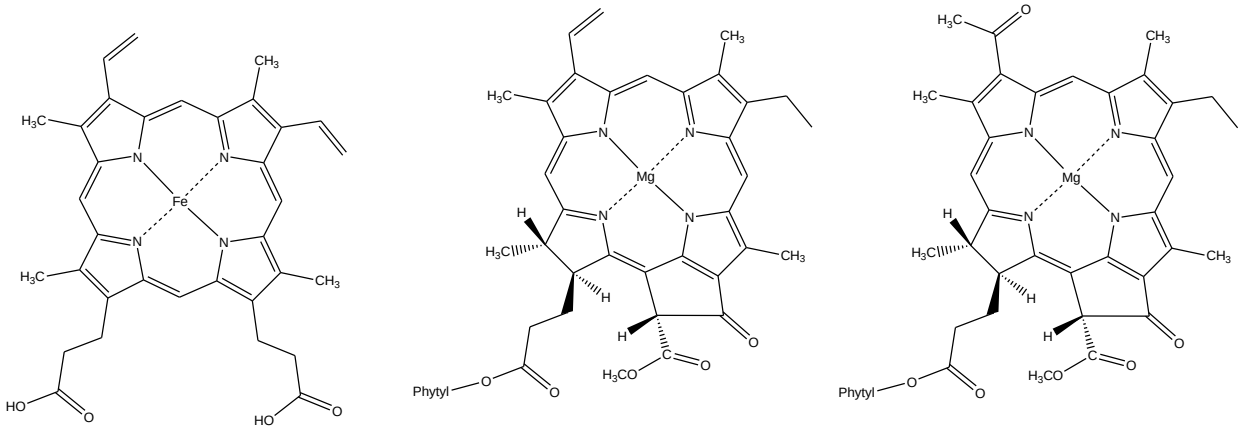

Figure 1-1: Examples of porphyrin derivatives that occur in nature

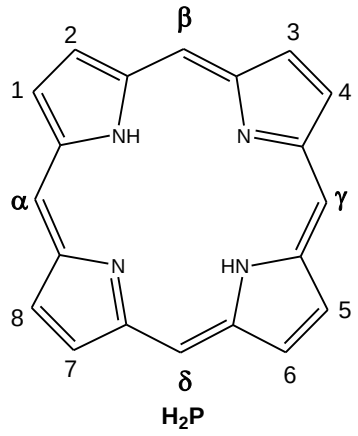

Figure 1-2: Porphyrin macrocycle

Porphyrins basically consist of four pyrrole rings joined by methane bridges to give a highly delocalized planar π-framework macrocycle. The structure of an unsubstituted porphine (H_2P) is shown in Figure 1-2, where 1 through 8 on H_2P correspond to the external pyrrolic carbons and α, β, γ, and δ correspond to the *meso* carbons. Porphyrins consist of 22 π-electrons to make up six different pathways for an 18-π electron system (Scheme 1-1), which follows Huckel's 4n+2 rule for aromaticity.[6]

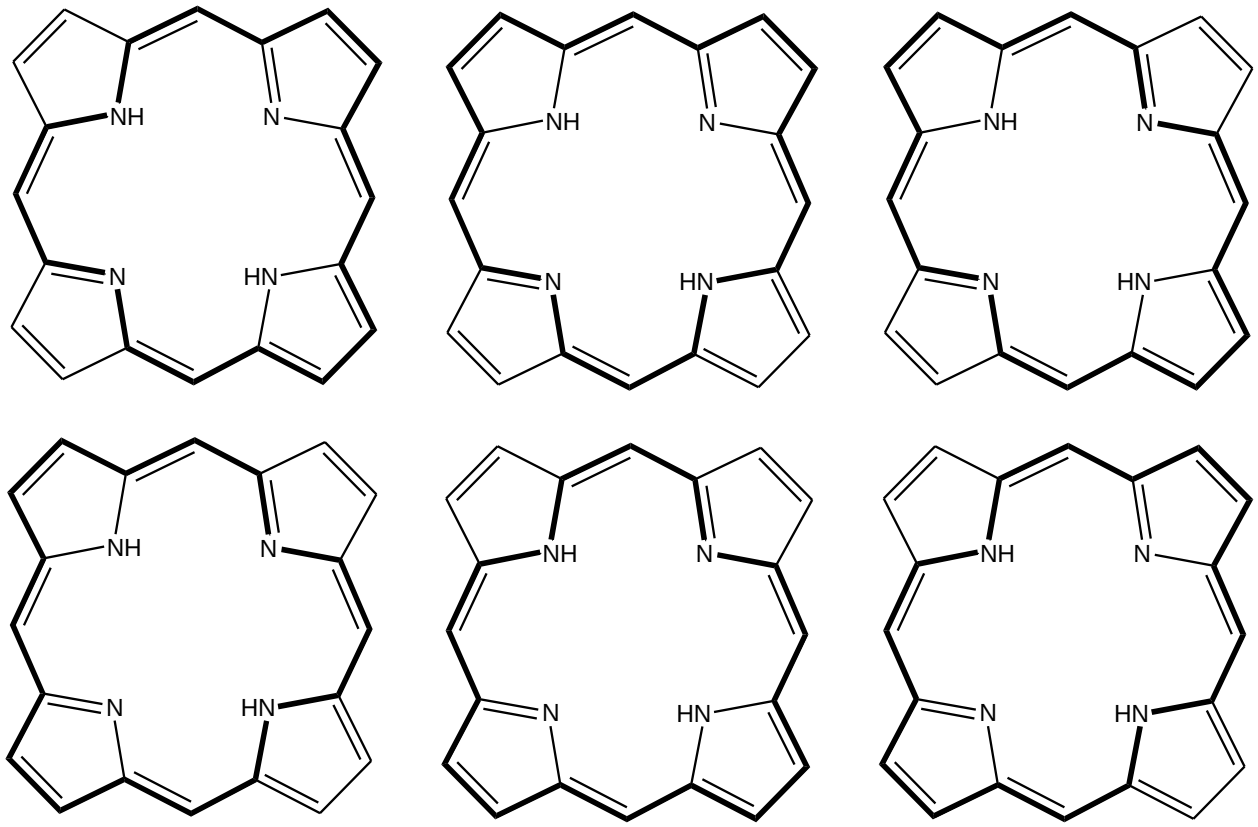

Scheme 1-1: 18-π electron pathways, which make up the aromatic character of the porphyrin ring system

There are many biologically active systems that have the porphyrin core structures, including chlorin, phorbin, bacteriochlorin, porphrazine, and phthalocyanine (Figure 1-3).

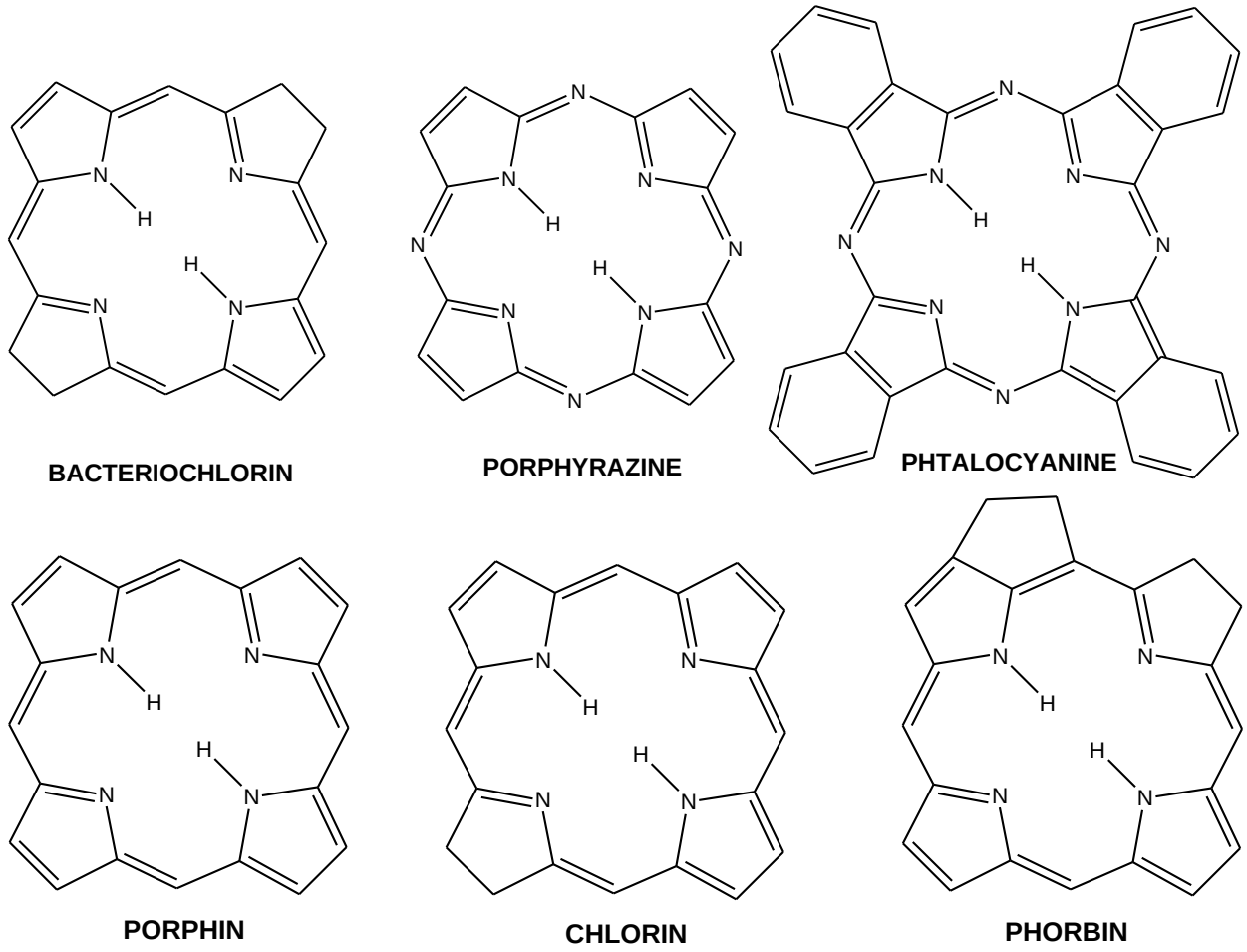

Figure 1-3: Biologically active systems containing the porphyrin core structure

The porphyrin macrocycle and its derivatives are considered to be amphoteric due to the inner pyrrolic, amine and imine, nitrogen atoms possessing acidic and basic properties.[7] As a result; the nitrogens inside the ring of the porphyrin can be deprotonated with strong bases to give the porphyrinato ion, while the two-imine nitrogens can be easily protonated with acids. These dianion species with their central cavities exhibit remarkable ligation characteristic towards metal ions.[8,9]

The porphyrinate dianion is suitable for acting as a tetradenate ligand with metal ions. Therefore, the minimum possible coordination number of a metalloporphyrin is four, yielding complexes with tetragonal geometries.[10] Coordination numbers greater than four result from

the addition of other ligands, either neutral or anionic; metalloporphyrins in which the metal ion has a coordination number of five, six, seven, or eight have been characterized. The five-coordinate complexes have square-pyramidal geometry with the single axial ligand occupying the apex of the square pyramid. The six-coordinate metalloporphyrins have octahedral geometries with two axial ligands found to be on opposite sides of the porphinato plane. In principle, the two axial donor atoms could be placed on the same side of the porphinato plane, but such complexes have not been characterized. The seven- and eight-coordinate derivatives, however, do have three or four axial donor groups bonded to the metal ion on the same side of the porphinato plane.[10]

The ^{1}H NMR spectrum of the aromatic porphyrin shows anisotropic effects.[11] The ring current generated by the applied field induces a local magnetic field similar to that in benzene. Therefore, the NH protons inside the ring shift upfield to as high as -5 ppm, whereas the deshielded *meso* protons appear downfield (~10 ppm). The pyrrolic protons are also deshielded and tend to resonate from 8 to 9 ppm, versus ~6 ppm in pyrrole. The tendency toward aggregation in some cases and the aromaticity of these porphyrin systems makes their NMR more difficult to assign.[12]

There are three different groups of dynamic processes that have been studied in the NMR of porphyrins. This includes rotational processes, macrocyclic inversion of non-planar porphyrins, and N-H tautomerism. Among the three processes, N-H tautomerism has been investigated in the most detail.[13]

Tautomerism, a dynamic process observed for all porphyrins, is an intramolecular proton transfer route paired with the migration of double bonds.[14] Free-base porphyrins undergo rapid tautomerism at room temperatures, so that the central hydrogen atoms exchange between opposite pairs of central nitrogen atoms. This N-H tautomerism (Scheme 1-2)

involves the shifting of highly conjugated double-bond systems.[15-18] It is impossible to differentiate between the two tautomers using spectroscopic methods at room temperature because the rate of the switching between the tautomers is too rapid. However, at -53 ^{o}C, it is possible to see the difference spectroscopically.

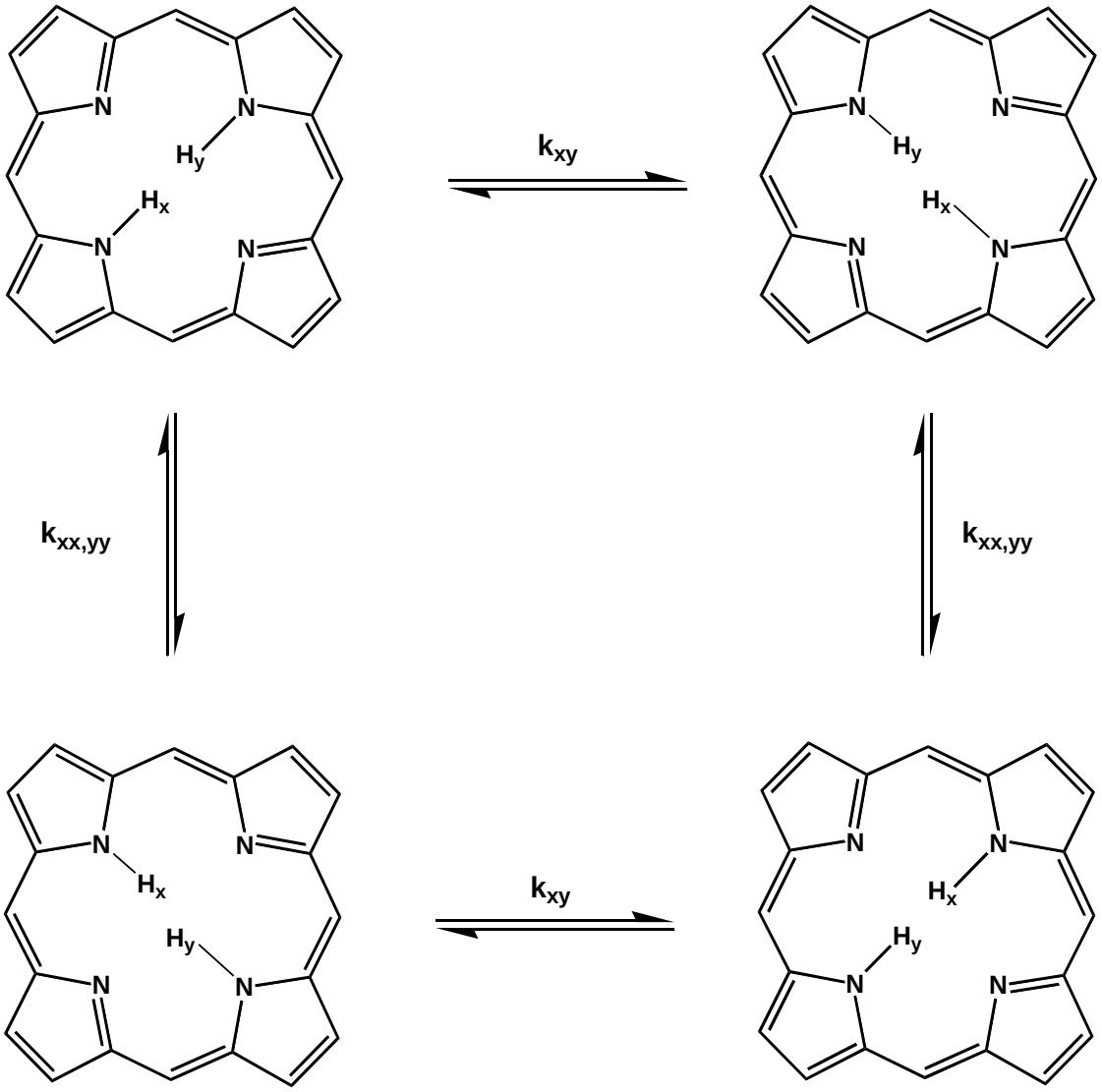

Scheme 1-2: N-H tautomerism in porphyrins[14]

1.2 Photophysical and electronic properties of free-base porphyrins and metalloporphyrins

The electronic heart of a porphyrin is the inner 16-membered ring with 18-π electrons, which are responsible for the unique porphyrin-type optical spectra. The photophysical behavior of porphyrins and their derivatives have attracted incredible attention during the past two decades due to their interesting optical properties and similarities to pigments found in biological organisms. Therefore, understanding these properties will continue to help advance our knowledge of fundamental photochemical processes such as electron and energy transfer, electronic excited states, solvent dynamics, solar cells, and kinetics.

1.2.1 Fundamental concepts of photophysical processes

Visible and ultraviolet (UV) light are small portions of the electromagnetic spectrum, as the range of the entire possible frequencies of electromagnetic radiation, which is shown in Figure 1-4. Molecules in the ground state S_0 can absorb a photon of radiation, so long as the energy of that radiation is greater than or equal to the difference in energy between the ground state and the first singlet excited state, S_1.

$$wavelength\ (\lambda) = \frac{c}{\nu} = \frac{1}{\bar{\nu}} \qquad (1)$$

Equation 1 represents the energy of the absorbed radiation, which can be expressed by its wavenumber ($\bar{\nu}$), its wavelength (λ), or its frequency (ν), where c is the speed of light (3×10^8 m·sec^{-1}).

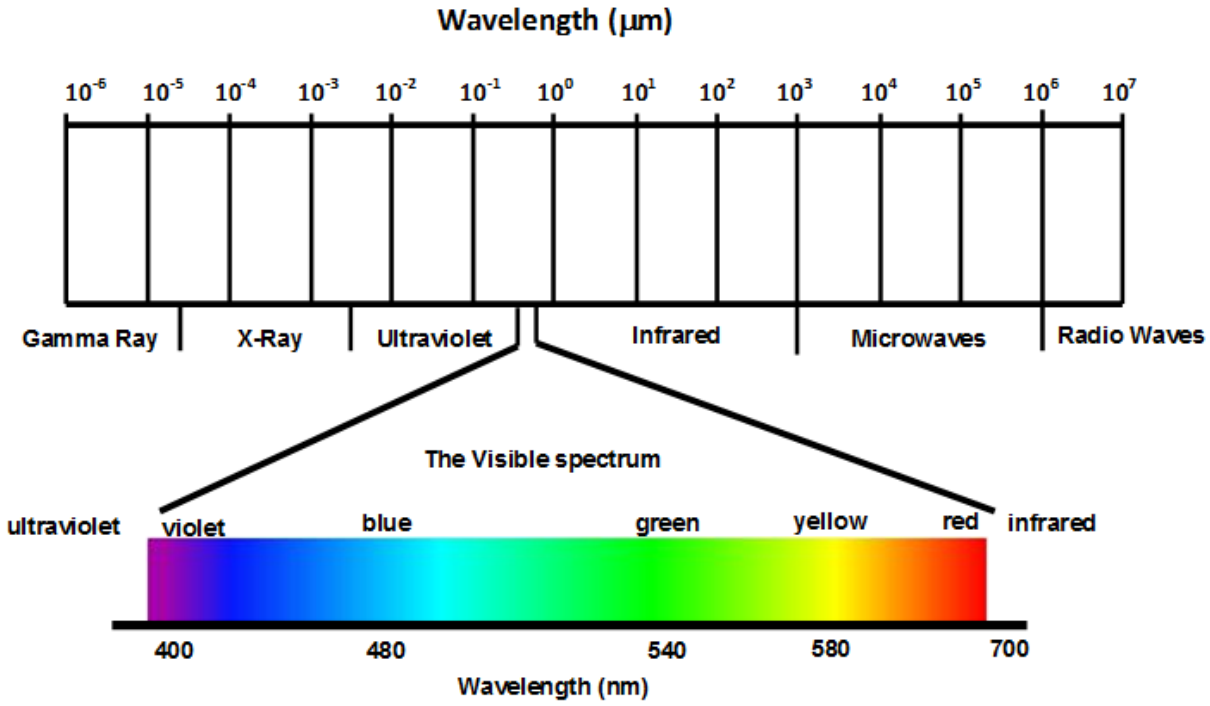

Figure 1-4: Electromagnetic spectrum, with the visible light region enlarged

The photophysical processes occurring in electronically excited organic molecules involve transitions from one state to another through radiative and radiationless transitions. The interaction of light with matter will result in these transitions without chemical changes in the molecules. The most important energy states when studying photophysical processes in organic molecules are the ground state (S_0), the first (lowest) excited state (S_1), and the first (lowest) triplet state (T_1). In photophysics, the promotion of an electron from the highest occupied molecular orbital (HOMO) to the lowest unoccupied molecular orbital (LUMO) occurs when the electron gets excited with a photon of light (Figure 1-5).

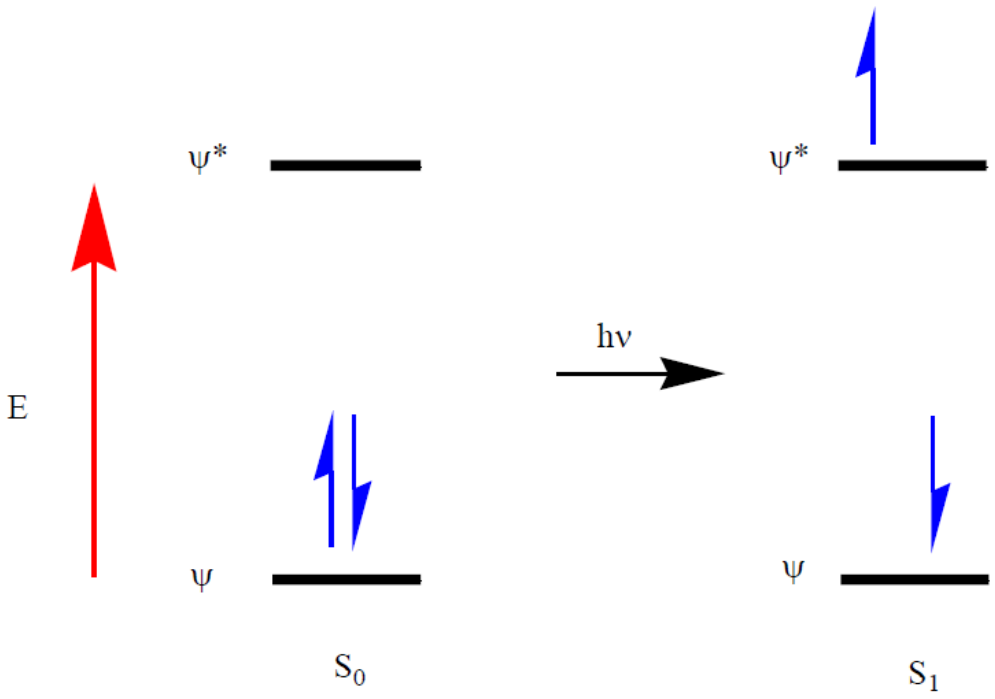

Figure 1-5: Electronic orbitals of an organic molecule showing the ground state (S_0) and the first excited singlet state (S_1)

1.2.2 Absorption spectra of free-base porphyrins and metalloporphyrins

All free-base porphyrins exhibit similar UV-visible absorption spectra. There is a stronger band in the region of 380 to 440 nm, called the Soret or B band, and four weak bands in the region between 500 and 700 nm, called the Q bands.[19] However, metalloporphyrins only show two Q bands, and a stronger Soret band compared to that of the free-base porphyrin.[20,21] These bands arise from π–π* transitions and can be explained by considering the four frontier orbitals (the HOMO and LUMO orbitals), as done in the Gouterman four-orbital model.[19,22]

1.2.2.1 Gouterman four-orbital mode

In the early 1960s, Martin Gouterman proposed the four-orbital model to explain the absorption spectra of porphyrins.[22] The absorption bands in porphyrin systems arise from transitions between two HOMOs and two LUMOs, while the identities of the metal center and the substituents on the ring affect the relative energies of these transitions (Figure 1-6). The two non-degenerate orbitals (HOMO) in this work have a_{2u} and a_{1u} symmetry, while the two degenerate orbitals (LUMO) were determined to have e_g symmetry. The transitions from a_{1u} to e_g give rise to the Soret band, while the Q bands were suggested to be the result of transitions from a_{2u} to e_g.

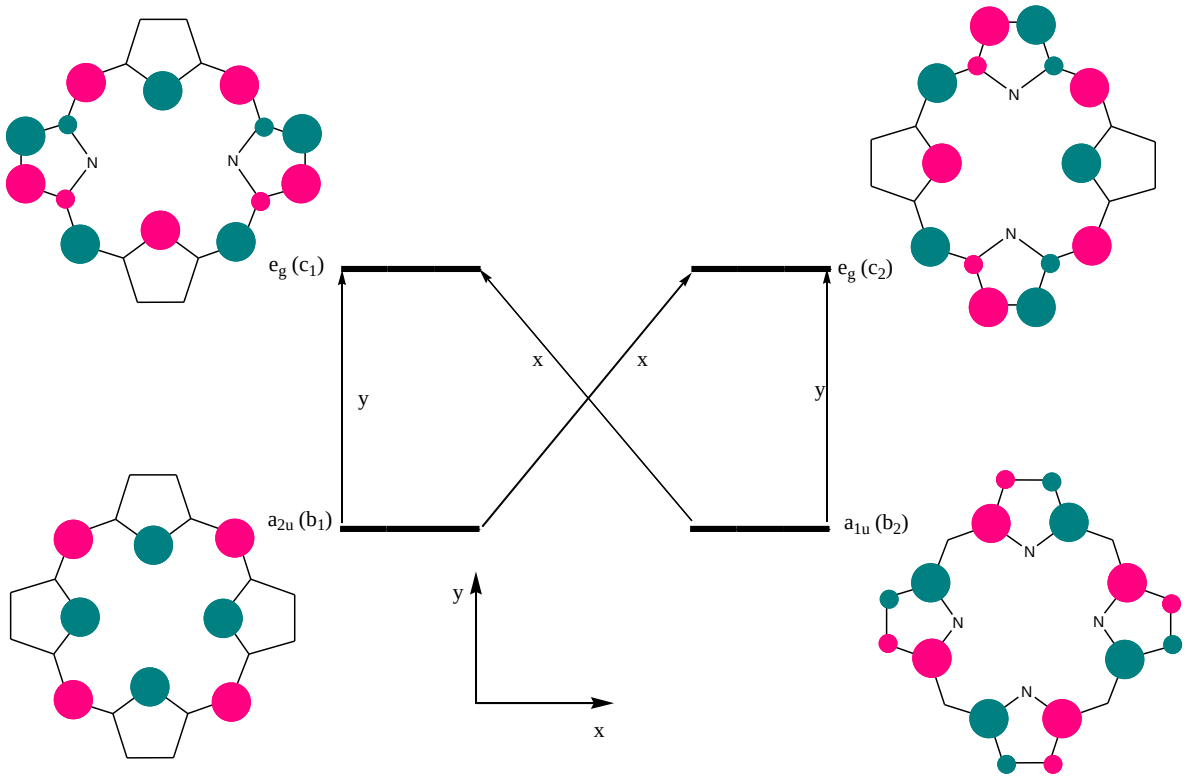

Figure 1-6: Porphine MOs showing the symmetry notations of porphine HOMOs and LUMOs; Gouterman's orbital re-labeling is shown in parentheses[19,22]

The group symmetry of a metalloporphine is D_{4h} (E, $2C_4$, C_2, $2C_2$, $2S_4$, $2\sigma_v$, σ_h, $2\sigma_d$) .[21] However, the change in substituents to two hydrogen atoms in the center of the porphyrin macrocycle reduces the group symmetry to D_{2h}. The Gouterman four-orbitals are shown in Figure 1.6; he was able to determine the transitions represented as a linear combination of b_1c_1-b_2c_2 and b_1c_2-b_2c_1 were responsible for the Q band transitions, and the transitions represented as a linear combination of b_1c_1+b_2c_2 and b_1c_2+b_2c_1 lead to the Soret band. Their intensities are represented in equations 2 and 3:

$$B_y = \frac{1}{z}(b_1c_1 + b_2c_2) \qquad B_x = \frac{1}{z}(b_1c_2 + b_2c_1) \qquad (2)$$

$$Q_y = \frac{1}{z}(b_1c_1 - b_2c_2) \qquad Q_x = \frac{1}{z}(b_1c_2 - b_2c_1) \qquad (3)$$

Gouterman explained the Soret and Q bands' intensities and band splitting of different porphyrins, as well as determining that the symmetry of the porphyrin's macrocycle affected the absorption spectra.[19] In the free-base porphyrin in the D_{2h} symmetry group, the transition dipoles in the x and y directions are different, where x polarization is along the H-H axis in the pyrrole rings. In the case of metalloporphyrins, where the symmetry is D_{4h}, the polarized x and y transition dipoles are equal to one another, as shown in Figure 1-7.

Two allowed transitions (Bx and By) yield the Soret band and two forbidden transitions (Qx and Qy) lead to the Q band transitions. The Bx and By, and the Qx and Qy, are degenerate transitions in the D_{4h} metalloporphyrins. Based on Gouterman's assumption that the b_1 and b_2 orbitals are degenerate, two Q bands (Q(1,0) and Q(0,0)) are observed for metalloporphyrins and four Q bands (Qy(1,0), Qy(0,0), Qx(1,0) and Qx(0,0)) for free-base porphyrins. These transitions represent the fundamental (0,0) and first vibrational (1,0) overtones of the Q band.

Introduction of a metal or hydrogen atoms to the center of the macrocyclic free-base porphyrin dramatically changes the orbital energy.[22] For example, hydrogen atoms tend to stabilize the free-base porphyrin ring and thus decrease the energy of the b_1 and c_2, whereas the metal, which is more electropositive (as is the case for zinc), increases the b_1 orbital energy (Figure 1-7).

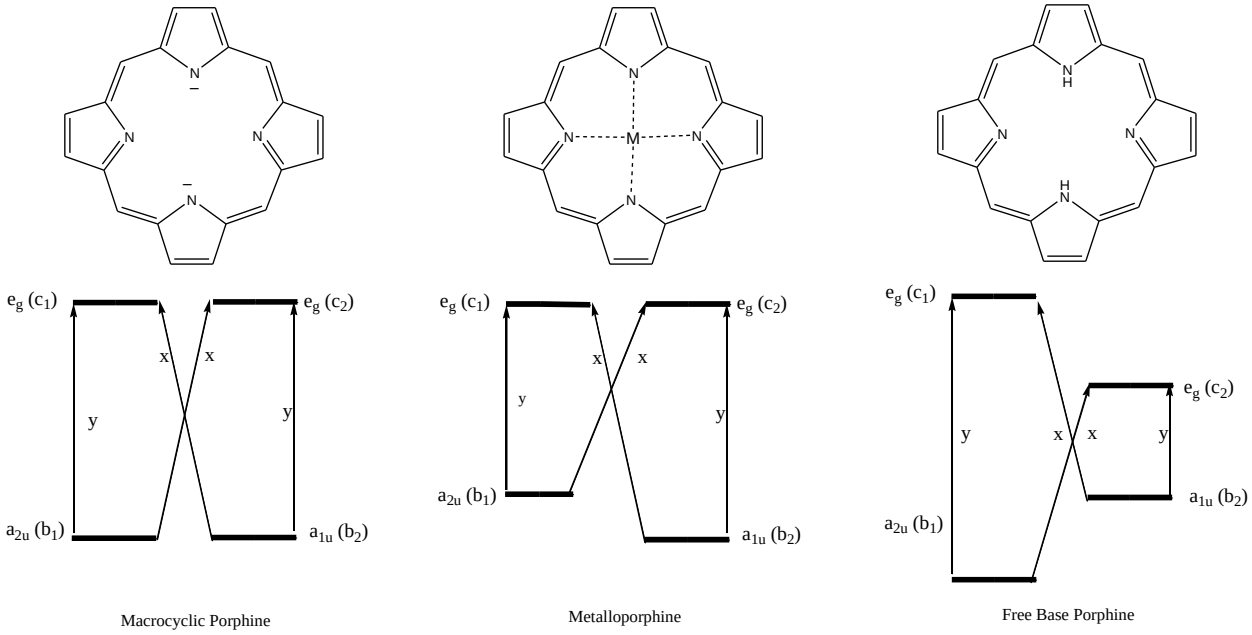

Figure 1-7: The changes induced in the orbitals upon introducing a metal or hydrogen atoms to the center of the macrocyclic porphyrin

The absorption maxima of free-base porphine (H_2PP) and zinc porphine (ZnPP) are summarized in Table 2.1, and their absorption spectra are shown in Figure 1-8.[23]

Table 1-1: The absorption maxima of H_2PP and ZnPP in benzene at room temperature

Compound	Soret (nm)	Q (nm)			
H_2PP	419	515	550	590	645
ZnPP	419	548		585	

The positions of these bands are affected by the substitution (electron-withdrawing or electron-donating groups), π-conjugation, protonation of the inner nitrogen atoms, or central metal and solvent polarity.

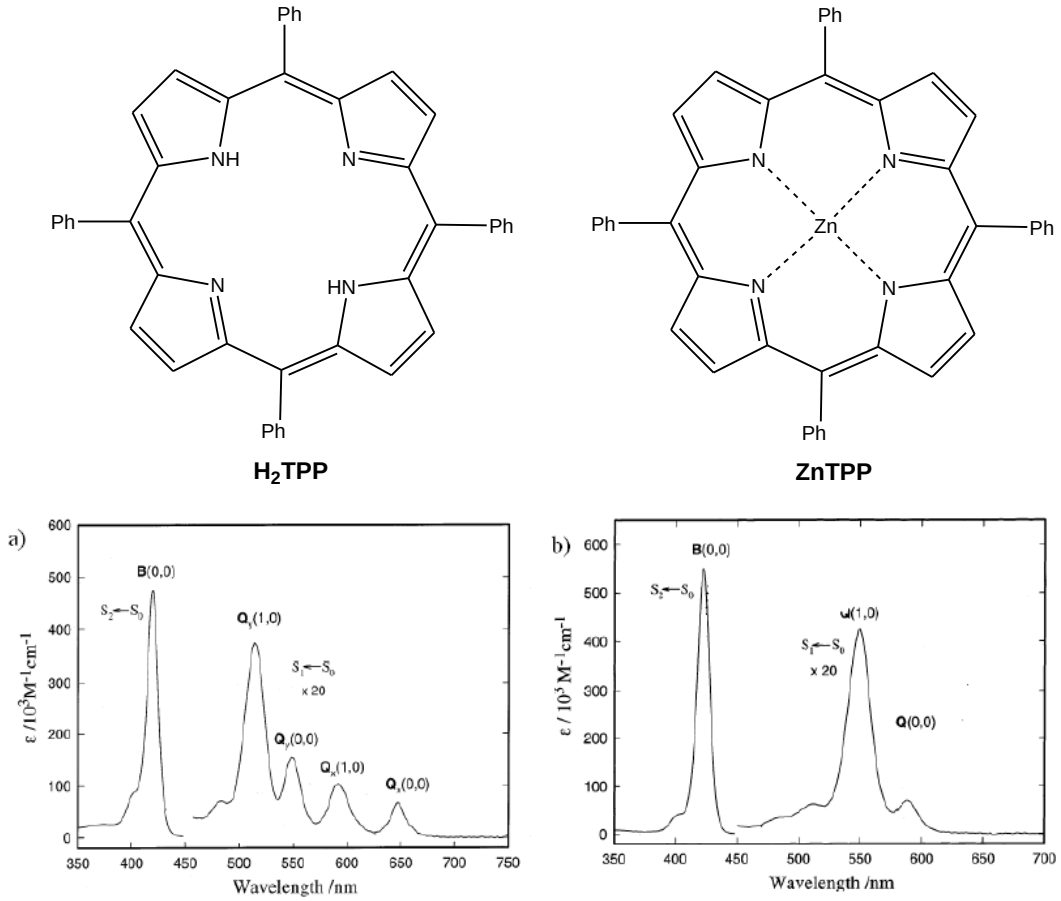

Figure 1-8: UV-vis absorption of a) free-base tetraphenylporphyrin (H_2TPP) and b) zinc tetraphenylporphyrin in benzene (the Q band intensities are expanded 20 times from the actual intensities). Reprinted with permission from *J. Phys. Chem. A* 2002, *106*, 9837- 9844 and *J. Phys. Chem. A*. 2002, *106*, 9845-9854.[24,25]

1.2.2.2 Substituent effects on *meso*-substituted porphyrin absorption spectra

Properties of free-base porphyrins can be modified by substitution at the *meso*-positions. As a result, they have attracted much interest. The porphyrin's ring often distorts in the presence of these peripheral substituents. This out-of-plane distortion is the cause of the red shift in the absorption spectra of the porphyrin. The HOMO b_1 orbital has a larger amount

of electron density at the *meso*-positions than the b_2 orbital (Figure 1-6). As a result, the energy gap between the electronic states becomes smaller with the attachment of phenyl rings as the b_1 orbital increases in energy with the addition of aryl groups at the *meso* positions (Table 1-1, Figure 1-8).

A series of studies have been done on *ortho*-substituted and *para*-substituted phenylporphyrins, and *meso*-tetraalkylporphyins, showing the steric and electronic effects as a result of the varied substitution.[24, 26-28]

The presence of electron-donating or electron-withdrawing groups resulted in changes of the intensities of the absorption bands, as well as a red shift or blue shift in the Soret and Q band absorption maxima.

1.2.3 Emission spectra of the free-base porphyrin and metalloporphyrin

The energy level diagram that is applicable for most aromatic compounds with singlet ground states is shown below (Figure 1-9). Upon exciting the electrons from the ground state S_0 to any excited state, S_x, fast radiationless decay will occur to the lowest excited singlet state, S_0. The decay from the highest state to the lowest can follow different pathways: from S_1, the molecule can emit fluorescence radiation via $S_1 \rightarrow S_0$ with a rate of K_f, decay without radiation with a rate of K_1 via $S_1 \rightarrow S_0$, or can convert internally to the lowest triplet state $S_1 \rightarrow T_1$ with rate K_2.[29]

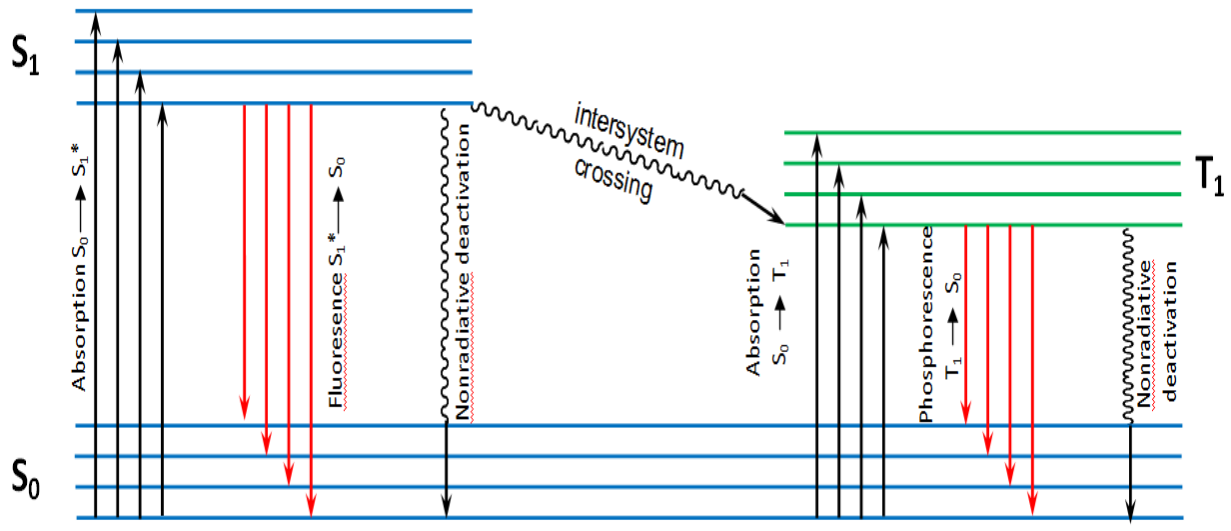

Figure 1-9: Decay scheme for singlet and triplet relaxation; the radiationless processes are shown as wavy lines and the radiation processes are shown by straight lines

In the transition from T_1, the molecule can emit phosphorescence radiation as $T_1 \rightarrow S_0$; the molecule can decay from $T_1 \rightarrow S_0$ without radiation or can be re-excited to the first excited singlet, $T_1 \rightarrow S_1$. Internal conversion does not involve a change in the electronic spin quantum number and occurs very fast. The excited molecule decaying through internal conversion undergoes vibrational relaxation to the ground state, with the excess energy converted to heat by collision with the solvent molecules. Intersystem crossing, however, involves a change in the spin quantum number of one electron, which is often a slow process.

Fluorescence and phosphorescence generally occur at shorter wavelengths in metalloporphyrins than their free-base analogues due to possessing higher singlet and triplet state excitation energies. The presence of a heavy metal atom in the porphyrin cavity generally leads to an increase in phosphorescence and a decrease in fluorescence. Unlike all other d^8 complexes, porphyrin-Ni complexes do not exhibit any luminescence as a result of low-lying d-d transitions.

The fluorescence spectra of the free-base porphyrin and metalloporphyrin usually consist of two peaks: the emission from the first excited single states, Q(0,0), and a vibronic overtone Q(0,1), which are mirror images of those seen in the absorption spectrum (Figure 1-10).

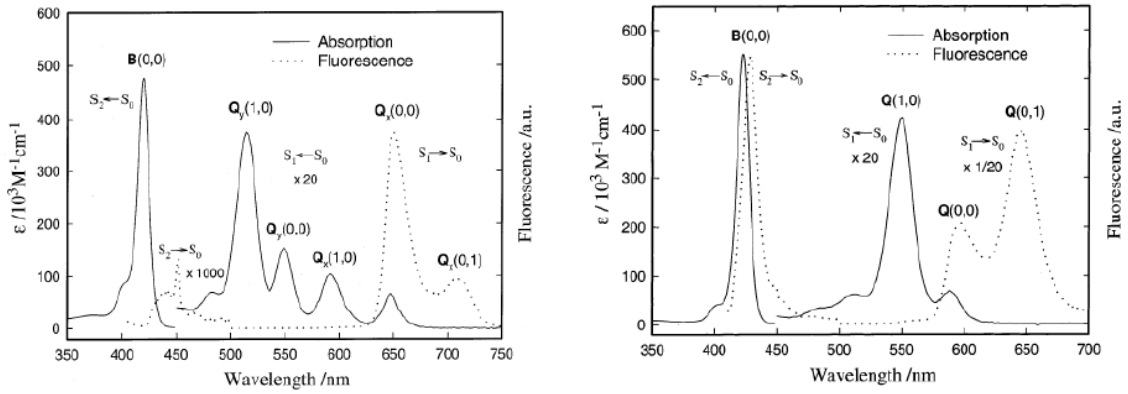

Figure 1-10: Absorption (solid line) and fluorescence (dashed lines) spectra of H_2TPP (left) and ZnTPP (right) in benzene. Reprinted with permission from *J. Phys. Chem. A.* 2002, *106*, 9837-9844 and *J. Phys. Chem. A.* 2002, *106*, 9845-9854.[24,25]

1.3 The synthesis of tetraphenylporphyrins and their metal analogues

Many *meso*-substituted porphyrins have been synthesized to resemble naturally occurring porphyrins in order to serve as biomimetic models and useful dyes. In 1935, Rothemund reported the first synthesis of a *meso*-substituted porphyrin.[30] He synthesized several *meso*-substituted porphyrins using a condensation reaction between substituted aldehydes and pyrrole in methanol at different temperatures in a sealed vessel. In total, three different *meso*-substituted porphyrins were prepared using acetaldehyde, benzaldehyde, and butyraldehyde yielding *meso*-substituted porphyrins in 4-5% yields.[31]

Thirty years later, Adler *et al*. reported the synthesis of tetraphenylporphyrin (TPP) via the condensation reaction between benzaldehyde and pyrrole using a wide range of acidic conditions including acetic acid, metallic salts in acetic acid, and benzene containing

trifluoroacetic acid.[32,33] The highest yield, ~30%, was isolated using the acidified reactions in benzene. The isolation of TPP was improved further when propionic acid was employed as the acid and the solvent.

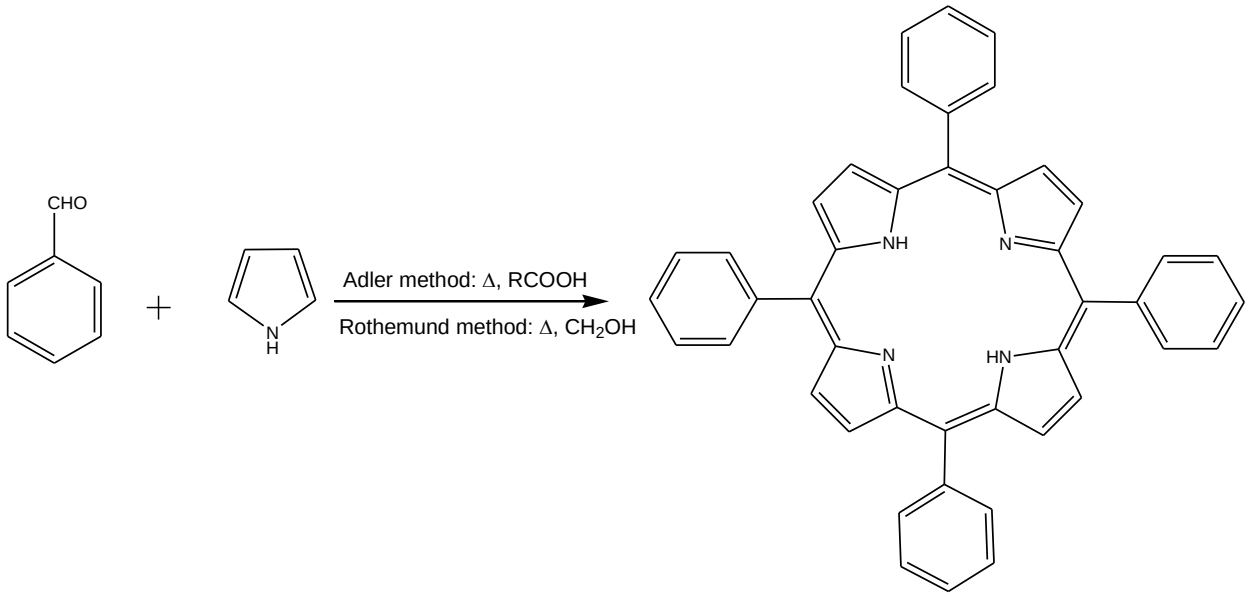

Scheme 1-3: Synthesis of tetraphenylporphyrin (TPP)

Both methods employ harsh reaction conditions (Scheme 1-3) which lead to the formation of porphyrin in low yields. Also, the synthesis of porphyrins containing sensitive functional groups was difficult to achieve, and so new methods were developed to broaden the extent and the scope of substitution on the porphyrin ring. Lindsey *et al*. developed a new approach in 1986 for synthesizing various *meso*-substituted porphyrins using mild conditions.[34,35] The Lindsey method involves a two-step one-flask reaction. The first step utilizes a condensation reaction between pyrrole and an aldehyde in the presence of acid as a catalyst to form the tetrapyrrolic macrocycle, while the second step entails an oxidation by 2,3-dichloro-5,6-dicyanobenoquinone (DDQ) or *p*-chloranil to form the porphyrin. This method involves the addition of a catalytic amount of trifluoroacetic acid (TFA) or BF_3

etherate to a solution of pyrrole and an aldehyde at 10 mM each, in dichloromethane or chloroform. The oxidation step converts the porphyrinogen to the corresponding porphyrin upon the addition of stoichiometric quantities of *p*-chloranil or DDQ (Scheme 1-4).

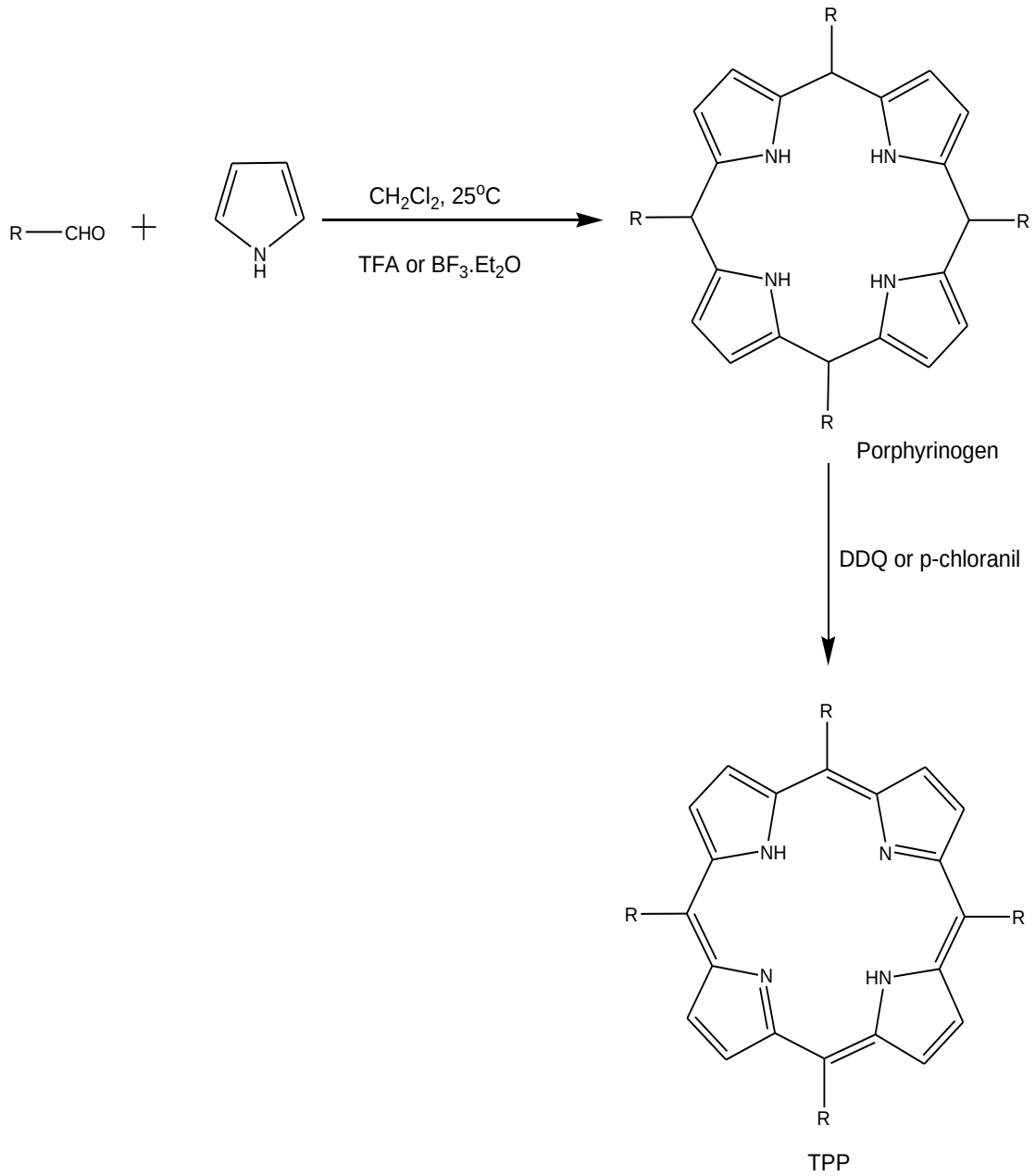

Scheme 1-4: Lindsey's method of synthesis of TPP

1.4 Porphyrin dendrimers

The unique properties associated with perfectly branched dendritic architectures have been heavily researched during the last two decades. Natural porphyrin derivatives, including hemes, chlorophylls, and bacteriochlorophylls, are integrated into protein scaffolds that are essential for their biological activities.[36] For instance, in myoglobin and hemoglobin, the embedded active iron centers are protected sterically and hydrophobically against irreversible oxidation, thus enabling reversible O_2 binding to take place. Also, the protein matrices of hemoproteins provide active centers with a specific steric hindrance.[37] Additionally, in the light harvesting complexes of purple bacteria, porphyrins play a major role in the efficient capturing of energy from sunlight and transferring it to the photosynthetic reaction center.[38,39]

The synthesis of porphyrin dendrimers began in 1993 by Aida and co-workers, when a porphyrin unit was integrated into the center of a poly(benzyl ether) dendrimer to form a synthetic model of a hemoprotein.[40] A year later, Diederich *et al*. reported the synthesis and redox properties of poly(ether-amide) porphyrin dendrimers.[41] In 1996, Suslick and co-workers studied the action of manganese porphyrin-cored poly(aryl ester) dendrimers for oxidation.[42]

1.4.1 Synthetic strategies and structural variation

A step-by-step iterative synthesis of a dendrimer allows porphyrins to be precisely positioned in the molecule's structure, as illustrated in Figure 1-11.

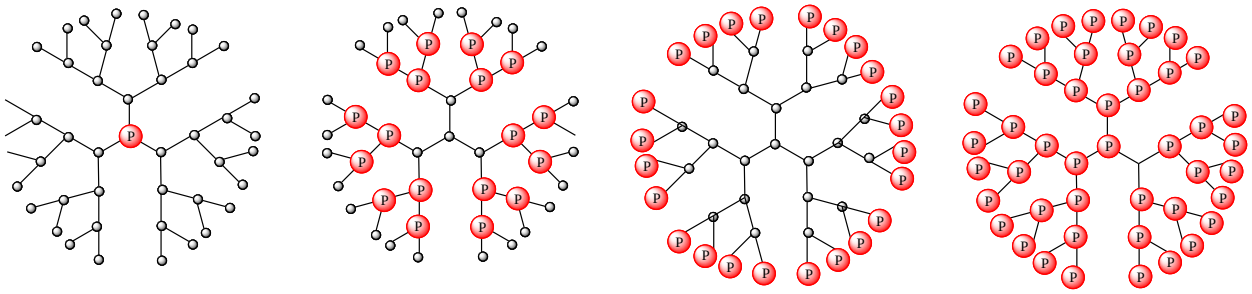

Figure 1-11: Structural classification of porphyrin dendrimers as reported thus far; symbol "P" denotes a porphyrin unit. = generic atom)

Most of these dendrimers have been synthesized by the introduction of dendritic substituents to the porphyrin core at the *meso*-position (Figure 1-12 A).

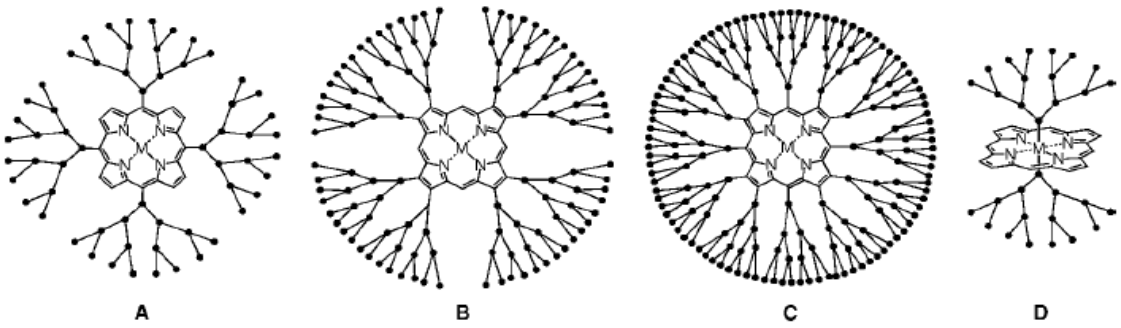

Figure 1-12: Structural classification of porphyrin dendrimers

There are two ways to synthesis the porphyrin dendrimers: either by divergent synthesis (route 1) or a convergent approach (routes 2 and 3), as shown in Scheme 1-5. Diederich and co-workers were the first to follow the divergent route to synthesize a poly(ether-amide) dendrimer from a porphyrin core.[43]

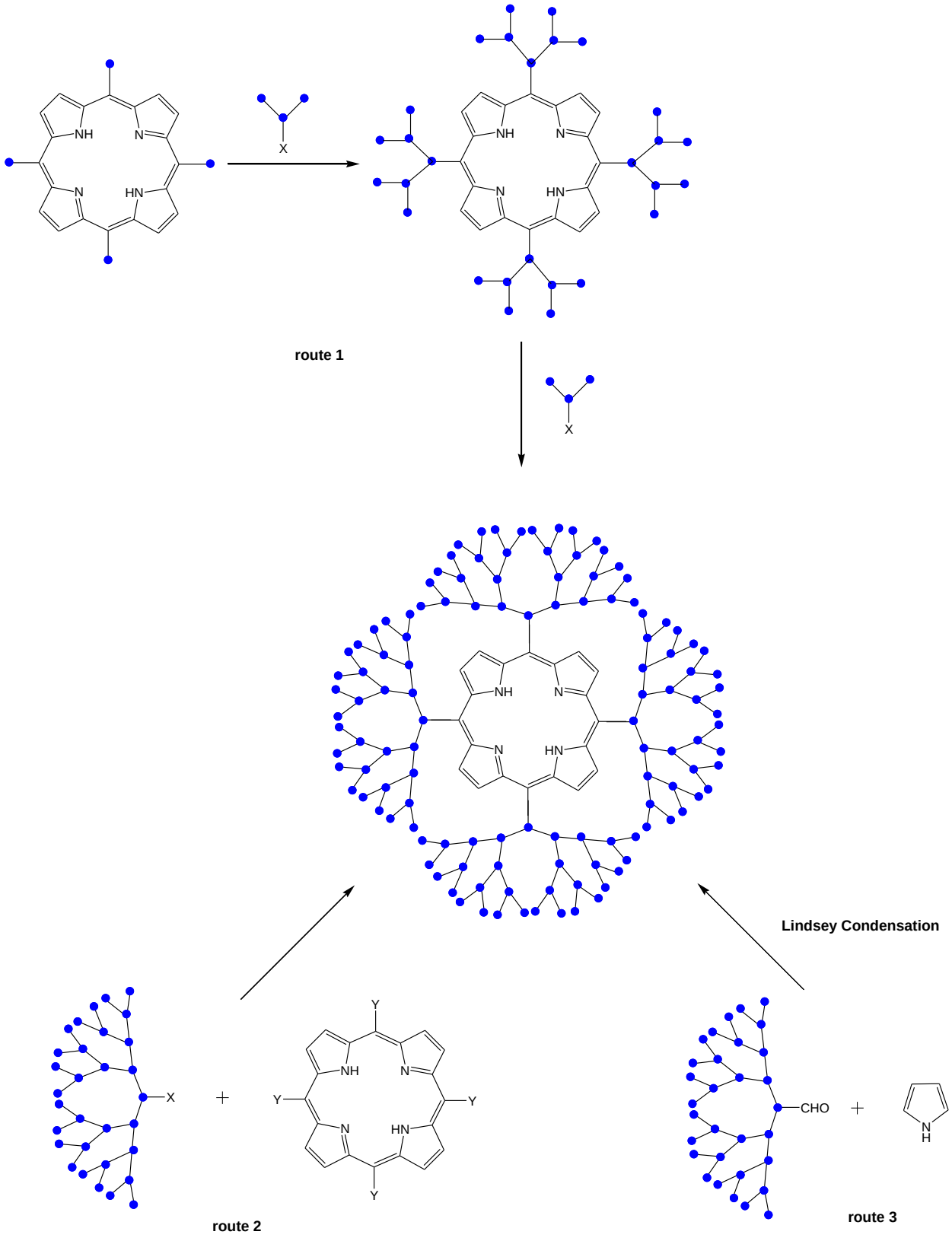

Scheme 1-5: The synthetic routes towards porphyrin dendrimers

The divergent approach may sometimes suffer from the disadvantage that the final products contain structural defects. However, this problem can be overcome by using the convergent approach.

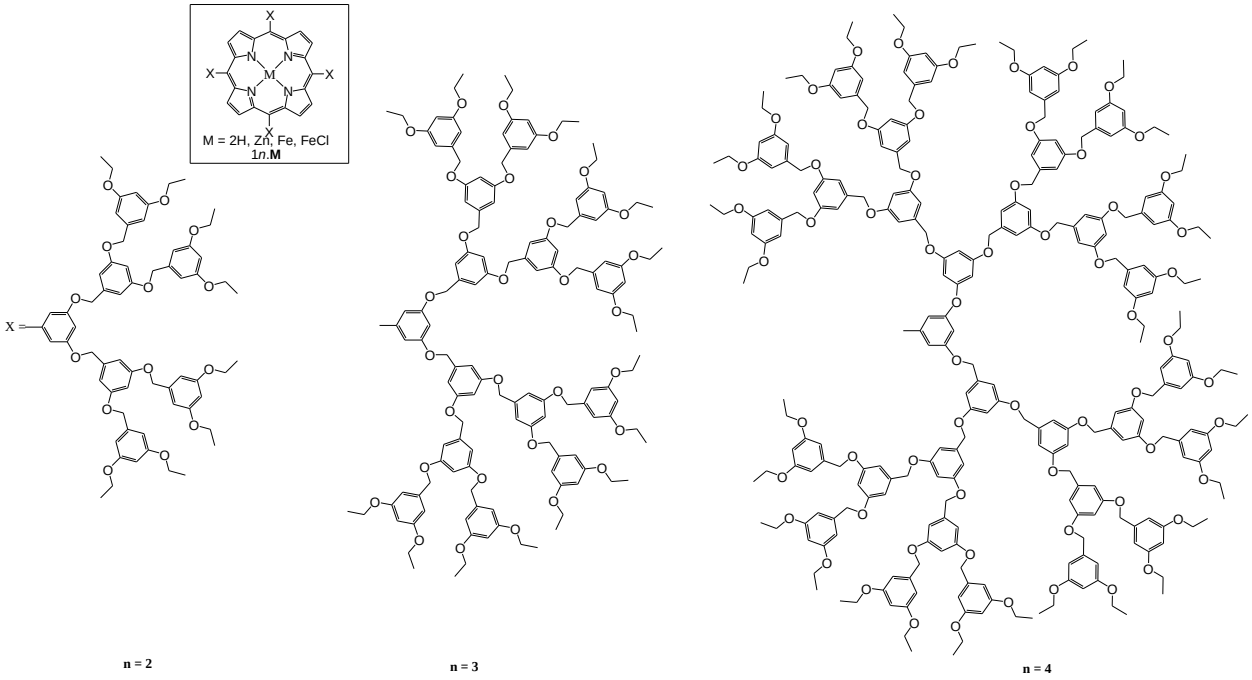

Figure 1-13: Porphyrin unit integrated into the center of poly(benzyl ether) dendrimer[40]

Using route 2, Aida and co-workers first reported the synthesis of a porphyrin dendrimer in 1993, synthesizing it via a Williamson condensation (Figure 1-13).[40] In 1998, Frechet *et al*. chose a new convergent approach (route 3) by a condensation reaction of pyrrole with poly(benzyl ether) dendrons with an aldehyde group at the focal core.[44] All previous synthetic strategies were employed to obtain a porphyrin dendrimer by the introduction of dendritic substituents at the *meso*-position. However, dendritic substituents have also been attached to axial and pyrrole-β positions (Figure 1-12 B-D). Vinogradov and co-workers reported a dendrimer where the arms are attached to the pyrrole-β, as well as the *meso*-position

(Figure 1-14).[45] Dendritic units were also successfully attached to the axial position (Figure 1-12 D) to prepare a rhodium(III) porphyrin complex.[46]

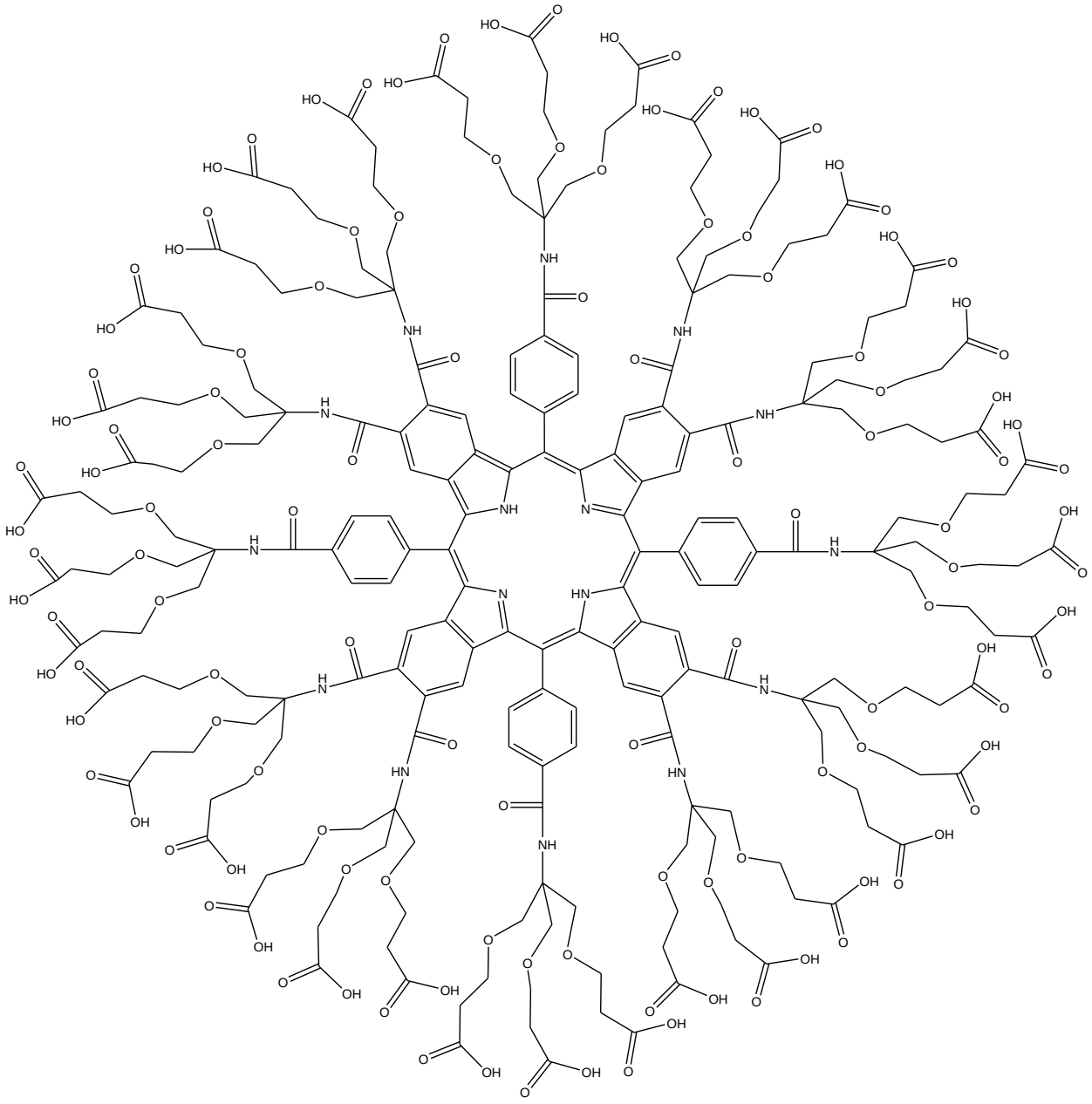

Figure 1-14: Dendrimer with arms attached to both pyrrole-*β* and *meso*-positions[45]

1.5 Applications

In recent years, porphyrins and related macrocycles have received a great deal of attention because they display interesting electrochemical, photochemical, and photophysical properties. The well-designed porphyrinoid ligand provides the chromophore for a multitude of iron, magnesium, cobalt, and nickel complexes, which are primary metabolites.[47,48]

Porphyrins and metalloporphyrins have been greatly studied through the past decade, both for their optical properties and their applications as sensors. Porphyrins and metalloporphyrins have applications as field-responsive materials, particularly for optoelectronic applications, including mesomorphic materials and optical-limiting coatings. For example, the substitution of the periphery of various porphyrins has resulted in a series of liquid crystalline materials with excellent thermal stability, where the extended conjugated macrocyclic rings give large non-linear optical effects in their physical properties, making their chemical modification easy.[48-51] Porphyrin-based macromolecules also absorb light energy over a wide spectral range and convert it into the highly directional transfer of electrons.[52-54]

A biomimetic method to the photosynthetic apparatus may also lead to applications of similar systems as optoelectronic devices. Due to their stability, unique optical properties, and synthetic versatility, porphyrins and metalloporphyrins are great candidates for sensing materials. Another focus in this area is the incorporation of synthetic porphyrins and metalloporphyrins into a variety of material matrices, such as polymers, glasses, and films.[55] They can also be used in the detection of organic vapours and ionic species in solution. Meanwhile, metalloporphyrins of aluminium, zinc, manganese, cobalt, and rhodium complexes have been explained as effective initiators for controlled anionic and free radical polymerizations.[56]

Dendrimers containing free-base porphyrins or metalloporphyrins participate in electron and energy transfer events in natural photosynthesis. As a result, they present potential applications as light harvesting devices and switches. The chromophore orientation is a key factor for their function, and thus a variety of covalently and non-covalently assembled multiporphyrins have been studied to further understand biological photosynthetic systems, as well as to devise artificial molecular systems that can achieve effective charge separation. A popular trend is to use the host-guest molecular recognition strategy with the aim to mimic similar processes employed in natural systems.[57,58]

Currently, porphyrin dendrimers have been used as sensitizers for photodynamic therapy (PDT).[59,60] PDT is a therapeutic technique which uses the combination of light and a drug to bring about a cytotoxic effect to cancerous tissues. This method can destroy unwanted tissue while sparing the normal tissue. It has no side effects to both healthy and abnormal tissue, and is only activated when exposed to a carefully regulated dose of light.[61] This technique is used to control the cancer by killing the cancer cells with lethal doses of radiation, chemotherapy, or a combination of these therapies. Despite the chemotherapy, radiotherapy and surgery effectively extend the lives of approximately 50% of patients who develop malignant tumors. In the PDT method, the side effects in normal tissues are minimal due to the photosensitizer property.[62,63]

In a bewildering array of proteins, porphyrins play a very important role.[64] Their functions include O_2 transport (hemoglobin Hb), O_2 storage (myoglobin Mb), bonds (cytochrome P_{450}), and oxygen reduction. In the case of cytochrome P_{450}, the axial ligand is the sulfur atom of a cysteinate, while the axial ligand is the nitrogen atom of a histidine residue in Mb and Hb. The diversity of functions of these natural hemoproteins is mainly

dictated by the number and nature of the axial ligands, the nature of the polypeptide chain, the spin and the oxidation state of the metal center, and the geometry of the porphyrin ring.[65-67]

In the field of the organic light-emitting diode (OLED) devices, porphyrins have received considerable attention for their saturated red chromaticity and the narrow emission width in the range of 635–660 nm.[68-71] Many porphyrins, such as substituted tetraphenylporphines, have been used as red-emitting materials.[72] It was found that the electroluminescent properties of OLEDs are strongly coupled to the molecular structures of the dopants in red-emitting OLEDs with the non-porphyrin dopants, and substituted electroluminescence materials exhibited a larger electroluminescent efficiency than the unsubstituted analogues.[73]

1.6 The chemistry of ferrocene

After the discovery of ferrocene in 1951, it has been widely used as either part of a backbone or a substituent in ancillary ligands due to its particular and unique geometries and redox properties, by which switching the redox state of the ferrocene backbone ensures control of the reactivity at the metal centre. All manner of ligands formed via substitution of ferrocenes using different donor heteroatoms have found wide applications.[74,75]

One of the cyclopentadienyl rings of ferrocene can be exchanged by an arene, resulting in a cationic η^6-arene-η^5-cyclopentadienyliron complex. In 1963, Nesmeyanov *et al*. first reported that η^6-arene-η^5-cyclopentadienyliron cations could be prepared by the reaction of benzene or substituted benzenes with ferrocene and $AlCl_3$, with aluminum powder also present in the reaction mixture to minimize the formation of ferrocenium ions from ferrocene; this reaction is called a ligand exchange reaction.[76,77]

1.7 Organoiron complexes based on cyclopentadienyliron cations

The ligand exchange reaction of ferrocene with chlorobenzene or 1,4-dichlorobenzene is shown in Scheme 1-6 as an example. The η^6-dichlorobenzene-η^5-cyclopentadienyliron complex, which can be subsequently treated with ammonium tetrafluoraborate or ammonium hexafluorophosphate and isolated as a neutral salt, is formed by ferrocene and monochlorobenzene or 1,4-dichlorobenzene in the presence of powdered aluminum at temperatures between 80-165°C for 5 hours catalyzed by $AlCl_3$. Because 1,4-dichlorobenzene is liquid under reaction temperatures, additional solvent is not required.

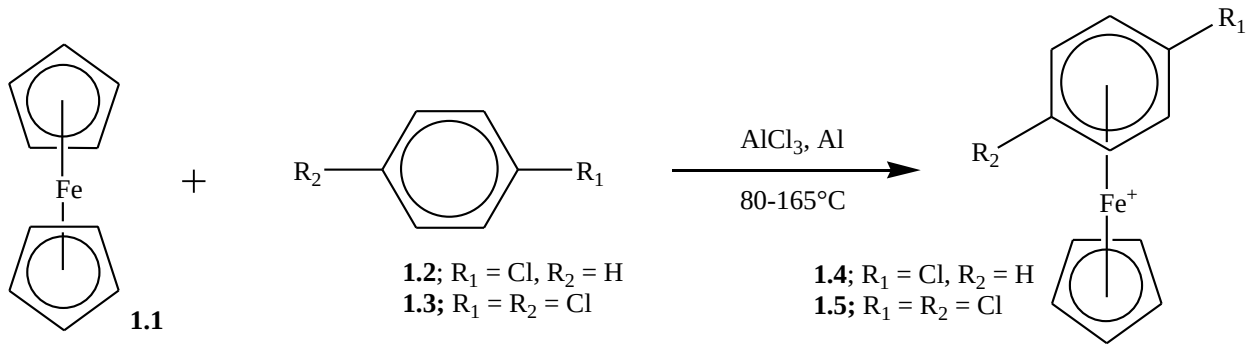

Scheme 1-6: Ligand exchange reaction of ferrocene

The proposed ligand exchange reaction mechanism, a Friedel-Crafts reaction, is shown in Scheme 1-7. The cyclopentadienyliron rings of the ferrocene molecule are coordinated by the $AlCl_3$, resulting in a disruption of the bond between the ring and the iron, cleaving the ring from the ferrocene and creating the cyclopentadienyliron cation. The cyclopentadienyliron cation then coordinates to the arene, giving the η^6-dichlorobenzene-η^5-cyclopentadienyliron complex.[78,79]

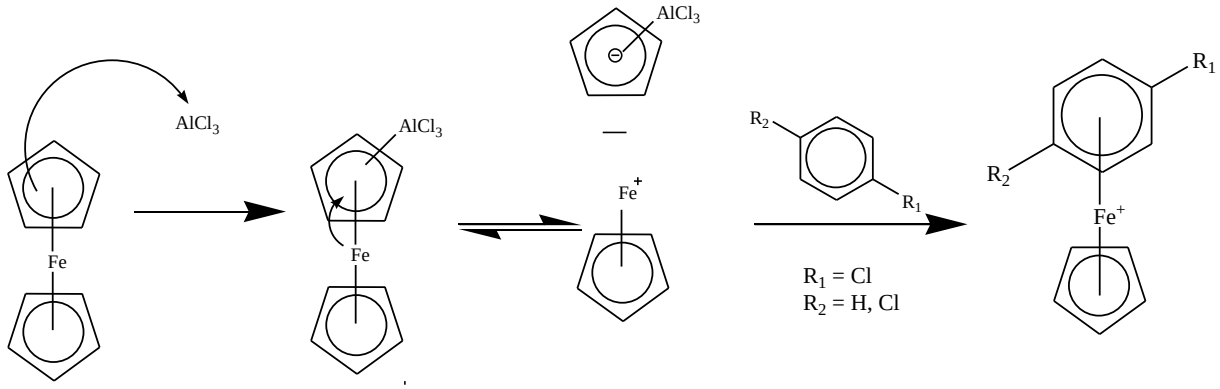

Scheme 1-7: Proposed mechanism for the ligand exchange of ferrocene[79]

The coordination of the cationic cyclopentadienyliron moiety to mono- or dihalobenzene increases the activity of the arene group to nucleophilic aromatic substitution because of the electron-withdrawing nature of the cyclopentadienyliron moiety.[80-88]

An aromatic substitution reaction of chlorobenzene with phenolic groups requires long reaction times, high temperature and pressure, or harsh catalysts. However, η^6-chlorosubstitutedarene-η^5-cyclopentadienyliron complexes are easily substituted by phenolic groups at room temperature in the presence of weak bases, such as K_2CO_3 (Scheme 1-8).[78,79]

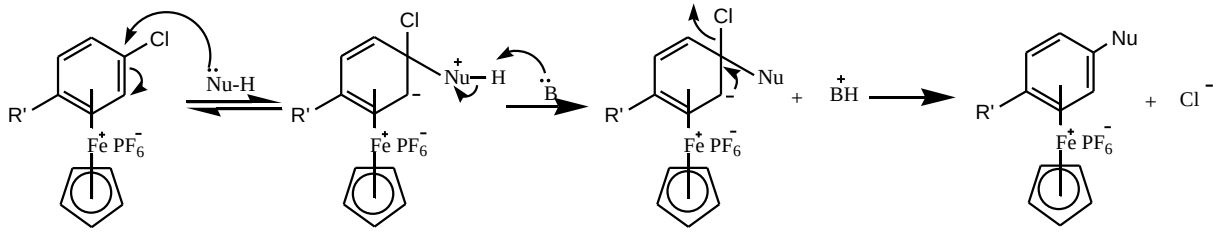

Nu-H = ROH, R_2NH, or RSH
B: = K_2CO_3 or R_2NH
R' = H, Cl

Scheme 1-8: Metal-mediated nucleophilic reaction of an η^6-dichloroarene-η^5-cyclopentadienyliron(II) hexafluorophosphate complex[79]

The coordination of the organoiron moiety to arenes offers an excellent method of analysis in ^{1}H NMR and ^{13}C NMR spectroscopy. In both NMR analyses, the resonances of the complexed arene appear at a significantly lower chemical shift than non-complexed arene rings. For example, when the ^{1}H NMR spectrum of *p*-dichlorobenzene is compared with the η^{6}-dichlorobenzene-η^{5}-cyclopentadienyliron(II) hexafluorophosphate complex (Figure 1-15), the proton resonances due to dichlorobenzene are approximately 7.42 ppm, whereas the resonances due to the complexed arene of η^{6}-dichlorobenzene-η^{5}-cyclopentadienyliron are closer to 7.00 ppm. The destabilization of the anisotropy of the arene due to coordination of the π-system to the iron centre results in an upfield shift in the signals of the ^{1}H NMR spectrum due to the electron-withdrawing nuture of the cyclopentadienyliron moities. These particular resonances can be used as diagnostic peaks to determine successful reactions due to differences between the resonances of complexed arenes versus other arenes.

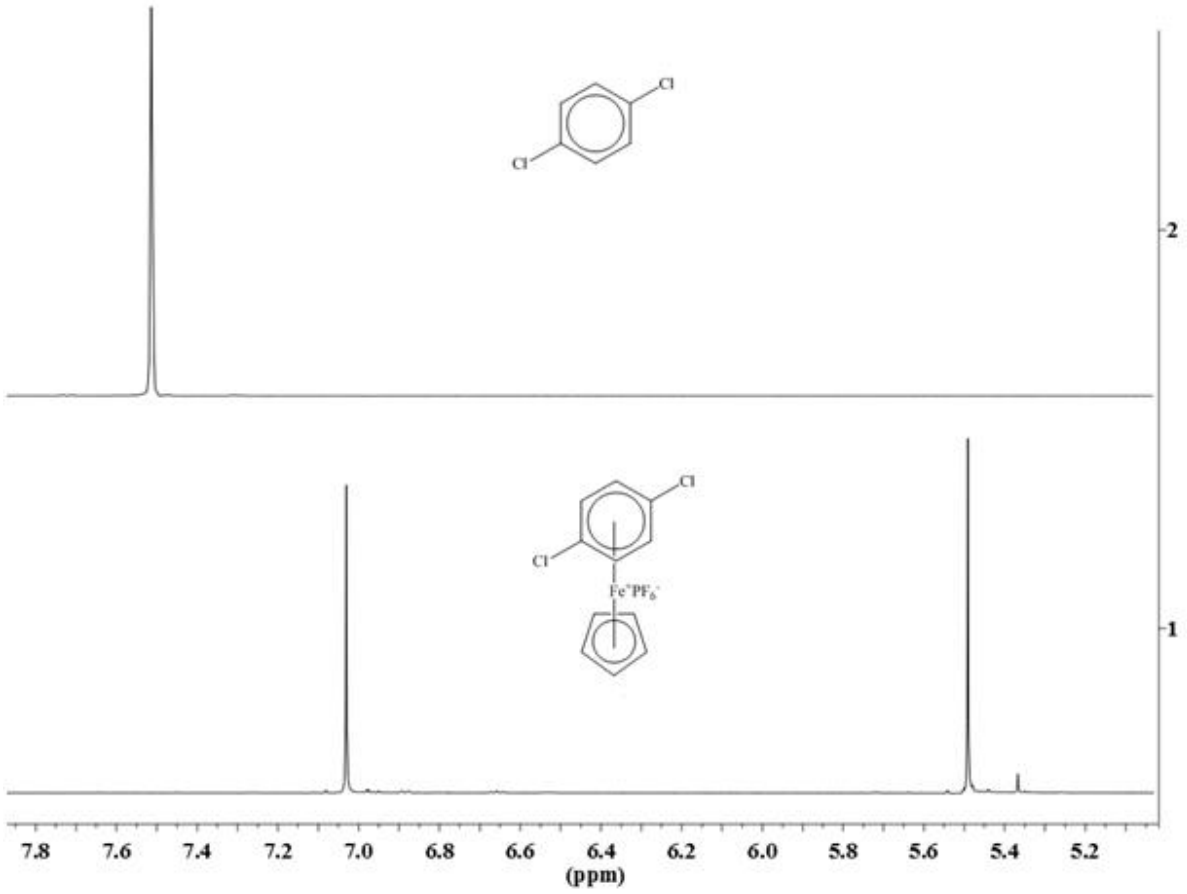

Figure 1-15: Comparison of 400 MHz ^{1}H NMR spectrum of dichlorobenzene 1.3 (spectrum 2) and complex 1.5 (spectrum 1)

As shown in Scheme 1-9[89], ferrocene undergoes a single electron reversible electrochemical oxidation, resulting in the reduction to the 16-, 17-, 18-, and 19-electron states.[90,91] The cationic cyclopentadienyliron complexes go through two single-electron reductions, providing oxidation states of 17-, 18-, 19-, and 20-electrons, which gives them unique electrochemical properties. Depending on the substituent of the arene ring and the cyclopentadienyliron ring, the reduction to form the 20-electron species shows the ability to be reversibly reduced to the 19-electron state. The 19-electron complex is fully reversible to either the 18-electron or 20-electron states, and 18-electron complexes are fully reversible to either the 17-electron or 19-electron states.[92] Electron-withdrawing groups attached to the

complexed arene will result in the complex undergoing reduction at more positive voltages than those with electron-donating groups due to the increased electron delocalization.[93-95]

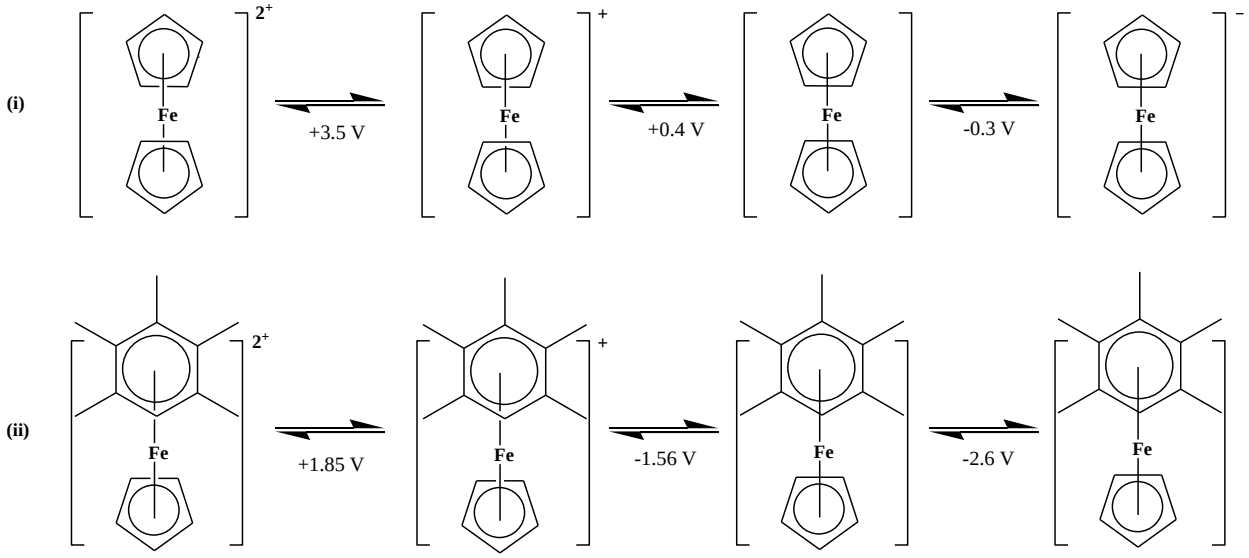

Scheme 1-9: Potentials for the oxidation states determined by cyclic voltammetry of (i) ferrocene and (ii) η^6-hexamethylbenzene-η^5-cyclopentadienyliron(II); potentials are given versus a saturated calomel reference electrode[89]

The cyclopentadienyliron moiety can easily be removed, giving purely organic analogues of the iron complex and thus providing an advantage in arene-coordinated cyclopentadienyliron complexes. Two main methods to remove the cationic iron moiety can be followed: pyrolysis and photolysis. However, electrolysis has also been used.[96,97] To cleave the cationic moiety via pyrolysis requires either excessive heating in a solvent with a high boiling point, such as dimethylsulfoxide (DMSO) or diphenyl ether. The organic analogues should be thermally stable if pyrolysis is used, otherwise decomposition of the product may occur.

Photolysis is an effective method to remove the cationic cyclopentadienyl moiety.[98] Under ultraviolet light (300 nm) using highly coordinating solvents, such as acetonitrile,

photolysis of the cationic group of the arene-coordinated cyclopentadienyliron complex is achieved.[98-102] Ferrocene, iron salts, and the organic arene are formed after this procedure, which can be isolated and purified through extractions and column chromatography. The mechanism of photolysis (Scheme 1-10) stimulates the arene-coordinated cyclopentadienyliron complexes into their triplet states, which results in "ring-slippage" from η^6 to η^4 and makes available a coordination site on the iron atom. A highly coordinating solvent or the complex's counter ion can fill the rapidly-formed coordination site, which produces a new intermediate complex that readily decomposes to give ferrocene, iron salts, and the organic compound.

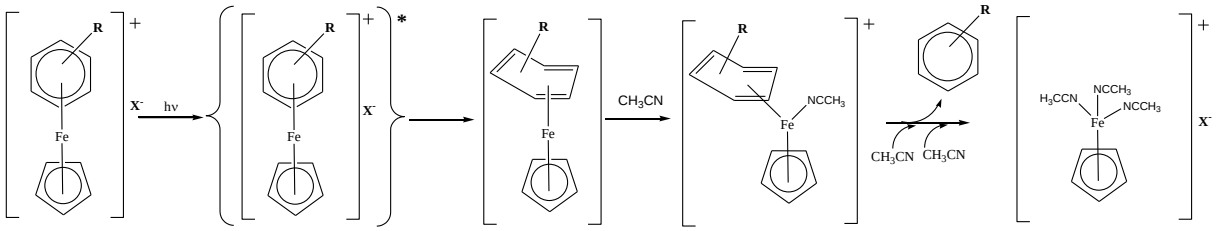

Scheme 1-10: Mechanism of the photolytic cleavage of the cationic cyclopentadienyliron moiety. X^- is a counter ion such as PF_6^-

1.7.1 The synthesis and chemistry of the η^6-haloarene-η^5-cyclopentadienyliron(II) hexafluorophosphate complex with carboxylic groups

The Abd-El-Aziz group has prepared a series of carboxylic acid-functionalized organoiron complexes employing the nucleophilic substitution of the η^6-chlorosubstitutedarene-η^5-cyclopentadienyliron complexes. Two carboxylic acid complexes, a monometallic acid complex and a bimetallic acid complex, functionalized by organoiron, are first prepared in order to conduct further condensation reactions. The monometallic acid complex **1.7** is synthesized from the reaction of *p*-dichlorobenzene cyclopentadienyliron hexafluorophosphate (*p*-dichloro complex **1.5**) with 4-hydroxybenzoic acid (Scheme 1-11).

This metal-mediated nucleophilic aromatic substitution reaction is typically performed in the presence of K_2CO_3 in DMF for 12 hours at room temperature.[102]

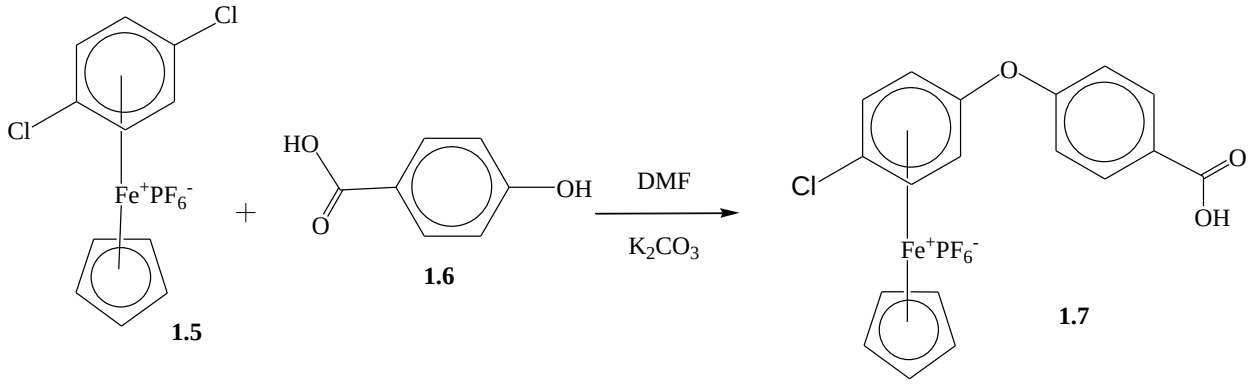

Scheme 1-11: Synthesis of the monometallic acid complex[102]

Bimetallic acid complex **1.9** is synthesized by the reaction of 4,4-bis(4-hydroxyphenyl)valeric acid with **1.5** (Scheme 1-12). The reaction is carried out in the same conditions as the monometallic acid complex, using K_2CO_3 in DMF at room temperature. However, a longer reaction time of 36 hours is required to make sure both phenolic groups are metal-mediated due to the ratio of the reagents.[102]

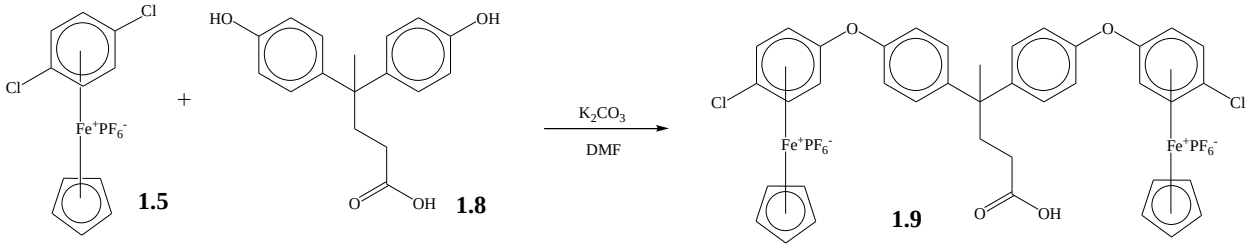

Scheme 1-12: Synthesis of bimetallic carboxylic acid complex 1.7[102]

1.8 Steglich esterification of bimetallic carboxylic acid complex

There are many effective and consistent methods for the esterification of carboxylic acids; for example, reacting their sodium, potassium, or calcium salts with alkyl halides, or

using the Fischer-Speier procedure in the presence of mineral acids. Steglich esterification is a competent method widely used under mild conditions, resulting in the condensation reaction of carboxylic acids and alcohols to form esters. The reaction utilizes dicyclohexylcarbodiimide (DCC) as a coupling reagent and 4-dimethylaminopyridine (DMAP) as a catalyst. The reaction is performed at 0°C for the first five minutes, and room temperature for the duration of the reaction for 3 hours (Scheme 1-13).

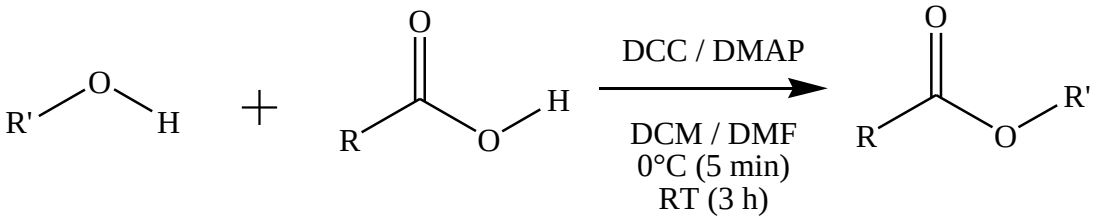

R', R = alkyl,aryl

Scheme 1-13: A simplified Steglich esterification[103]

The general mechanism of the Steglich esterification reaction is depicted in Scheme 1-14. Initially, the carboxylic acid is deprotonated by a strong nucleophile (DMAP) and subsequently reacted with DCC to form an *o*-acylisourea intermediate, which indicates some similarity with the analogous carboxylic acid anhydride, making it more reactive than the free acid. The protonated DMAP then acts as an acyl transfer reagent to yield a reactive amide, or "active ester". This intermediate cannot form intramolecular byproducts but undergoes reaction quickly with the alcohol. At last, the analogous ester is formed, along with dicyclohexylurea (DCU), a stable side product. DCU has low solubility in most common solvents such as acetone, dichloromethane, and water, and can therefore be removed from the product through filtration as a white precipitate.

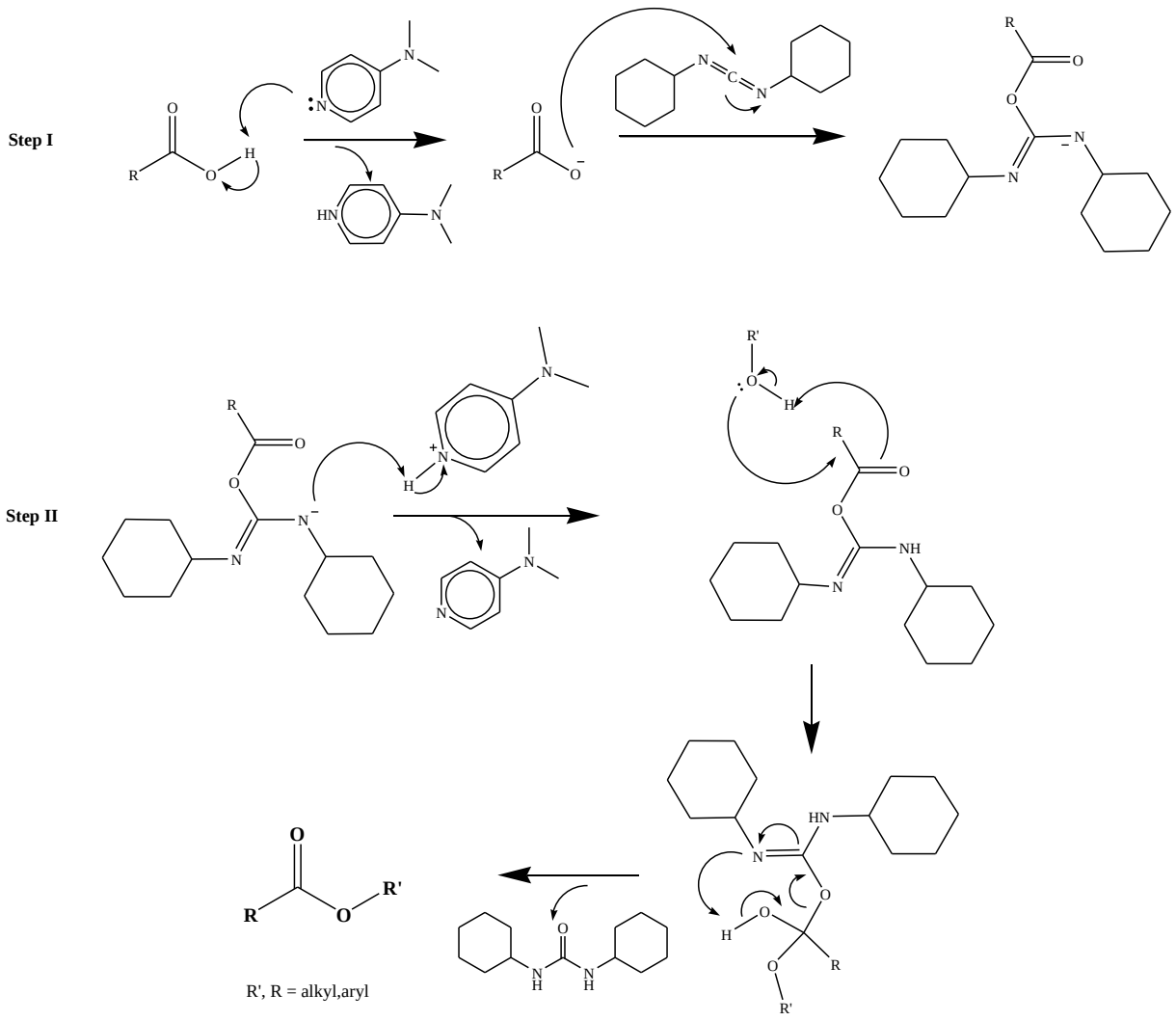

Scheme 1-14: Mechanism of the Steglich esterification using DCC/DMAP conditions

Chapter 2. Synthesis of porphyrin dendrimers containing organoiron complexes

2.1 Synthesis of free-base porphyrin 2.1, nickel 2.2a and Zinc 2.2b Porphyrins

Porphyrin T(P-OH)PPH_2 **2.1** was synthesized following the Alder approach,[32,33] where 4-hydroxybenzaldehyde and one equivalent of pyrrole were refluxed for one hour open to atmosphere in propionic acid (Scheme 2-1) to afford porphyrin **2.1** in 18% yield.

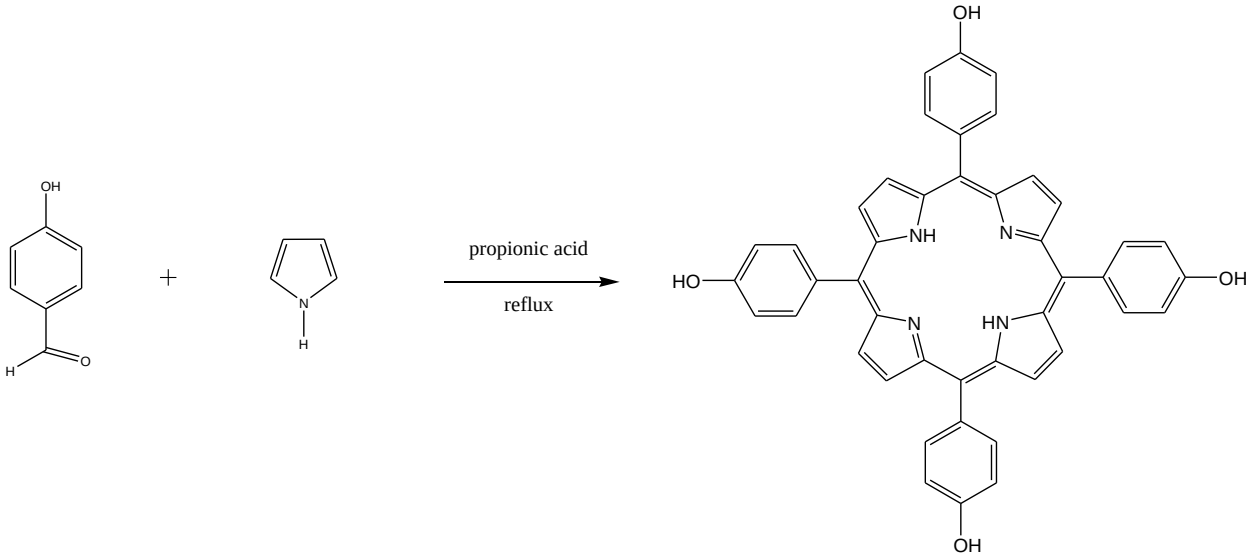

2.1

Scheme 2-1: Synthesis of 5,10,15,20-tetrakis(4-hydroxyphenyl) porphyrin

The ^{1}H NMR spectrum of **2.1** is shown in Figure 2-1. The internal proton N-H signals of the porphyrin resonated upfield at -2.87 ppm due to the ring current interaction. The signal for the pyrrole protons, however, was located downfield at 8.87 ppm. The phenyl protons resonated at 7.21-8.00 ppm (*ortho*- and *meta*-H-Ph), while the O-H proton appeared downfield at 9.96 ppm.

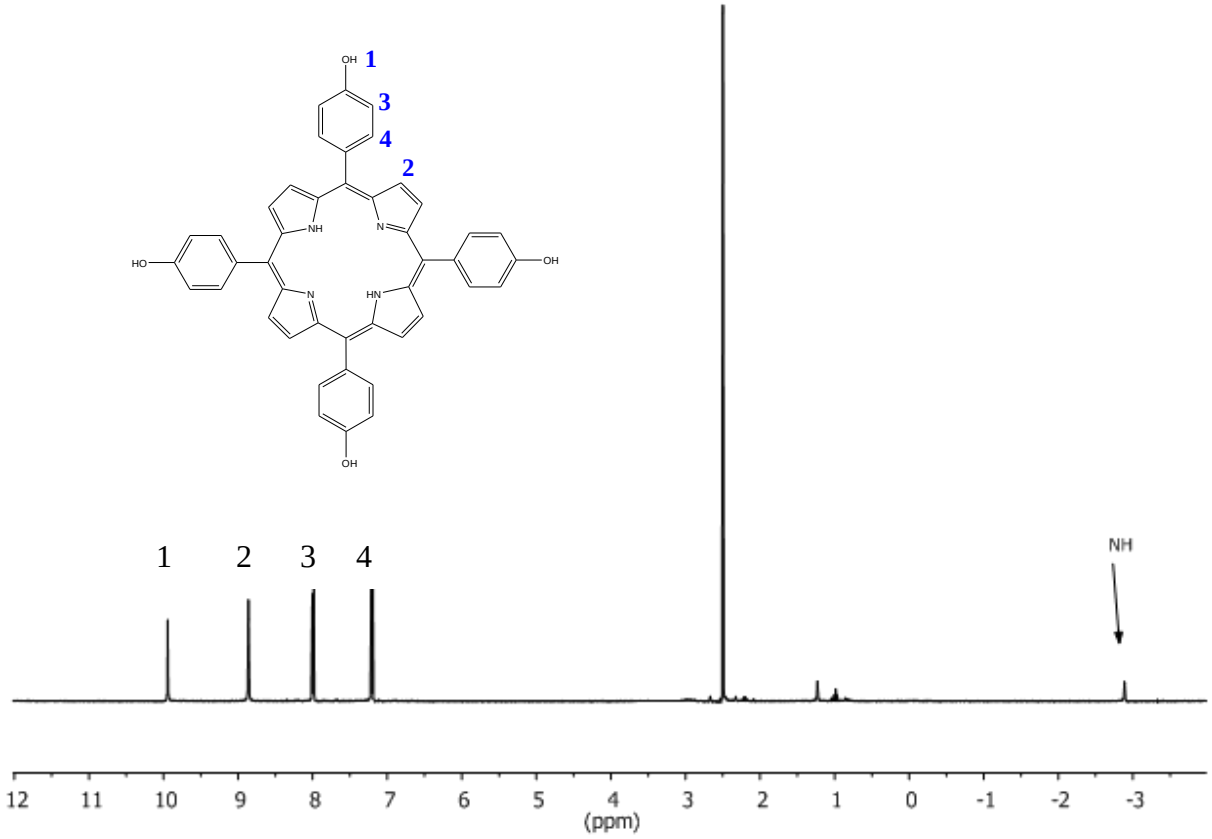

Figure 2-1: 400 MHz ^{1}H NMR spectrum of free-base porphyrin 2.1

The N-H tautomerism in free-base porphyrins shows exchange broadening of the pyrrole carbon signals at room temperature, which prevent some signals from being observed, particularly the α-carbon signals.[14-17] The ^{13}C NMR spectrum of **2.1** (Figure 2-2) shows only six observable peaks instead of the expected seven peaks. A very broad and small signal representing the *β*-carbon of pyrrole resonates at 131.9 ppm, close to the carbon 3 signal at 132.3 ppm. The *α*-carbon signal is not observed due to broadening by the conformational flexiblility of free-base porphyrin and the aforemention exchanely, which is lost in baseline noise. However, it appears as a sharp signal at 143.0 ppm when metallated.

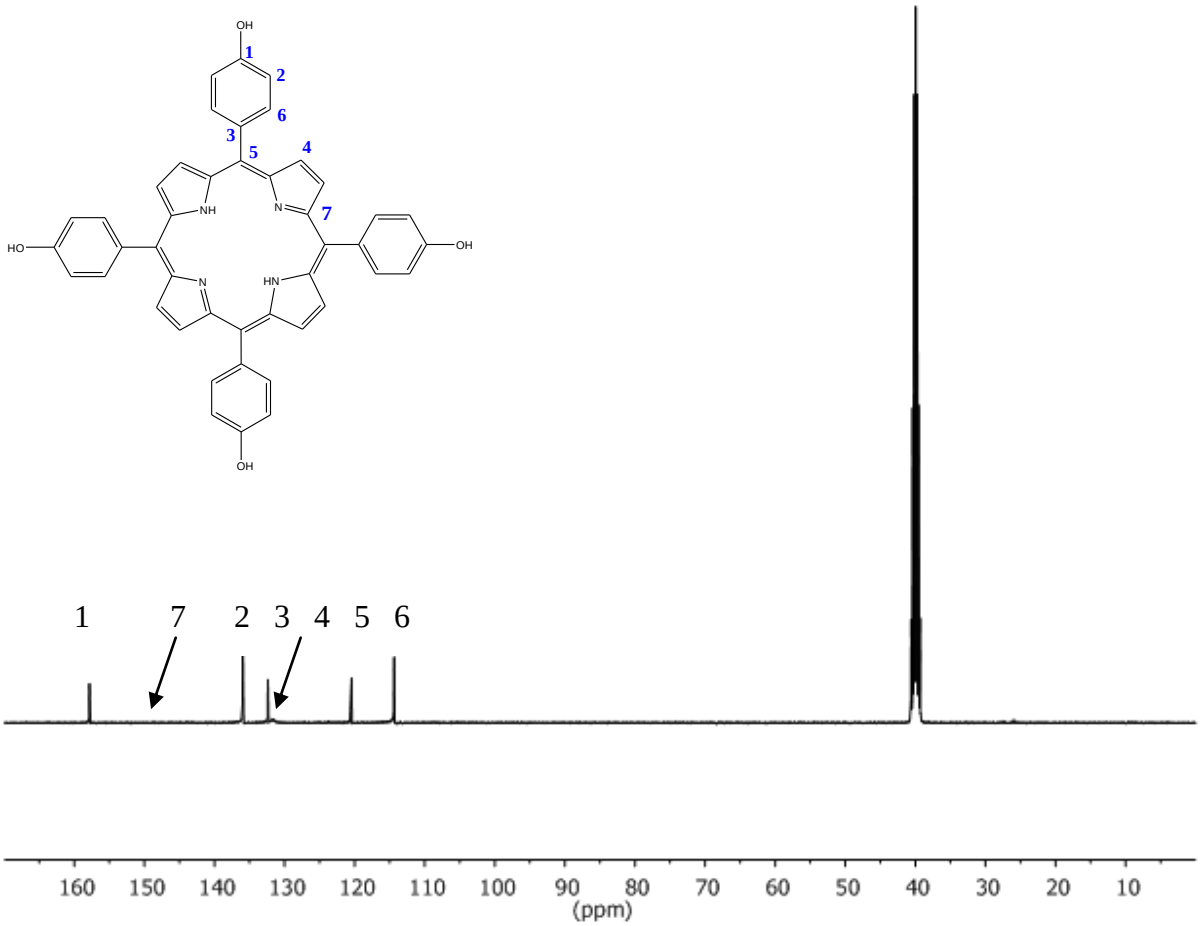

Figure 2-2: 101 MHz ^{13}C NMR spectrum of free-base porphyrin 2.1

The HSQC spectrum of **2.1** (Figure 2-3) further confirms the identity of the peak at 131.95 ppm by showing correlation between this peak and the *β*-proton of pyrrole located at 8.87 ppm. The phenyl carbons resonate at 114.08-135.66 ppm (*ortho*- and *meta*-C-Ph), and the carbon 1 that directly correlates to the O-H group resonated downfield at 157.65 ppm. Finally, the carbon 5 resonated at 120.44 ppm.

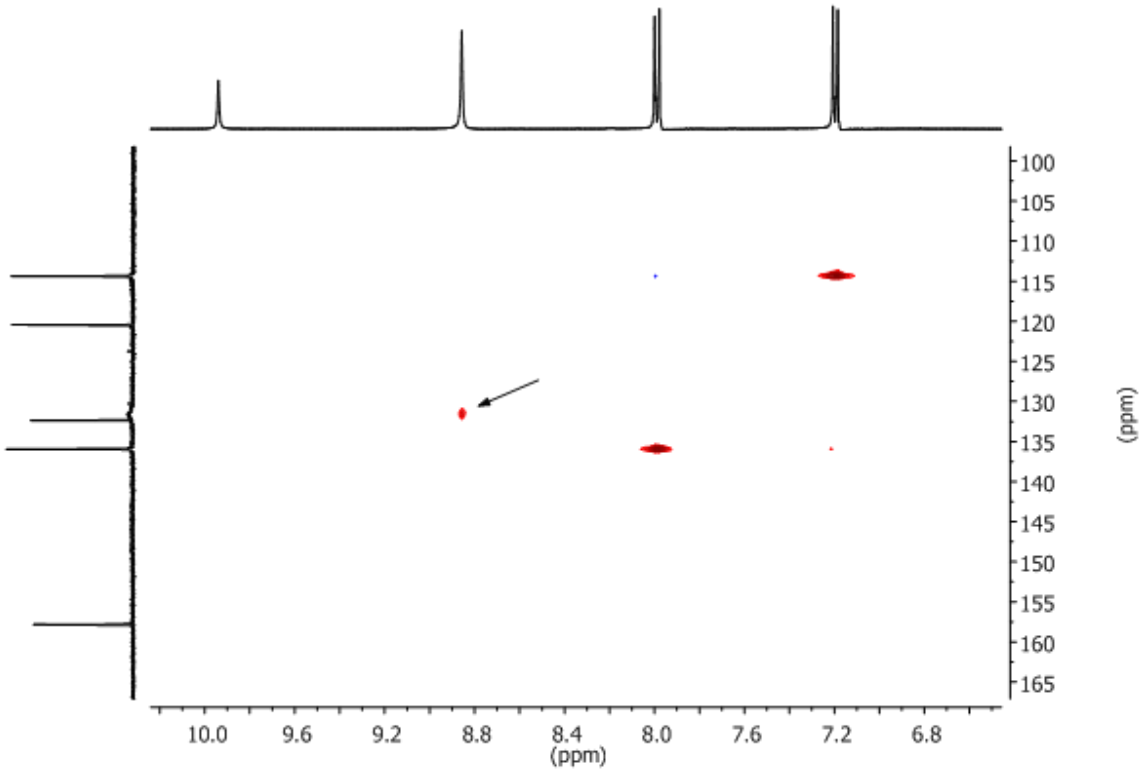

Figure 2-3: HSQC spectrum of free-base porphyrin 2.1

The nitrogens inside the ring of the porphyrin can be deprotonated with strong bases to give the porphyrinato ion, while the two-imine nitrogens can be easily protonated with acids. These dianion species with their central cavities exhibit remarkable ligation characteristic towards metal ions. As a result; metalloporphyrins are readily available upon refluxing metal chloride dihydrates in MeOH/DCM for 3 h,[32,33] as shown in Scheme 2-2, followed by chromatography over silica to give a reddish crystal in the case of T(P-OH)PPNi, and a dark purple crystal in the case of T(P-OH)PPZn, in 92% yield.

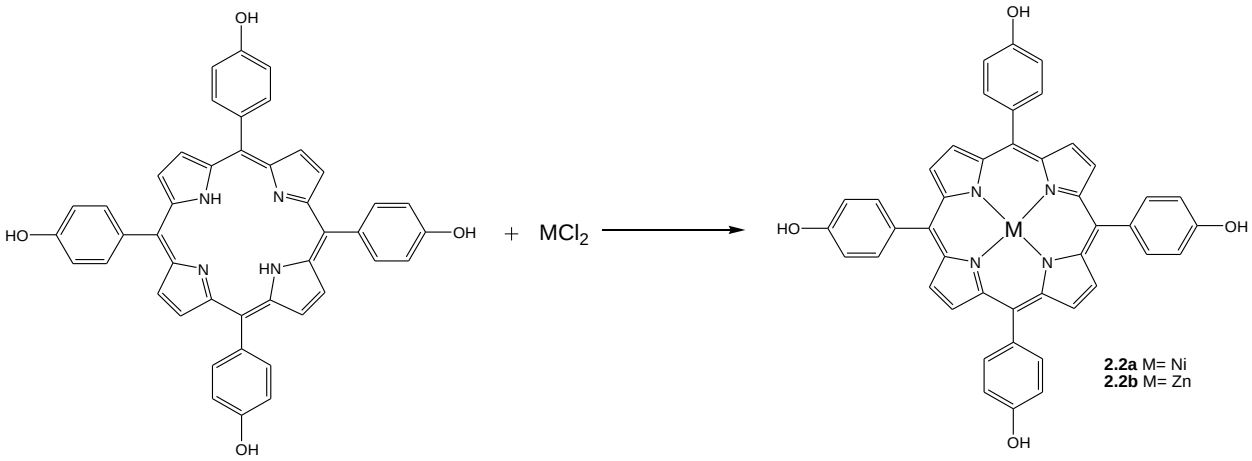

2.1

Scheme 2-2: Synthesis of 5,10,15,20-tetrakis(4-hydroxyphenyl) porphyrin metal complexes

The ^{1}H NMR spectrum of **2.2a** is shown in Figure 2-4. The disappearance of the resonance at -2.87 ppm representing the N-H protons confirms the formation of the nickel complex. Also, all the other resonances are shifted slightly upfield by approximately 0.06 ppm. Due to the high symmetry of T(P-OH)PPNi, the β-proton of pyrrole resonating at 8.75 ppm appeared sharper than the free-base peak located at 8.87 ppm.

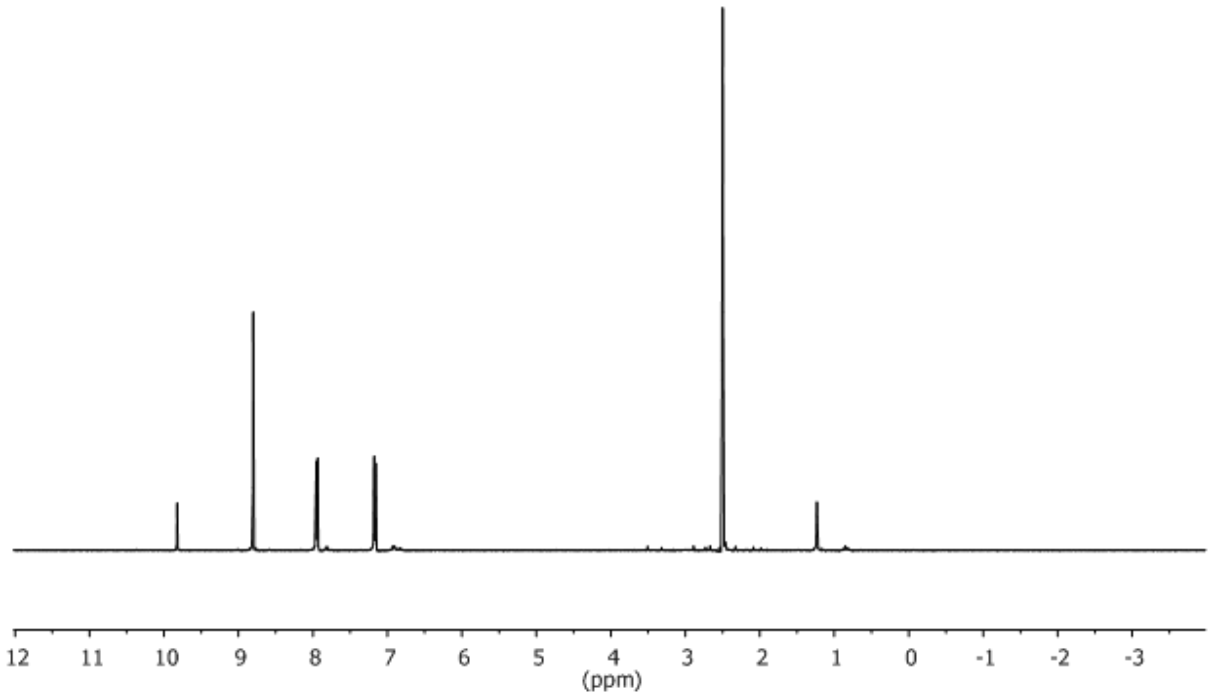

Figure 2-4: 400 MHz ^{1}H NMR spectrum of 2.2a, T(P-OH)PPNi

The ^{13}C NMR spectrum of **2.2a** (Figure 2-5) clearly shows the seven electronically different carbon environments of the metalloporphyrin, including the α-carbon and β-carbon of pyrrole, which completely disappeared in the case of the free-base porphyrin due to the N-H tautomerism. The signal located at 143.01 ppm represents the α-carbon of pyrrole and the resonance at 131.89 ppm results from the β-carbon of pyrrole.

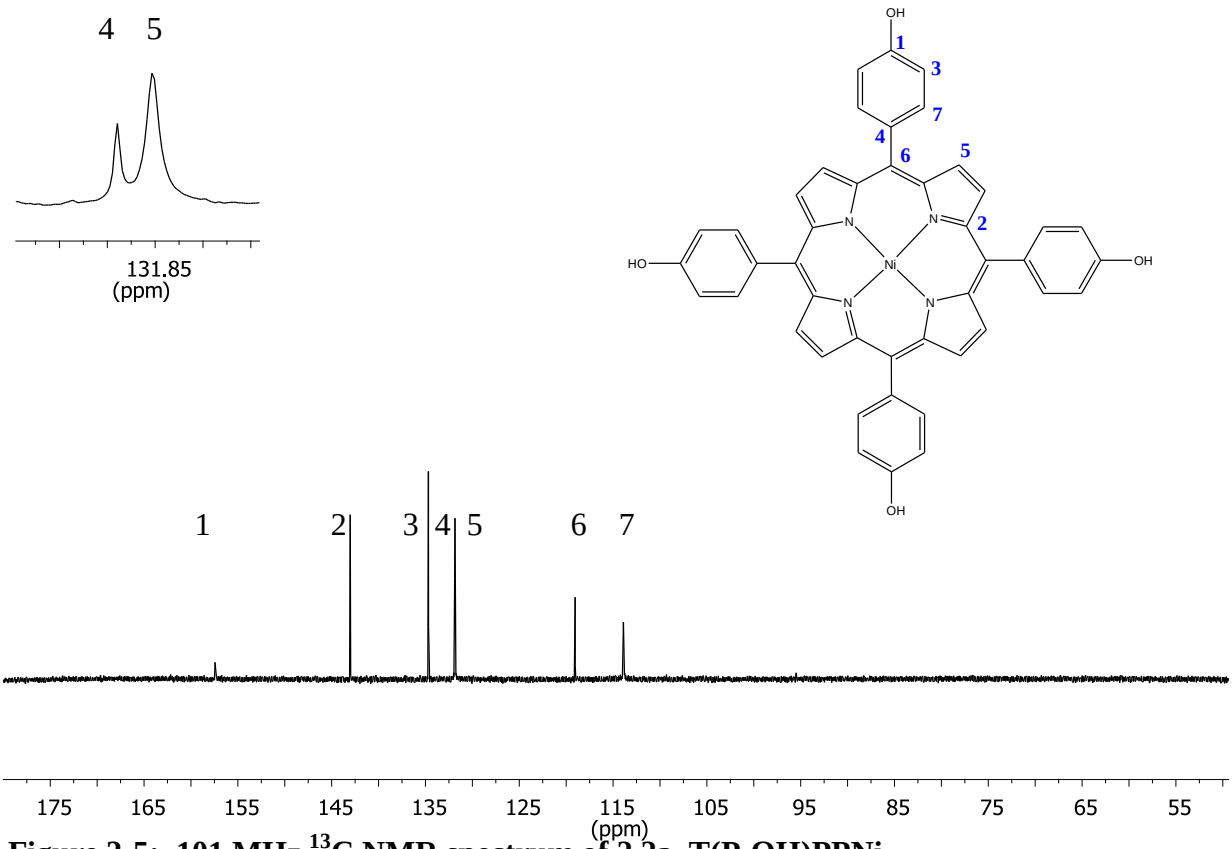

Figure 2-5: 101 MHz ^{13}C NMR spectrum of 2.2a, T(P-OH)PPNi

2.1.1 Absorption spectroscopy of free-base porphyrin 2.1, nickel complex 2.2a, and zinc complex 2.2b

The absorption spectra of free-base **2.1**, nickel porphyrin complex **2.2a**, and zinc porphyrin complex **2.2c** were obtained (Figure 2-6). The Soret band for free-base porphyrin **2.1** was observed at 423 nm and four Q-bands at 519 nm, 557 nm, 598 nm, and 652 nm in DMF. The Soret band of Ni-porphyrin complex **2.2a** was blue-shifted to 418 nm, and the absorbance spectrum shows only one Q-band at 531 nm. The Soret band of Zn-porphyrin complex **2.2b** was red-shifted by ~5 nm and found at 428 nm in DMF, with two Q-bands at 563 nm and 604 nm (Table 2-1).

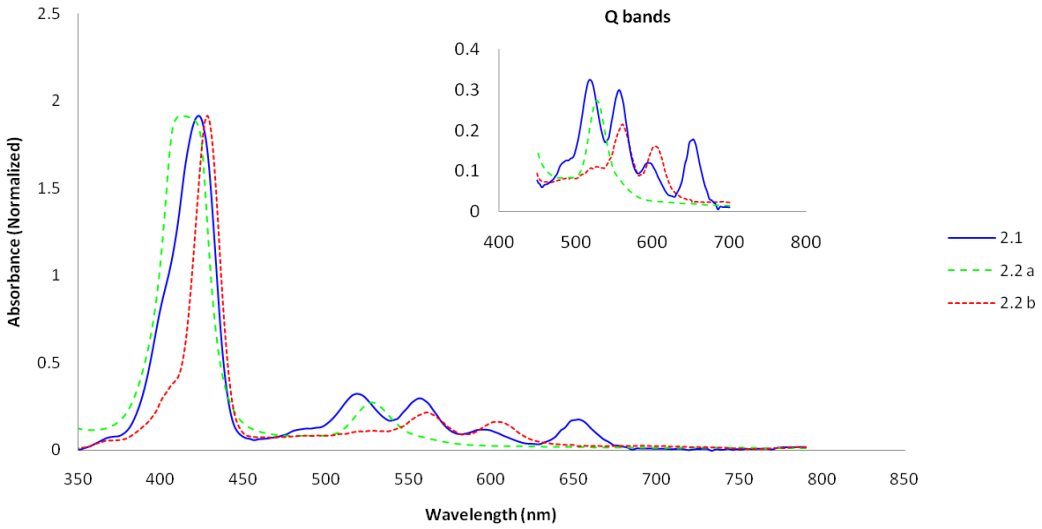

Figure 2-6: Absorption spectra of compounds 2.1, 2.2a, and 2.2b in DMF

Table 2-1: UV-visible data of compounds 2.1, 2.2a, and 2.2b in DMF (1.5×10^{-5} M)

Compounds	Absorption (λ_{max}/nm)				
	Soret band	Q band			
2.1	423	519	557	598	652
2.2 a	418	-	531	-	-
2.2 c	428	-	563	604	-

2.1.2 Fluorescence spectroscopy of free-base porphyrin 2.1 and Zn-porphyrin 2.2b

Fluorescence measurements were performed on both free-base porphyrin **2.1** and zinc porphyrin **2.2b.** The free-base porphyrin was observed to fluoresce at 658 nm and 716 nm, while the analogous zinc porphyrin complex exhibited fluorescence at 613 nm and 716 nm (Table 2-2, Figure 2-7).

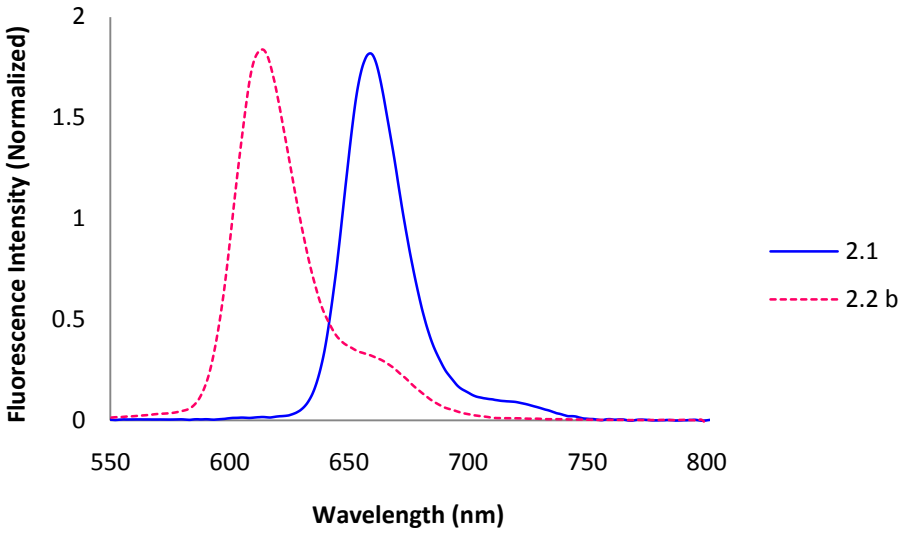

Figure 2-7: Fluorescence spectra of free-base porphyrin 2.1 and Zn-porphyrin 2.2b

Table 2-2: Fluorescence data of compounds 2.1 and 2.2b in DMF (1.5×10^{-5} M)

Compounds	Fluorescence (λ_{em}/nm)	
2.1	658	716
2.2 b	613	660

2.2 Porphyrin dendrimers containing cationic organoiron moieties

η^6-Dichlorobenzene-η^5-cyclopentadienyliron complexes readily undergo nucleophilic aromatic substitution reactions under mild conditions. The incorporation of these types of organoiron complexes into porphyrin frameworks should allow for a versatile method for producing functionalized porphyrins. This section will discuss the synthesis and characterization of porphyrin dendrimers and metalloporphyrins containing organoiron complexes. The preparation of porphyrins and metalloporphyrins based on η^6-dichlorobenzene-η^5-cyclopentadienyliron is interesting as the presence of the terminal chloro groups on the organoiron complex should allow for nucleophilic aromatic substitution reaction

to further functionalize the prepared porphyrin. The presence of the phenolic groups on porphyrin and metalloporphyrin allows for the addition of cationic organoiron groups to the molecule.

2.3 Synthesis of porphyrins and metalloporphyrins containing η^6- monochlorobenzene η^5-cyclopentadienyliron complexes

The η^6-monochlorobenzene-η^5-cyclopentadienyliron complex **1.4** was reacted with free-base porphyrin **2.1** (5,10,15,20-tetrakis(4-hydroxyphenyl) porphyrin) or with metalloporphyrins **2.1a** or **2.1b** in DMF, with an excess amount of potassium carbonate as a base to give porphyrins **2.3a-c** containing four cationic organoiron moieties (Scheme 2-3). This reaction was carried out at room temperature to give deep purple crystals.

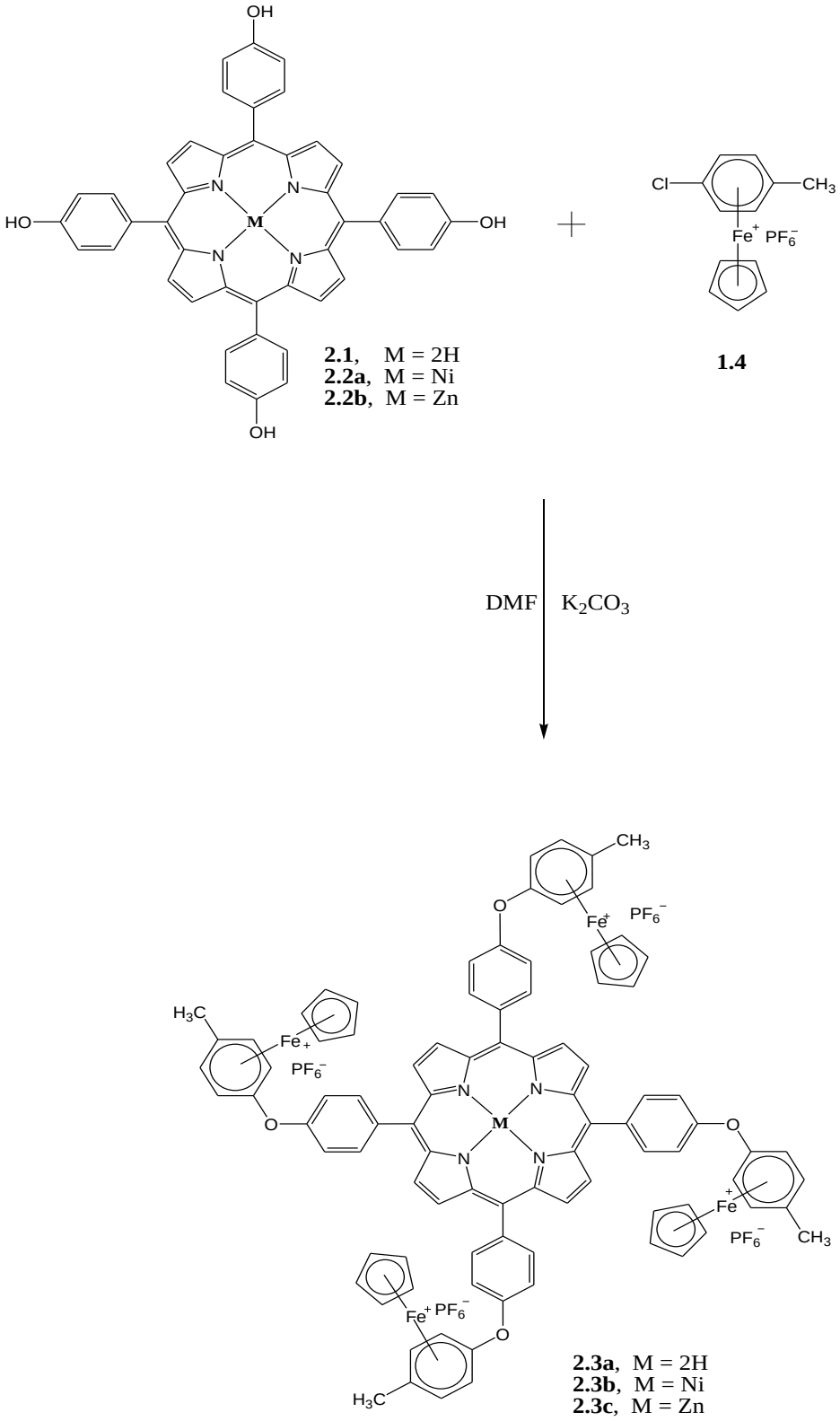

Scheme 2-3: Synthesis of free-base porphyrin and metalloporphyrins 2.3a-c

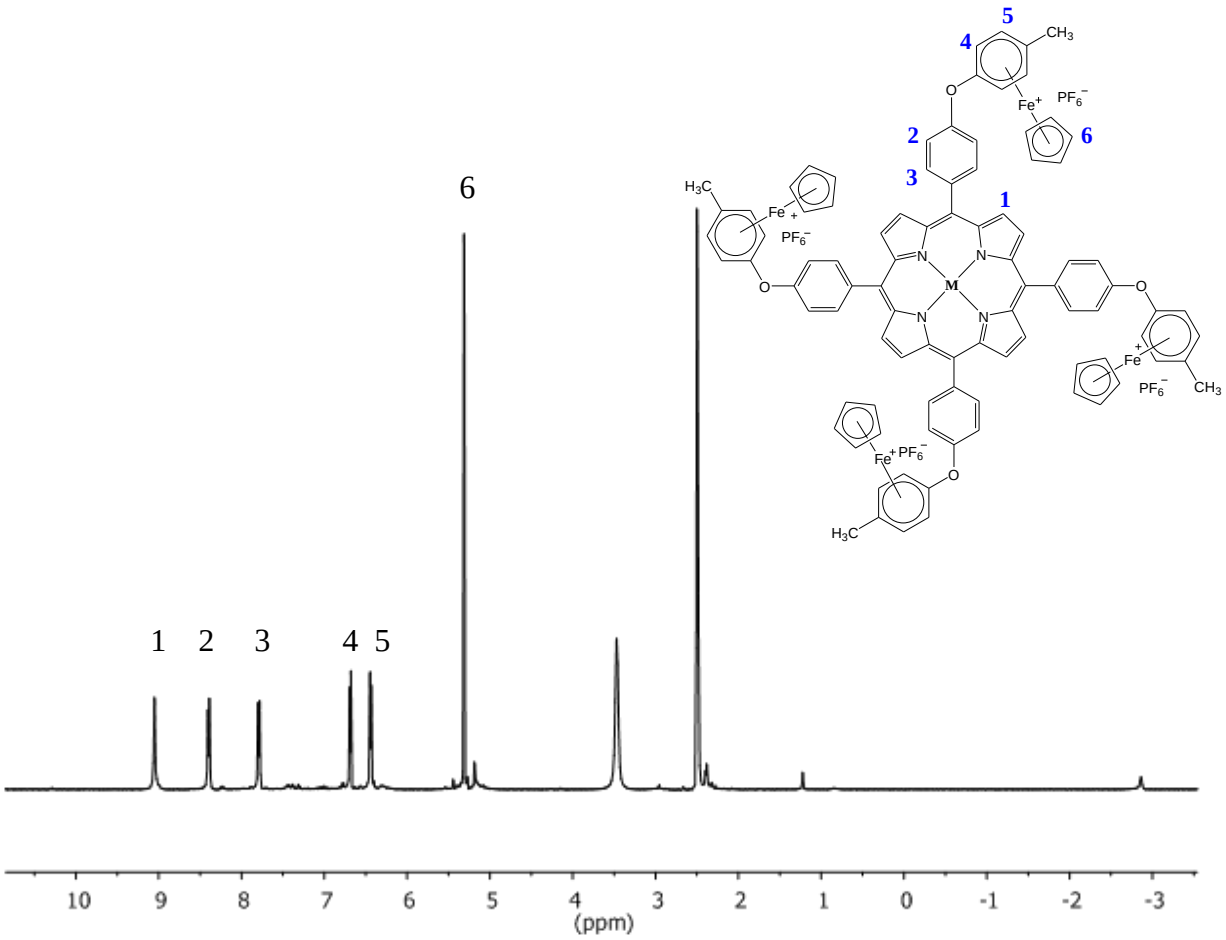

Figure 2-8: 400 MHz ^{1}H NMR spectrum of free-base porphyrin 2.3a

The ^{1}H and ^{13}C NMR spectra of **2.3a** are shown in Figures 2-8 and 2-9. The ^{1}H NMR spectrum shows the successful incorporation of the organoiron unit to the porphyrin core due to the appearance of the Cp peak at 5.46 ppm. All the phenyl and pyrrole protons shifted downfield due to the incorporation of the organoiron complexes. For example, the *ortho*-H-Ph protons shifted from 7.21 ppm to 7.80 ppm as a result of the presence of a more electron-rich environment caused by replacing the chlorine with a phenolic group in the organoiron complex.

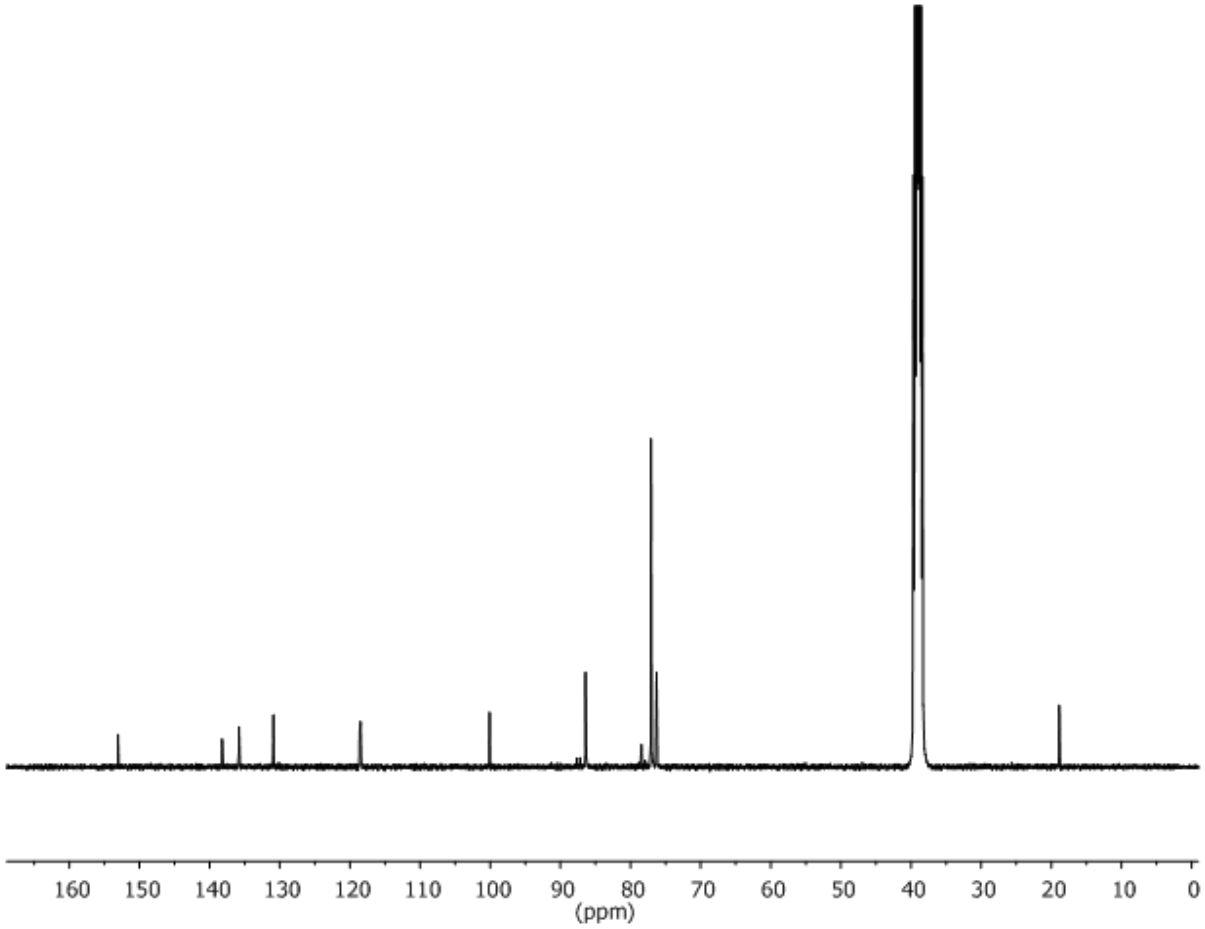

Figure 2-9: 101 MHz ^{13}C NMR spectrum of free-base porphyrin 2.3a

The ^{13}C NMR spectrum (Figure 2-9) clearly showed the incorporation of the organoiron complex. The attached methyl group to the cyclopentadienyliron complex resonated at 19.4 ppm. The resonance at 77.6 ppm was due to the Cp moiety and the complexed aromatics resonated at 76.8 ppm, 78.9 ppm, 86.9 ppm, and 100.6 ppm. The ^{13}C NMR spectrum also confirmed the formation of the ether from the shift in the phenyl *meso*-substituted porphyrin from 113.9 ppm to 119.0 and 120.0 ppm to 131.4 ppm, respectively.

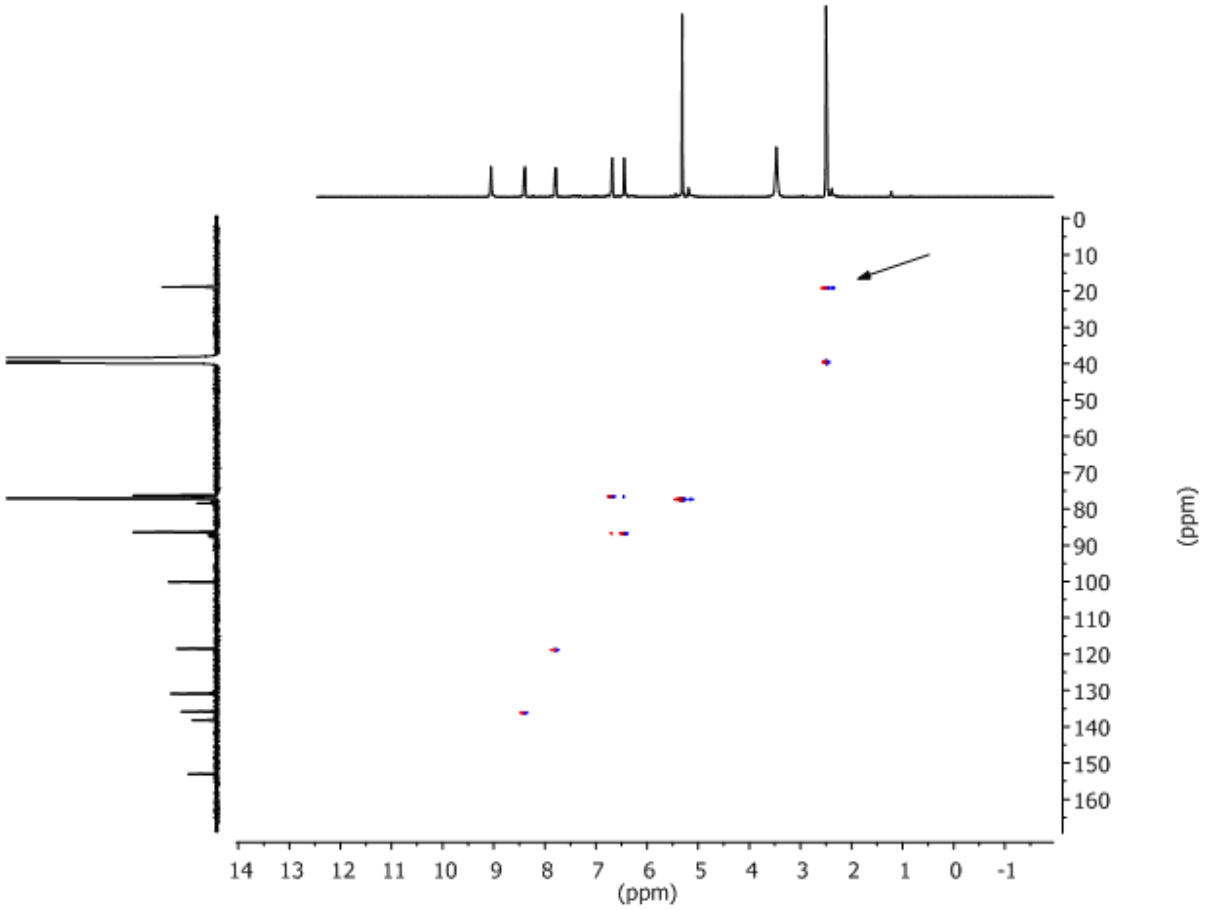

Figure 2-10: HSQC spectrum of porphyrin 2.3a

The HSQC spectrum of **2.3a** (Figure 2-10) further confirms the substitution of the iron complex with the porphyrin. The protons of the methyl group overlap with the DMSO solvent peak at 2.50 ppm, but nonetheless correlate to the methyl carbon at 19.4 ppm. The phenyl carbons resonate at 119.1-138.7 ppm (*ortho*- and *meta*-C-Ph) correlate to protons that resonate at 7.80-8.41 ppm respectively. The Cp protons show a correlation to a carbon which resonate at 77.6 ppm.

2.3.1 Absorption spectroscopy of complexes 2.3a-c

The absorption spectra obtained for free-base porphyrin **2.3a**, Ni-porphyrin complex **2.3b**, and Zn-porphyrin complex **2.3c** (Figure 2-11) were similar to the absorption of porphyrin cores **2.1**, **2.2a**, and **2.2b** (Figure 2-6). However, a new absorbed band at 309 nm was present as a result of the incorporation of the cyclopentadienyliron complex onto the porphyrin core. The Soret band for free base porphyrin **2.3a** was slightly blue-shifted and observed at 419 nm, and four Q bands appeared at 517 nm, 553 nm, 594 nm, and 649 nm in DMF. The absorption spectra of analogous nickel complex **2.3b** showed a blue shift in the Soret band to 415 nm upon incorporation of the iron complex, and showed only one Q band at 528 nm. The Soret band of zinc complex **2.3c** was also slightly blue-shifted by 2 nm and found at 426 nm in DMF, with two Q bands at 560 nm and 601 nm (Table 2-3). The metal ions in the metalloporphyrins behave as Lewis acids and accept lone pairs of electrons from the dianionic porphyrin ligand. Unlike most transition metal complexes, their color is due to absorptions within the porphyrin ligand involving the excitation of electrons from π to π^* porphyrin ring orbitals. The change in the spectrum, fewer peaks in the case of metalloporphyrins, is due to increased symmetry relative to the free-base porphyrin. The two hydrogens on the nitrogen atoms in the free-base porphyrin reduce the ring symmetry from square, in case of metalloporphyrins, to rectangular.

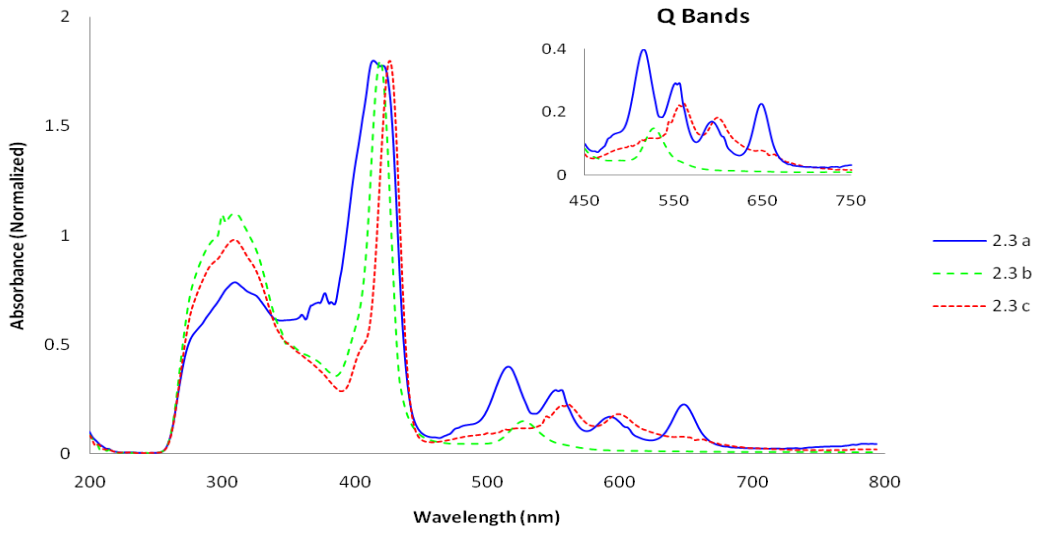

Figure 2-11: Absorption spectra of compounds 2.3a-c in DMF

There is significant metal to ligand π-backbonding via the π* orbital of the porphyrin in the Ni-porphyrin complex, which raises the porphyrin π* orbitals to higher energies, resulting in an increased porphyrin π to π* energy separation, and thus causing the electronic absorptions to undergo a blue shift. In contrast, the Zn-porphyrin complex has metal d-π orbitals that are relatively low in energy, having very little effect on the porphyrin π to π* energy gap in the electronic spectra of the porphyrin. As a result, electronic absorptions undergo red shifts.

Table 2-3: UV-visible data of compounds 2.3a-c in DMF (1.5 x 10^{-5} M)

Compounds	Absorption (λ_{max}/nm)				
	Soret band	Q band			
2.3 a	419	517	553	594	649
2.3 b	415	-	528	-	-
2.3 c	426	-	560	601	-

2.3.2 Fluorescence spectroscopy of free-base 2.3a and Zn-porphyrin complex 2.3c

Fluorescence measurements were performed on both free-base porphyrin **2.3a** and Zn-porphyrin complex **2.3c**. Similar to the absorption spectra, all the fluorescence bands were blue-shifted compared to that of porphyrin cores **2.1** and **2.2b** (Table 2-2, Figure 2-7). For example, free-base porphyrin **2.3a** was observed to fluoresce at 653 nm and 714 nm (Table 2-4, Figure 2-12), while analogous zinc porphyrin **2.3c** exhibited fluorescence at 606 nm and 655 nm (Table 2-4, Figure 2-13). This is most likely due to the incorporation of the iron complex decreasing the electron density in the porphyrin macrocycle, which raises the energy for electron transition, leading to a blue shift in the fluorescence bands.

Table 2-4: Fluorescence data of compounds 2.3a and 2.3c in DMF (1.5 x 10-5 M)

Compounds	Fluorescence (λ_{em}/nm)	
2.3 a	653	714
2.3 c	606	655

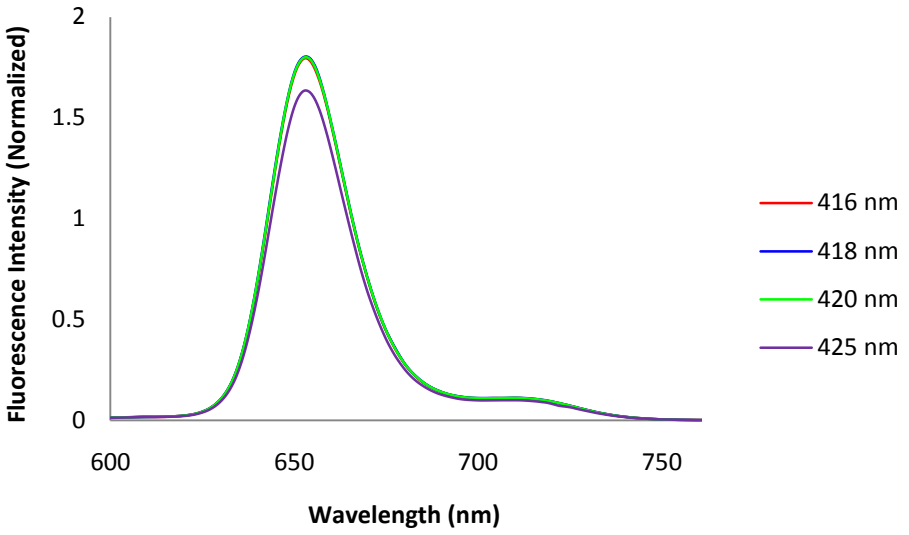

Figure 2-12: Fluorescence spectra of free-base porphyrin 2.3a excited at different wavelengths

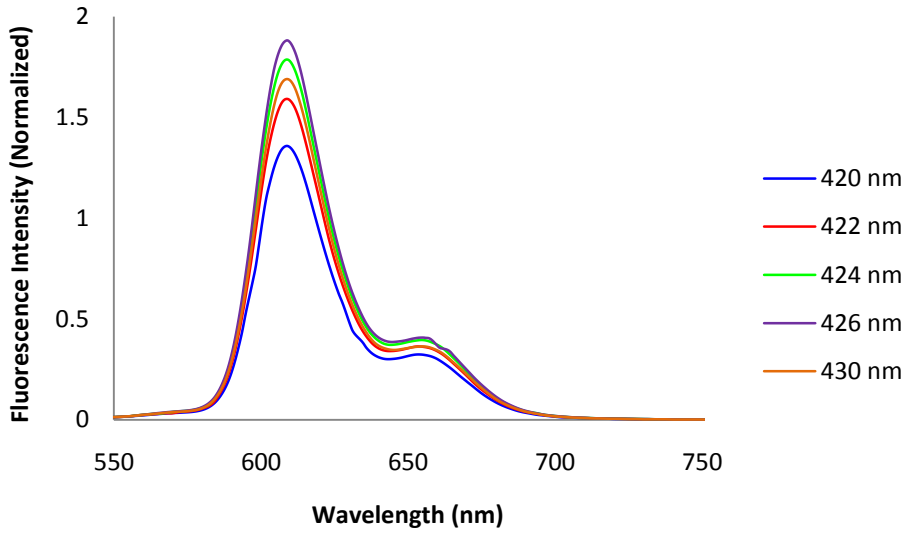

Figure 2-13: Fluorescence spectra of Zn-porphyrin 2.3c excited at different wavelengths

2.4 Syntheses of porphyrins and metalloporphyrins containing η^6-dichlorobenzene-η^5-cyclopentadienyliron complexes

η^6-Dichlorobenzene-η^5-cyclopentadienyliron complex **1.5** was reacted with free-base porphyrin **2.1** or with metalloporphyrins **2.1a** or **2.1b** to give porphyrins **2.4a-c** containing four cationic organoiron moieties (Scheme 2-4). This was the first step in making porphyrin dendrimers containing cationic iron moieties, ferrocene, and naphthalene.

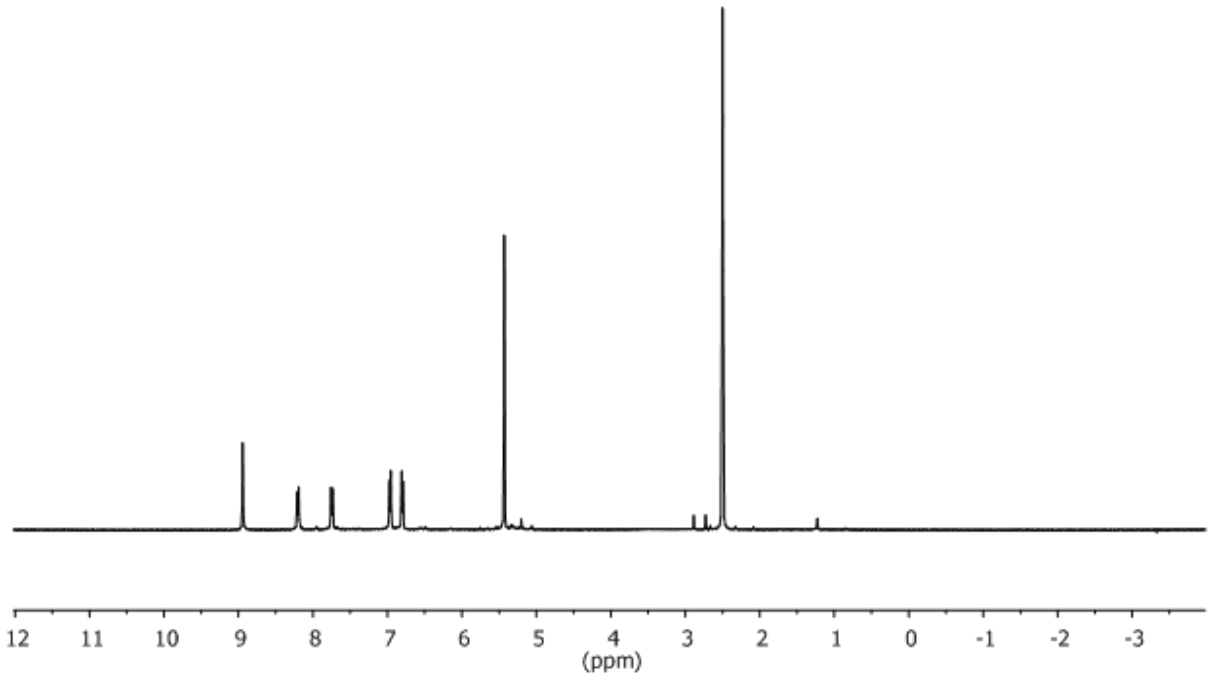

Figure 2-14: 400 MHz ^{1}H NMR spectrum of porphyrin complex 2.4b

The ^{1}H and ^{13}C NMR spectra of **2.4b** are shown in Figures 2-14 and 2-15, respectively. The appearance of the resonance at 5.37 ppm due to the cyclopentadienyliron moiety confirms the formation of porphyrin **2.4b**. Also, the four arene protons resonated at two different

positions, 6.96 ppm and 6.80 ppm, due to the attachment of the organoiron unit to the metalloporphyrin. All the phenyl and pyrrole protons shifted downfield due the incorporation of organoiron complexes. For example, the *ortho*-H-Ph shifted from 7.21 ppm to 7.75 ppm because of the replacement of the chlorine with a phenolic group.

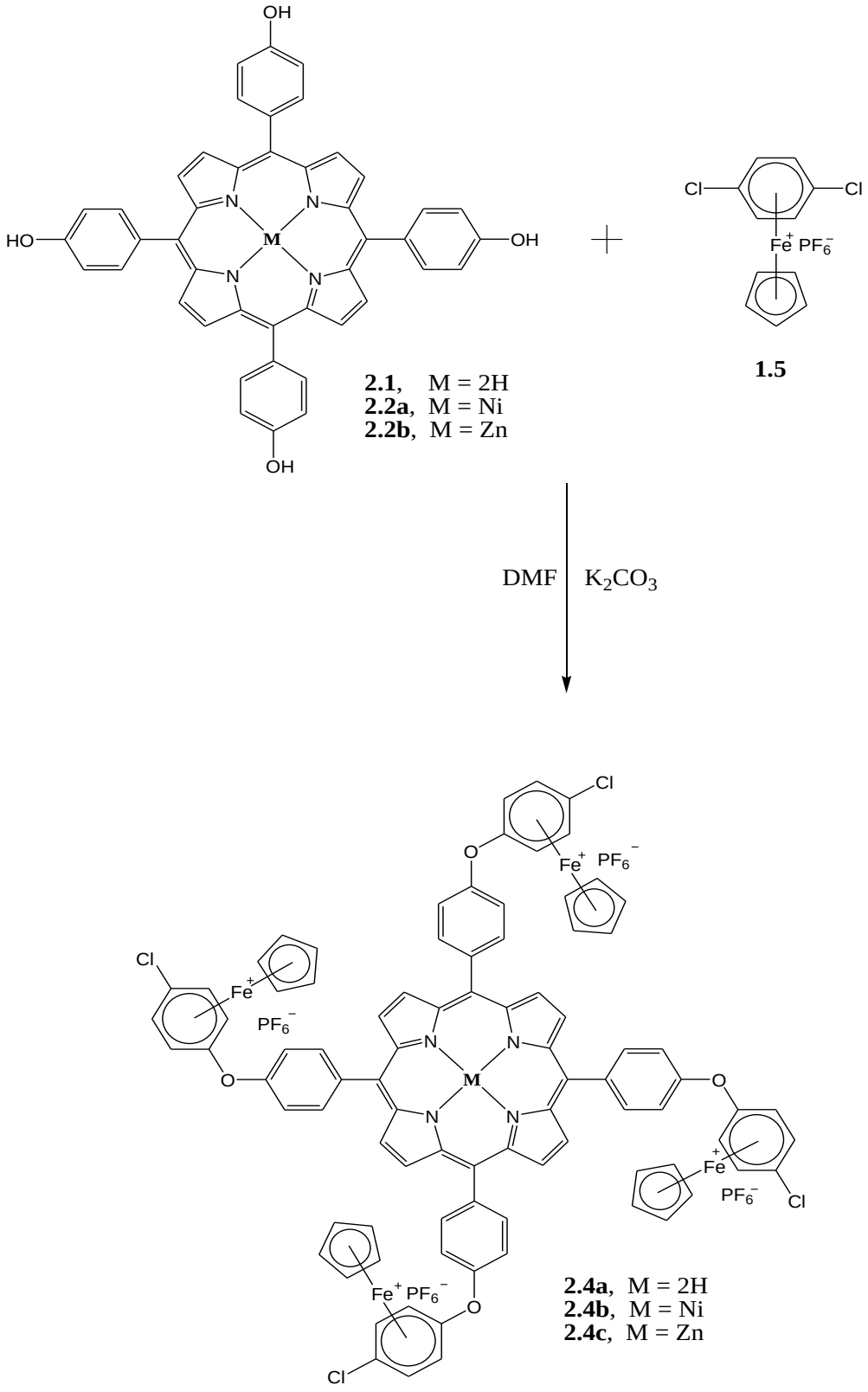

Scheme 2-4: Synthesis of free-base porphyrin 2.4a and metalloporphyrins 2.4b and 2.4c

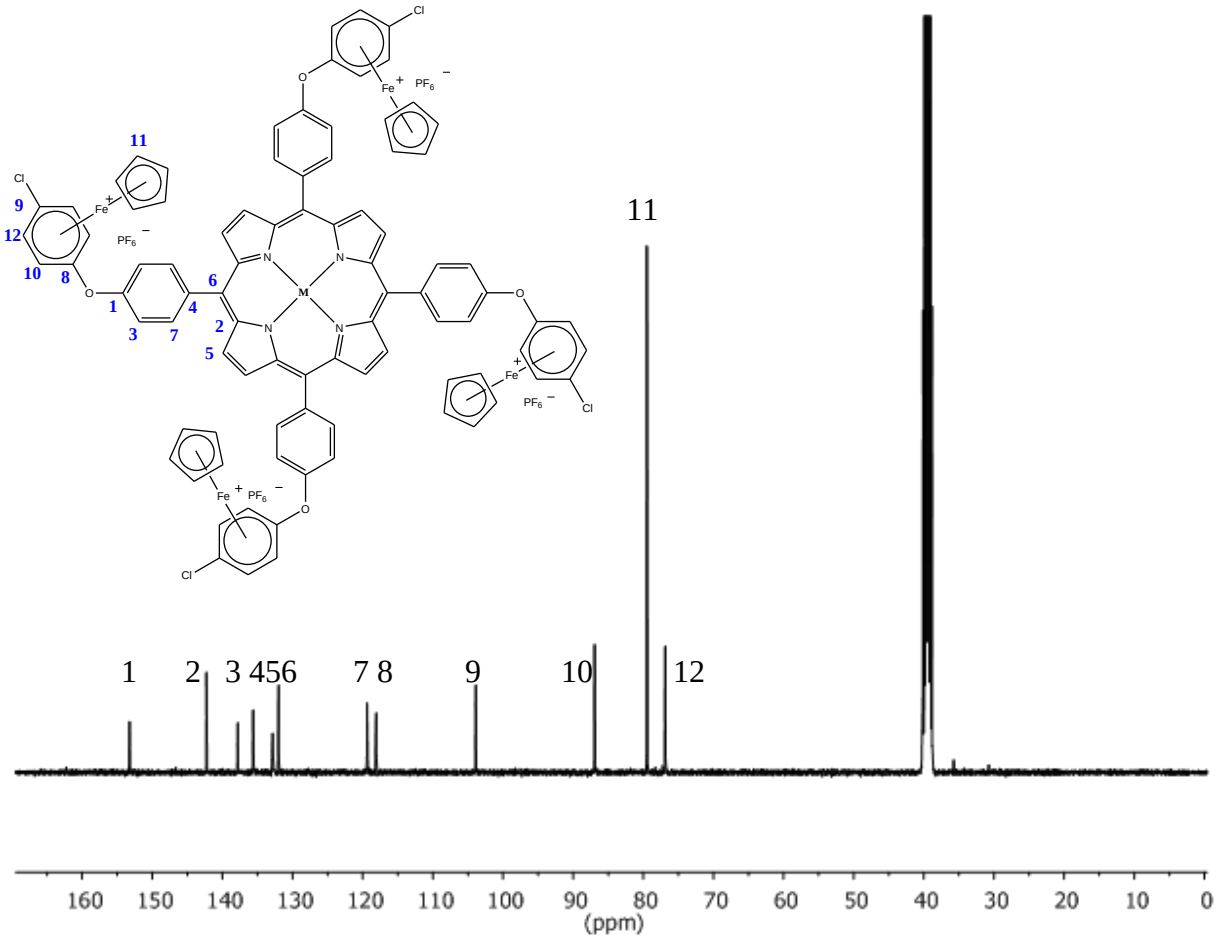

Figure 2-15: 101 MHz ^{13}C NMR spectrum of metalloporphyrin 2.4b

The incorporation of the organoiron complex to metalloporphyrin **2.2a** was confirmed by a ^{13}C NMR spectrum (Figure 2-15). The signal at 79.5 ppm was due to the Cp moiety, while the protons of the phenyl *meso*-substituted porphyrin shifted downfield from 115.4 ppm and 121.3 ppm to resonate at 119.4 ppm and 132.0 ppm, respectively.

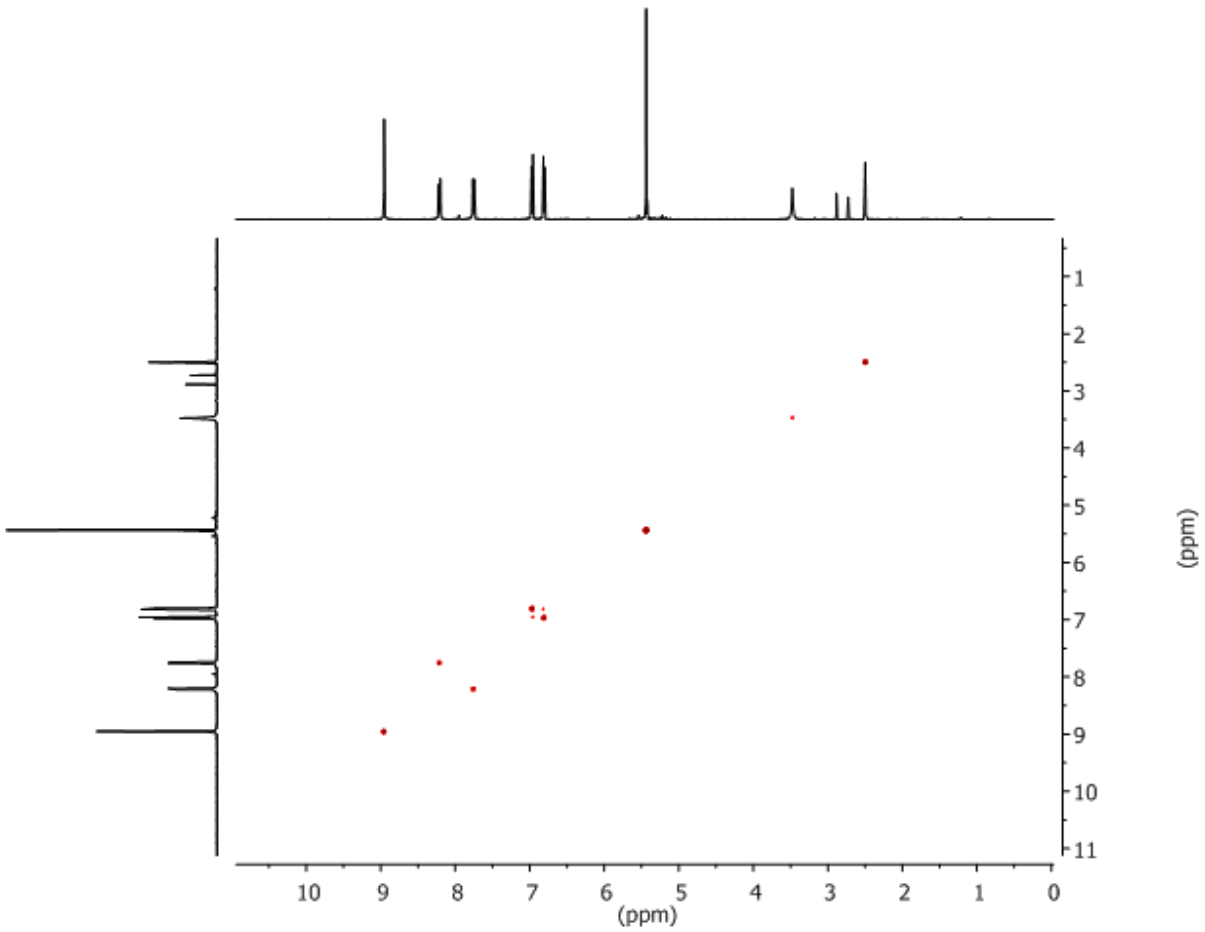

Figure 2-16: COSY spectrum of metalloporphyrin 2.4b

The COSY and HSQC of metalloporphyrin complex **2.4b** are shown in Figures 2-16 an 2-17, respectively. There is a clear correlation between protons of the arene complex with a *J*-coupling value of 6.8 Hz. Also, there is a coupling of phenyl protons with a *J* value of 8.4 Hz.

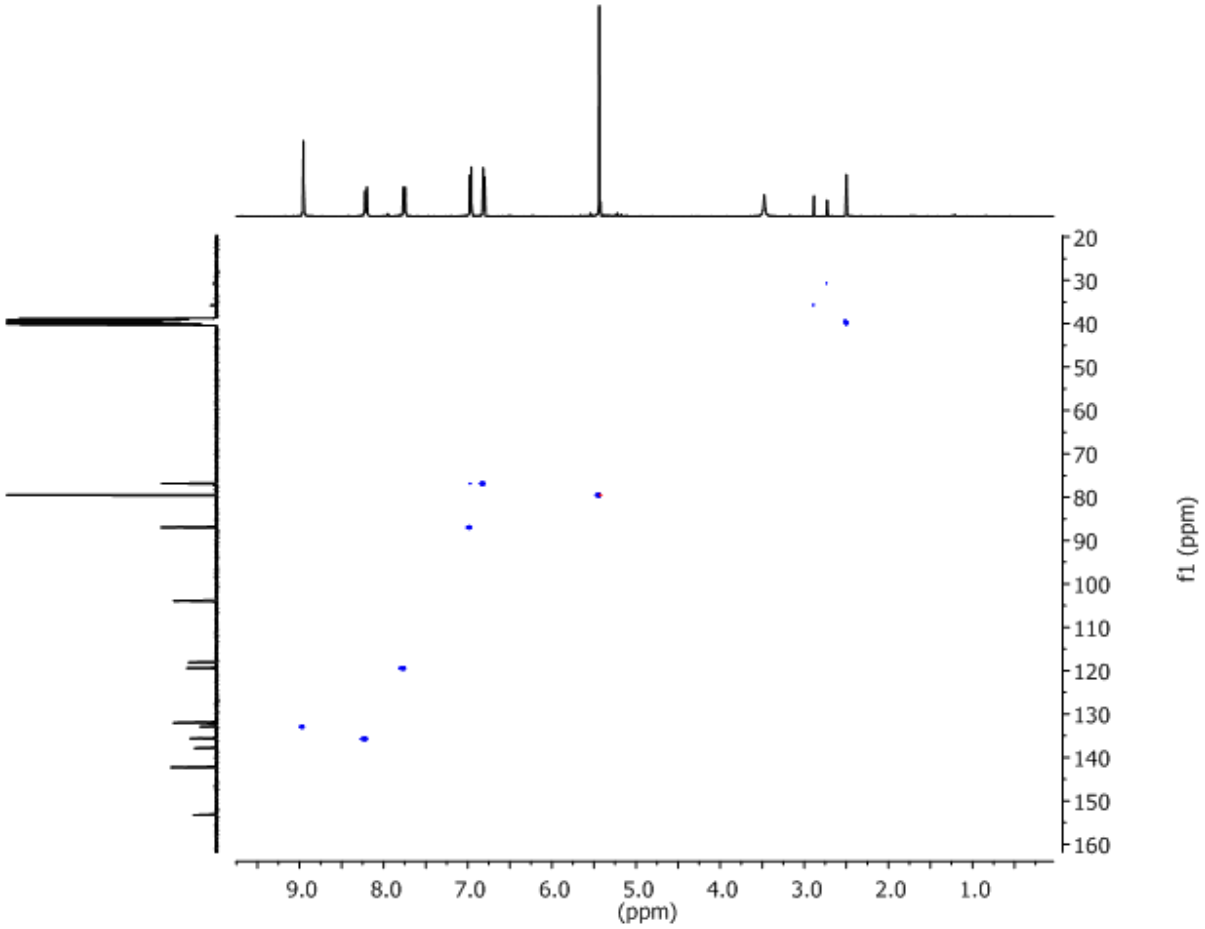

Figure 2-17: HSQC spectrum of metalloporphyrin 2.4b

2.4.1 Absorption spectroscopy of compounds 2.4a-c

The incorporation of dichlorobenzene-cyclopentadienyliron complex **1.5** into the porphyrin core, indicative of the absorption band at 268 nm, led to free-base porphyrin **2.4a** and porphyrin dendrimers containing nickel (**2.4b**) and zinc (**2.4c**) with similar absorption spectra to similar complexes **2.1**, **2.2a**, and **2.2b**. However, all the absorption bands are slightly blue shifted. For example, the Soret band for free-base porphyrin **2.4a** shifted slightly to 417 nm, along with four Q bands at 515 nm, 550 nm, 592 nm, and 647 nm in DMF. As expected, the absorption spectra of the analogous nickel complex **2.4b** showed the Soret band also blue-shifted to 414 nm after incorporate of the iron complex, with only one Q band at 526

nm. The Soret band of the zinc complex **2.4c** was slightly blue-shifted as well by ~3 nm to 425 nm in DMF with two Q bands at 557 nm and 598 nm (Table 2-5, Figure 2-18). The introduction of electron withdrawing groups (complex **1.4** or **1.5**) to the *para*-phenyl positions has been shown to lower the energy of the *b1* orbital by decreasing the amount of electron density in this orbital, leading to an increase in the energy of transition and hence blue shifted bands.

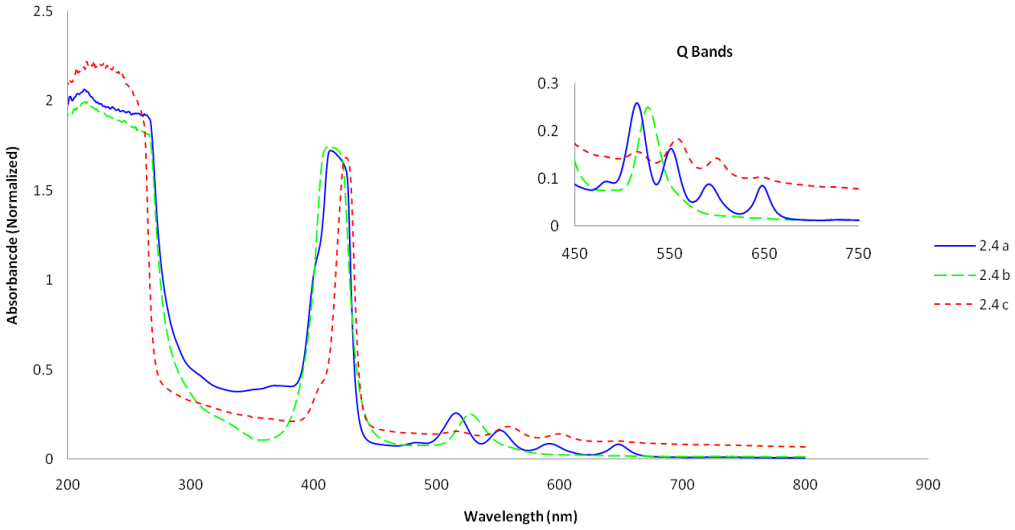

Figure 2-18: Absorption spectra of compounds 2.4a-c in DMF

Table 2-5: UV-visible data of compounds 2.4a-c in DMF (1.5 x 10^{-5} M)

Compounds	Absorption (Λmax/nm)				
	Soret band	Q band			
2.4 a	417	515	550	592	647
2.4 b	414	-	526	-	-
2.4 c	425	-	557	598	-

2.4.2 Fluorescence spectroscopy of free-base porphyrin 2.4a and Zn-porphyrin 2.4c

The fluorescence measurements of free-base porphyrin **2.4a** and Zn-porphyrin complex **2.4c** were performed. Like the absorption spectra, there was little change in the energies of the fluorescence bands observed for free-base dendrimer **2.4a.** Free-base dendrimer **2.4a** was observed to fluoresce at 651 nm and 711 nm (Table 2-6, Figure 2-19). These bands were blue-shifted compared to porphyrin core **2.1** (658 nm and 716 nm). The fluorescence spectrum of zinc porphyrin dendrimer **2.4c** (Table 2-6, Figure 2-20) was also blue-shifted by ~8 nm relative to the fluorescence spectra observed for zinc porphyrin core **2.2b** (613 nm and 660 nm).

Table 2-6: Fluorescence data of compounds 2.4a and 2.4c in DMF (1.5×10^{-5} M)

Compounds	**Fluorescence (λ_{em}/nm)**	
2.4 a	651	711
2.4 c	604	652

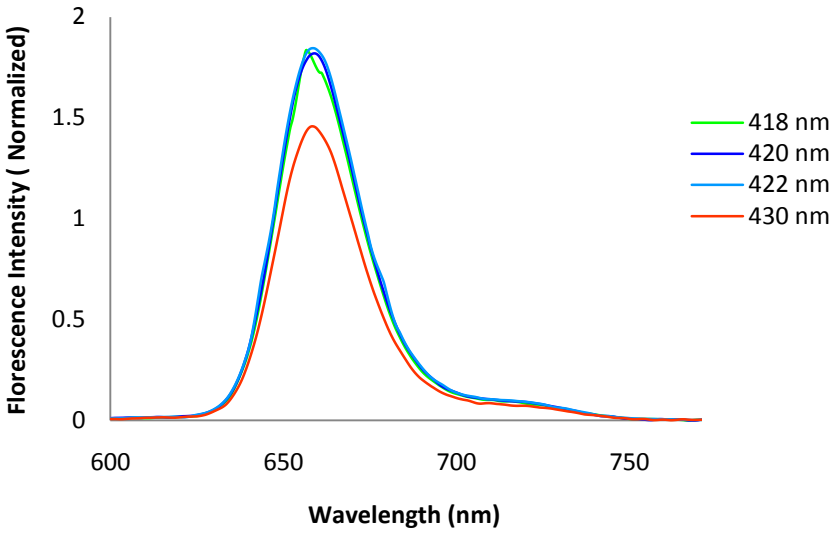

Figure 2-19: Fluorescence spectra of free-base porphyrin 2.4a excited at different wavelengths

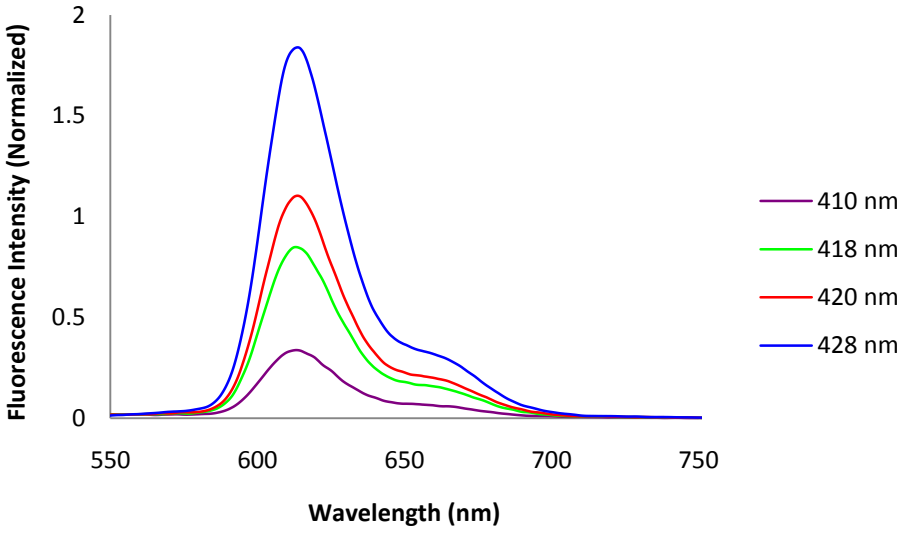

Figure 2-20: Fluorescence spectra of Zn-porphyrin 2.4c excited at different wavelengths

2.5 Synthesis of porphyrins and metalloporphyrins containing naphthalene

The presence of the cyclopentadienyliron moiety on the complexed arene allowed the chlorine group to readily undergo further nucleophilic aromatic substitution reactions in relatively mild conditions. The incorporation of naphthalene into a free-base porphyrin and metalloporphyrin can allow for wide potential applications in different fields such as organic light-emitting diodes (OLEDs), light harvesting, or switches. This section will describe the synthesis and characterization of free-base porphyrins and metalloporphyrins containing naphthalene.

Chloro-terminated free-base porphyrin **2.4a** and metalloporphyrin complexes **2.4b** and **2.4c** were reacted with 2-hydroxynaphthalene (**2.5**) in DMF in the presence of a weak base like potassium carbonate to give porphyrin dendrimers **2.6a-c** containing four cationic organoiron moieties (Scheme 2-5).

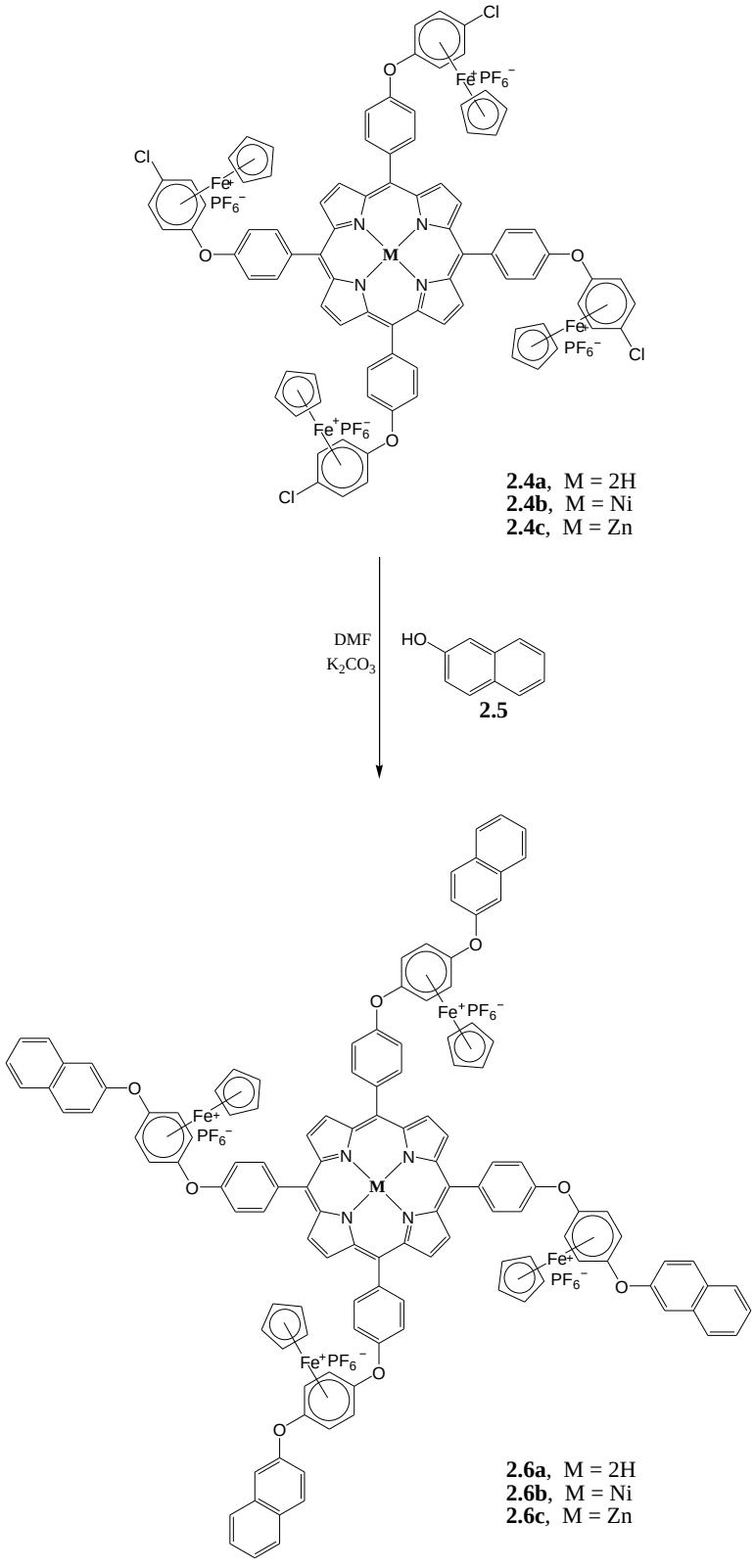

Scheme 2-5: Synthesis of free-base porphyrin 2.6a and metalloporphyrin dendrimers 2.6b and 2.6c

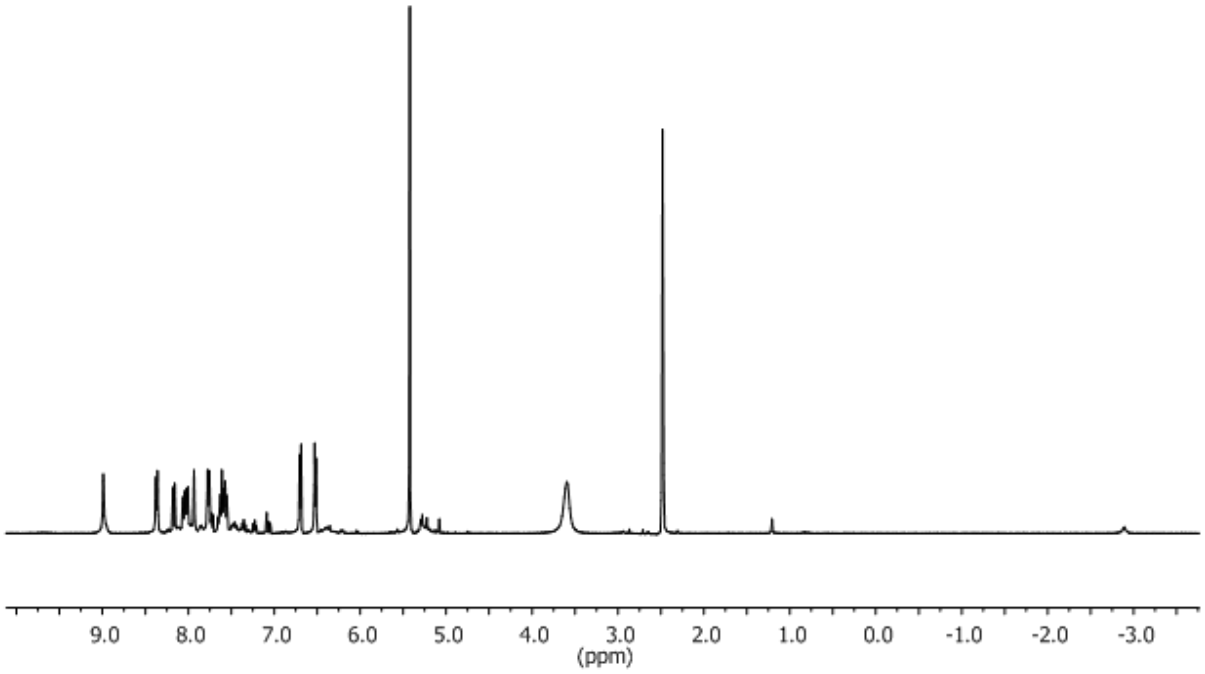

Figure 2-21: 400 MHz ^{1}H NMR spectrum of porphyrin dendrimer 2.6a

The ^{1}H NMR spectrum of **2.6a** is shown in Figure 2-21. The disappearance of the resonance at 10.02 ppm representing the phenolic hydroxyl proton confirms the formation of dendrimer **2.6a**. Also, the four arene protons shifted further upfield, from 7.00 ppm and 6.86 ppm in previous porphyrin **2.4a** to 6.72 ppm and 6.54 ppm in dendrimer **2.6a**, which confirmed the full substitution of the terminal chloro group.

The relatively weak coordination bonds between the cyclopentadienyliron and the arene ring in the cationic organoiron groups can be easily cleaved using UV light (300 nm) in a strongly coordinating solvent such as acetonitrile. Solutions of dendrimers **2.6a-c** in CH_3CN were exposed to 300 nm light for two hours to give dendrimers **2.7a-c** (Scheme 2-6). After cleavage of the cationic cyclopentadienyliron moieties, the solubility of the dendrimers in non-polar organic solvents drastically increased.

As seen in the ^{1}H NMR spectrum of dendrimer **2.7a** (Figure 2-22), the resonance at 5.44 ppm from the cationic cyclopentadienyliron moiety is completely removed, and the resonances due to the complexed aromatics have dramatically shifted from 6.54 ppm and 6.72 ppm to overlap with the resonances of the other aromatic environments.

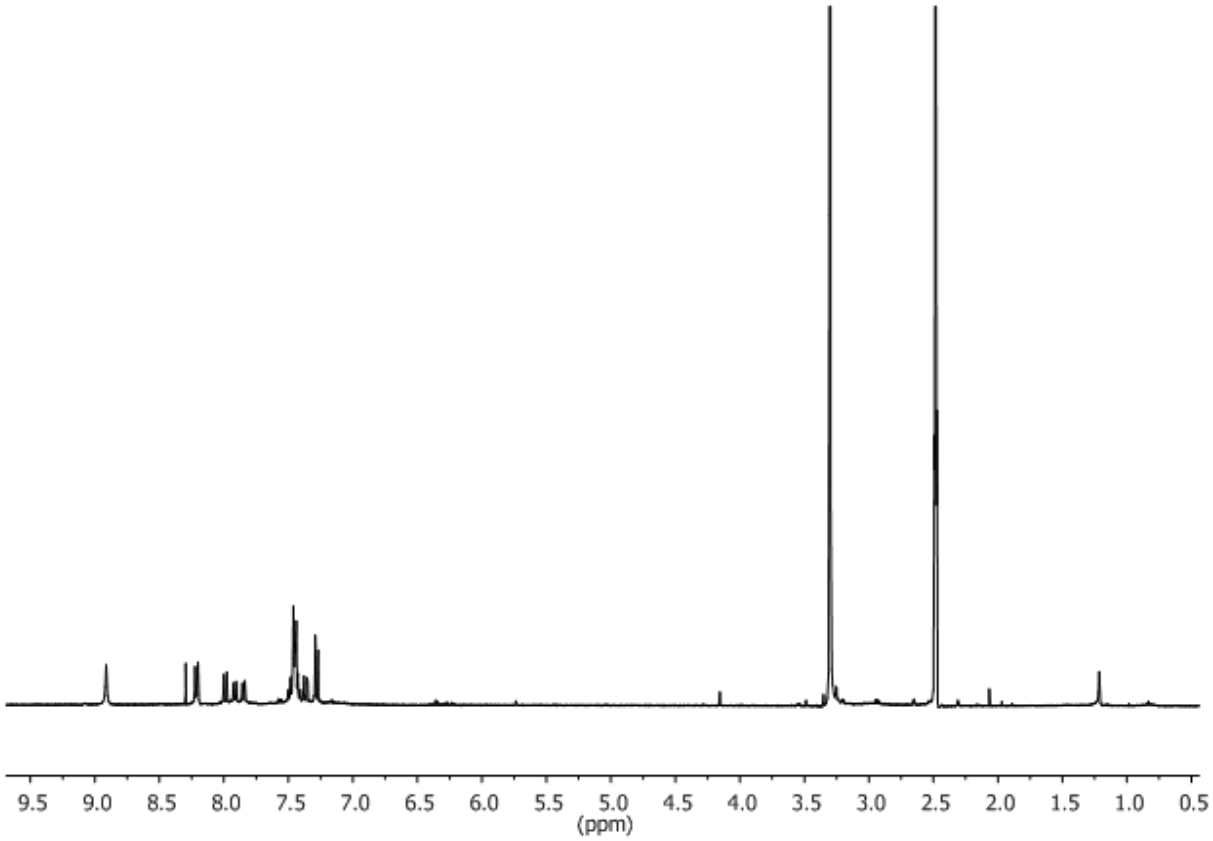

Figure 2-22: 400 MHz ^{1}H NMR spectrum of porphyrin dendrimer 2.7a

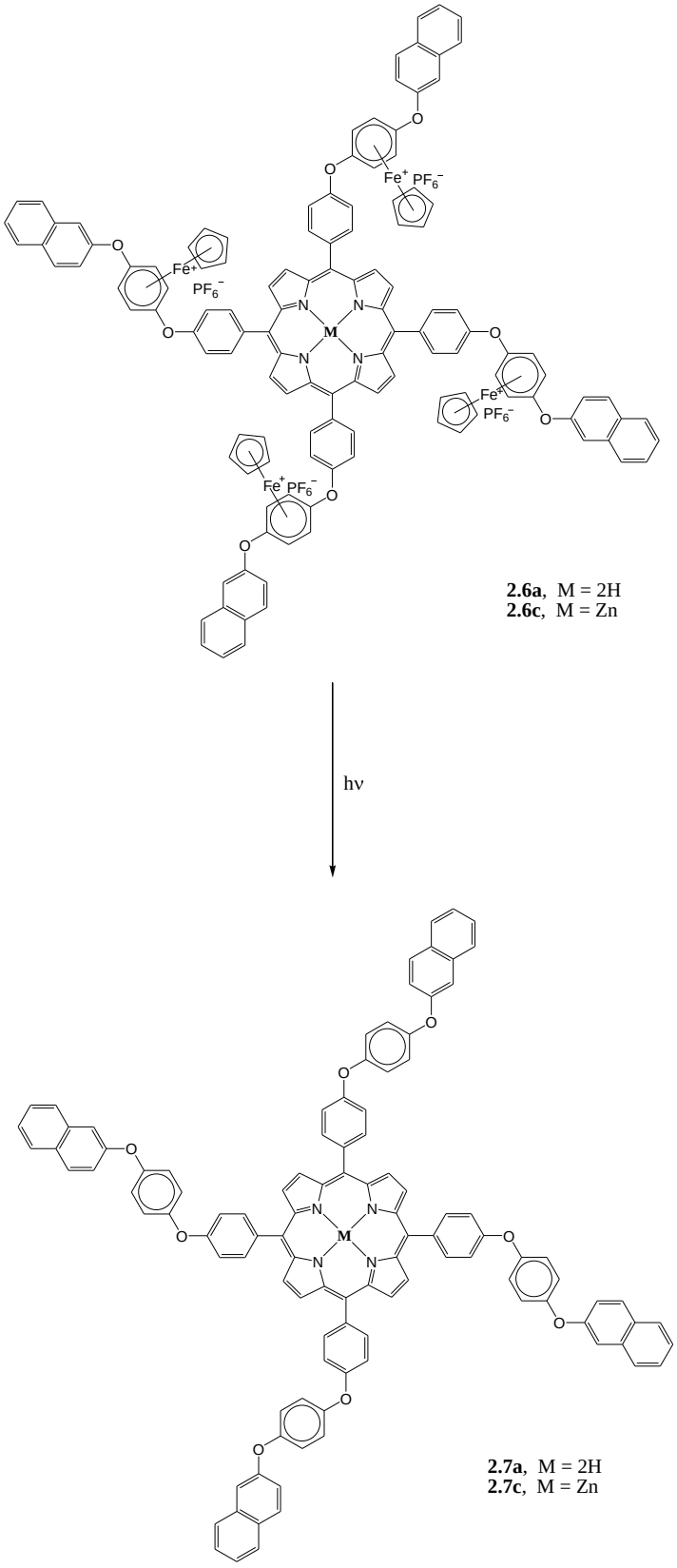

Scheme 2-6: Synthesis of free-base porphyrin 2.7a and metalloporphyrins 2.7c

2.5.1 Absorption spectroscopy of complexes 2.7a and 2.7c

The incorporation of naphthalene (**2.5**) into porphyrin complexes **2.4a** and **2.4c** led to free-base porphyrin **2.6a** and Zn-porphyrin dendrimer **2.6c**, which underwent photolysis to cleave the cyclopentadienyliron moiety and produce free-base porphyrin dendrimer **2.7a** and Zn-porphyrin dendrimer **2.7c**, both with similar absorption spectra to those of **2.4a** and **2.4c**, respectively (Figure 2-18).

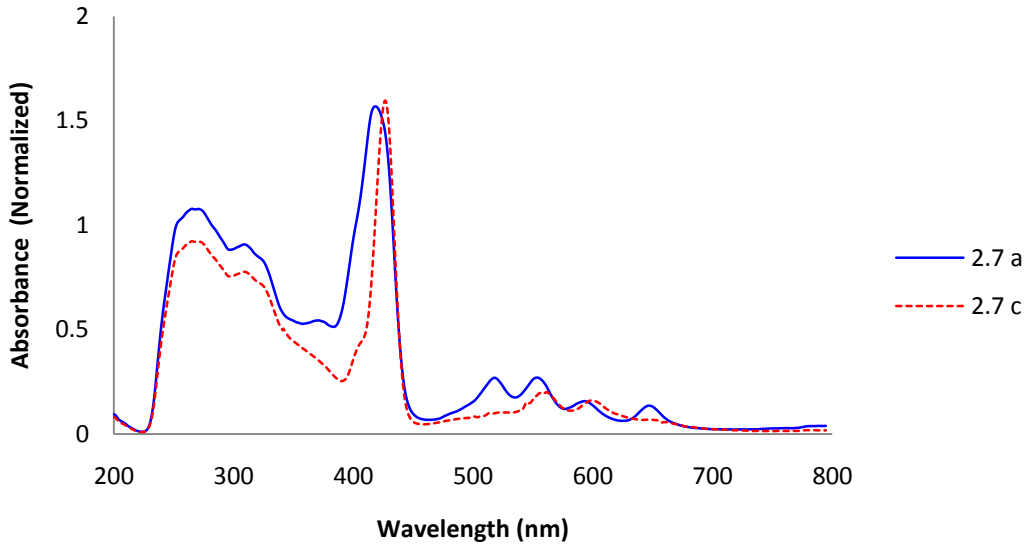

Figure 2-23: Absorption spectra of compounds 2.7a and 2.7c in DMF

Table 2-7: UV-visible data of compounds 2.7a and 2.7c in DMF (1.5 x 10^{-5} M)

Compounds	Absorption (λ_{max}/nm)				
	Soret band	Q band			
2.7 a	418	517	551	592	645
2.7 c	426	-	558	597	-

2.5.2 Fluorescence spectroscopy of free-base porphyrin 2.7a and Zn-porphyrin 2.7c

The presence of naphthalene moieties in free-base dendrimer **2.7a** and zinc porphyrin dendrimer **2.7c** has very little impact on the fluorescence spectroscopy, compared to the spectra of **2.4a** and **2.4c**. Similar to the absorption spectra, the change in the energies of the fluorescence bands was observed for free-base dendrimer **2.7a.** The free-base dendrimer fluoresced at 652 nm and 713 nm (Table 2-8, Figure 2-24). These bands are slightly red-shifted comparing to **2.4a** (651 nm and 711 nm). Surprisingly, the fluorescence spectrum of zinc porphyrin dendrimer **2.7c** did not show any shift relative to the fluorescence spectra observed for zinc porphyrin **2.4c** (Table 2-6, Figure 2-20).

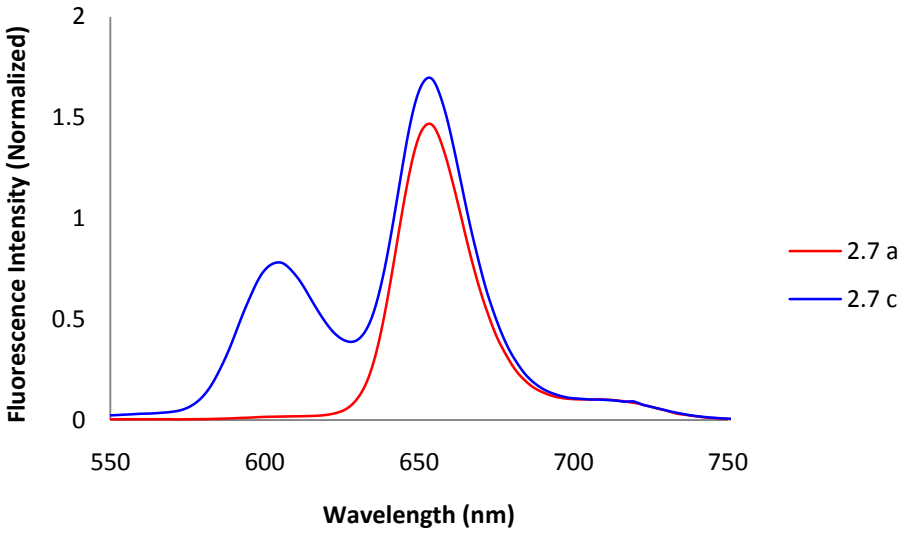

Figure 2-24: Fluorescence spectra of free-base porphyrin 2.7a and zinc porphyrin dendrimer 2.7c

Table 2-8: Fluorescence data for dendrimers 2.7a and 2.7c.in DMF (1.5 x 10^{-5} M)

Compounds	Fluorescence (λ_{em}/nm)	
2.7a	652	713
2.7 c	604	651

2.6 Synthesis of free-base porphyrin and metalloporphyrin dendrimers containing neutral and cationic organoiron species

The reaction of the previously prepared free-base porphyrin and metalloporphyrin dendrimers **2.4a-c** with 4-hydroxybenzyl alcohol (**2.8**) in the presence of a weak base gave dendrimers that possess terminal primary aliphatic alcohols (Scheme 2-7).

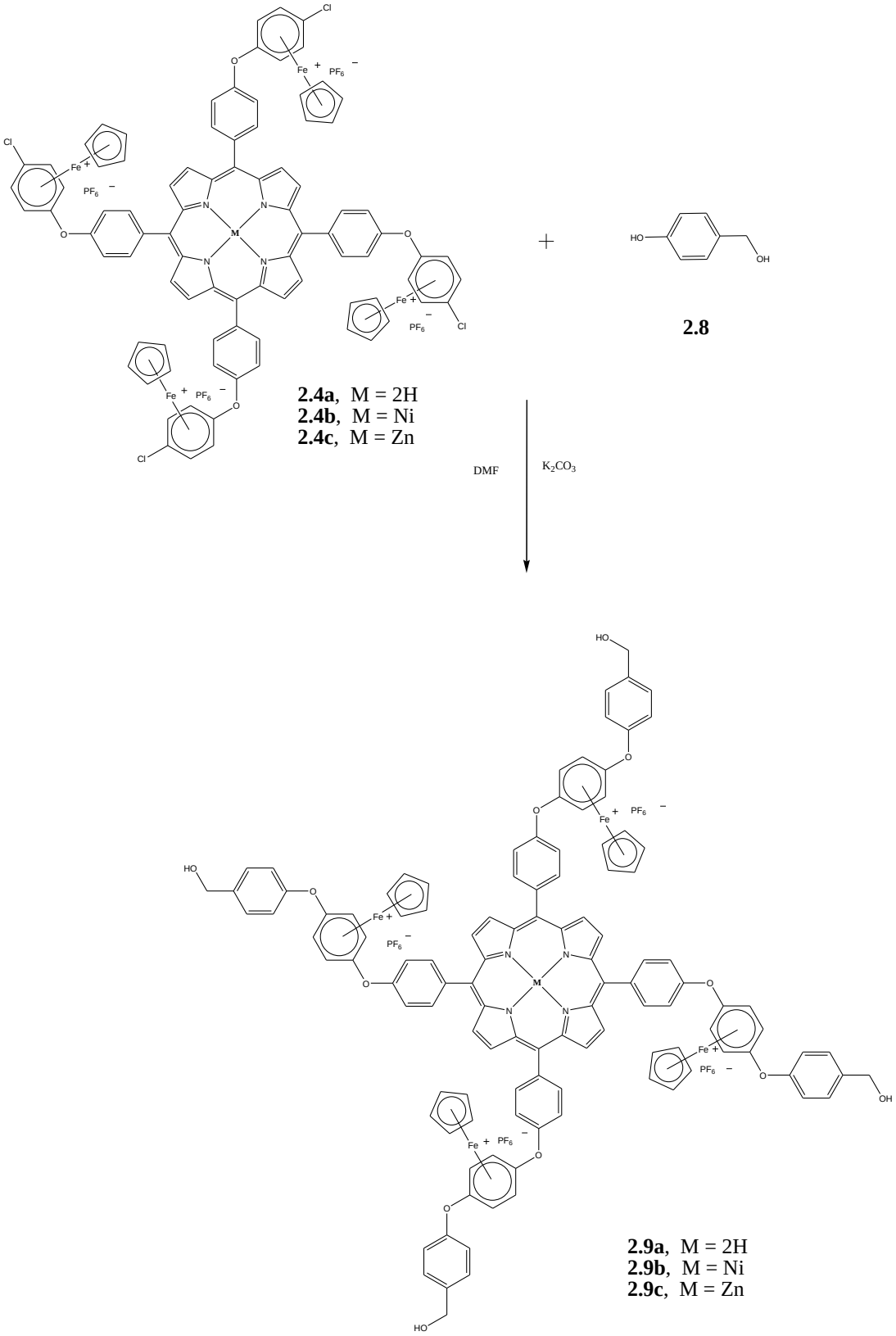

Scheme 2-7: Synthesis of tetrahydroxy-functionalized free-base porphyrin and metalloporphyrin dendrimers 2.9a-c

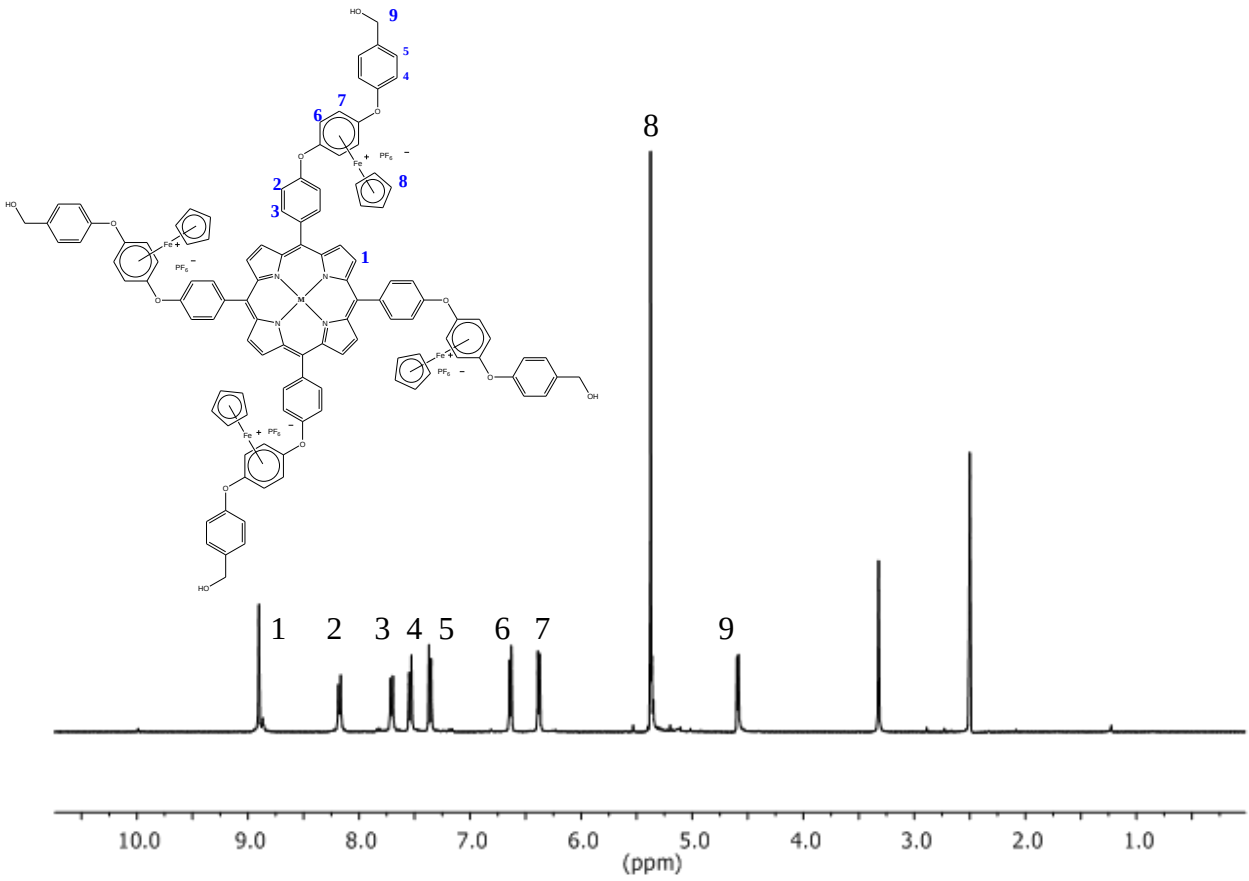

Figure 2-25: 400 MHz ^{1}H NMR spectrum of metalloporphyrin dendrimer 2.9b

The ^{1}H NMR spectrum clearly shows the incorporation of the 4-hydroxybenzyl alcohol due to the presence of a doublet at 4.59 ppm. This doublet is due to the presence of the benzyl methylene group; Figure 2-25 shows the ^{1}H NMR spectrum of complex **2.9b** as a representative sample of compounds **2.9a-c**. The OH should be a triplet but it is not observed, presumably due to overlap.

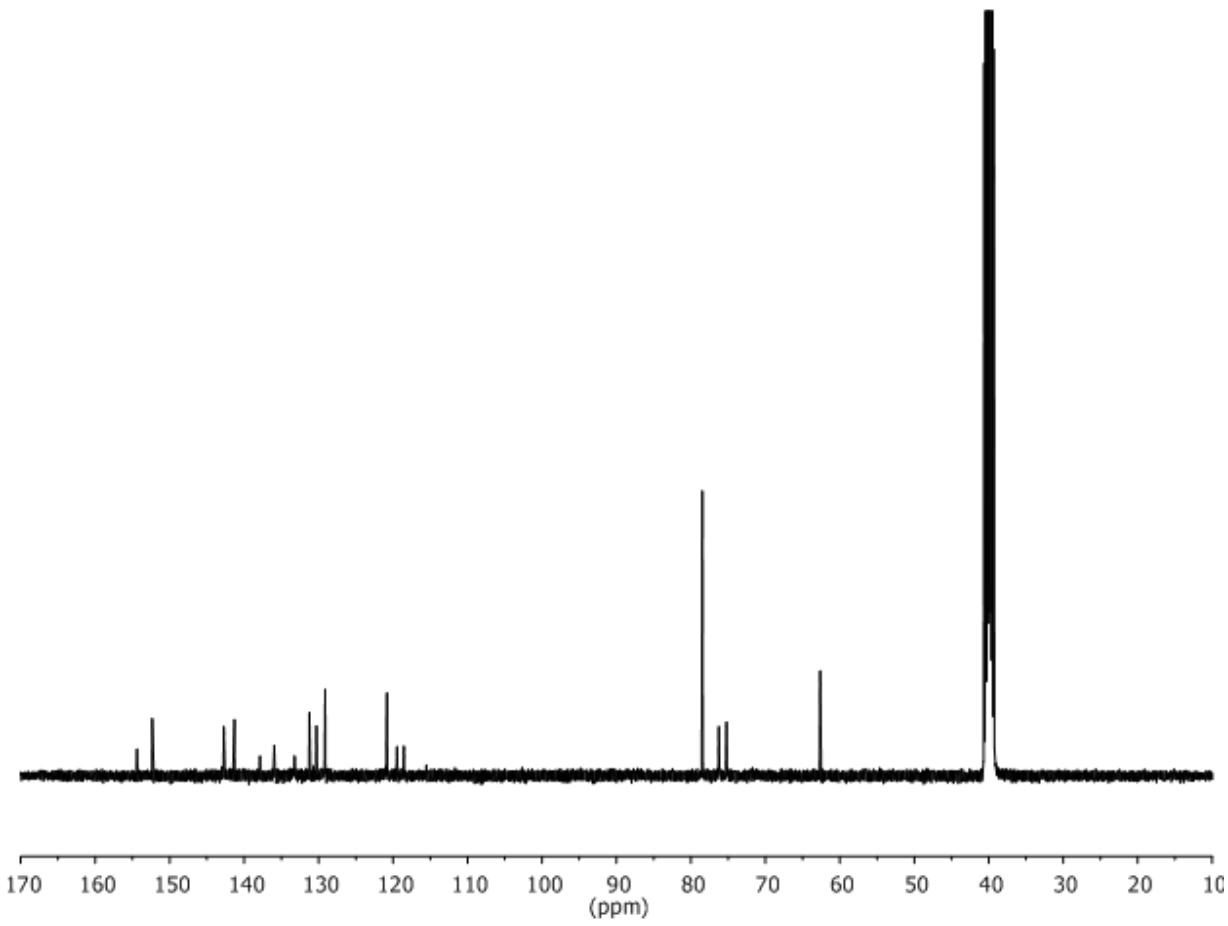

Figure 2-26: 101 MHz ^{13}C NMR spectrum of metalloporphyrin dendrimer 2.9b

The ^{13}C NMR spectrum of **2.9b** (Figure 2-26) clearly shows that the metal complex was successfully substituted due to the shift in the resonance of the complexed CH next to the chloro group from 87.0 ppm to 75.79 ppm due to the replacement of the chlorine with a phenolic group; this can be seen more clearly in the HSQC spectrum. The appearance of a new resonance at 62.18 ppm further confirms the successful substitution of the metal complex, representing the benzylic carbon.

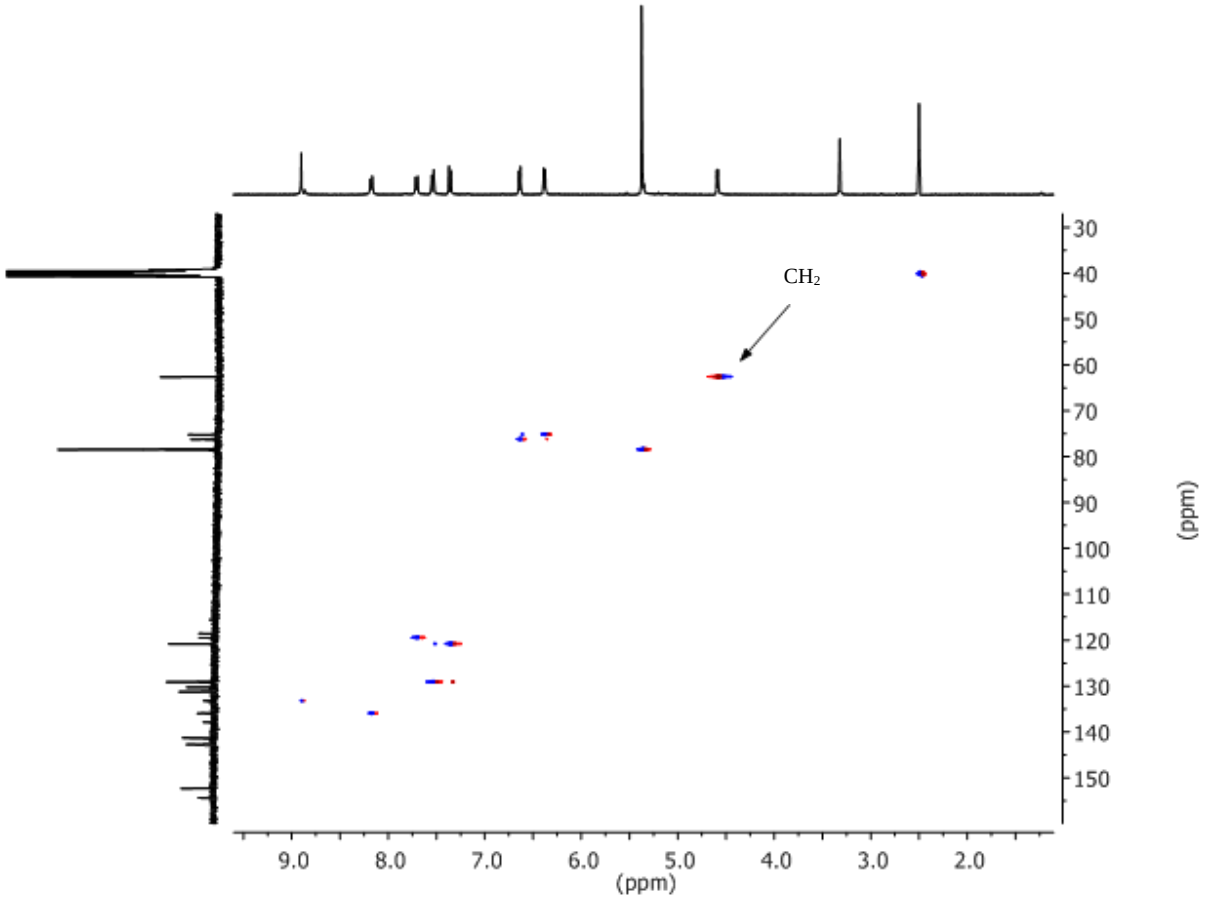

Figure 2-27: HSQC spectrum of metalloporphyrin dendrimer 2.9b

The HSQC spectrum (Figure 2-27) confirms that the benzylic CH_2 proton resonance at 4.59 ppm correlates to a carbon resonating at 63.90 ppm, which is again consistent with the structure of metalloporphyrin dendrimer **2.9b**.

2.6.1 Absorption spectroscopy of compounds 2.9a and 2.9c

The incorporation of 4-hydroxybenzyl alcohol into previously prepared porphyrin complexes **2.4a** and **2.4c** led to free-base porphyrin dendrimer **2.9a** and zinc-based metalloporphyrin dendrimer **2.9c** with red-shifted absorption spectra compared to those of **2.4a** and **2.4c** (Table 2-5, Figure 2-18). The Soret band for free-base porphyrin dendrimer **2.9a** was slightly shifted to 419 nm and the four Q bands were observed at 516 nm, 552 nm, 593

nm, and 648 nm in DMF (Table 2-9). As expected, the absorption spectrum of analogous zinc complex **2.9c** showed a red-shifted Soret band to 426 nm after incorporating the 4-hydroxybenzyl alcohol; two Q bands at 559 nm and 600 nm also appear (Table 2-9). The red shift in all of the absorbed bands after the introduction of 4-hydroxybenzyl alcohol moieties, is caused by the hydroxyl donating electron density, strengthening the electronic density on the phenyl ring. Therefore, the phenyl ring conjugates with the porphyrin macrocycle, which causes electron transition energy of the porphyrin macrocycle to reduce, resulting in red-shifted peaks in the absorption spectrum.

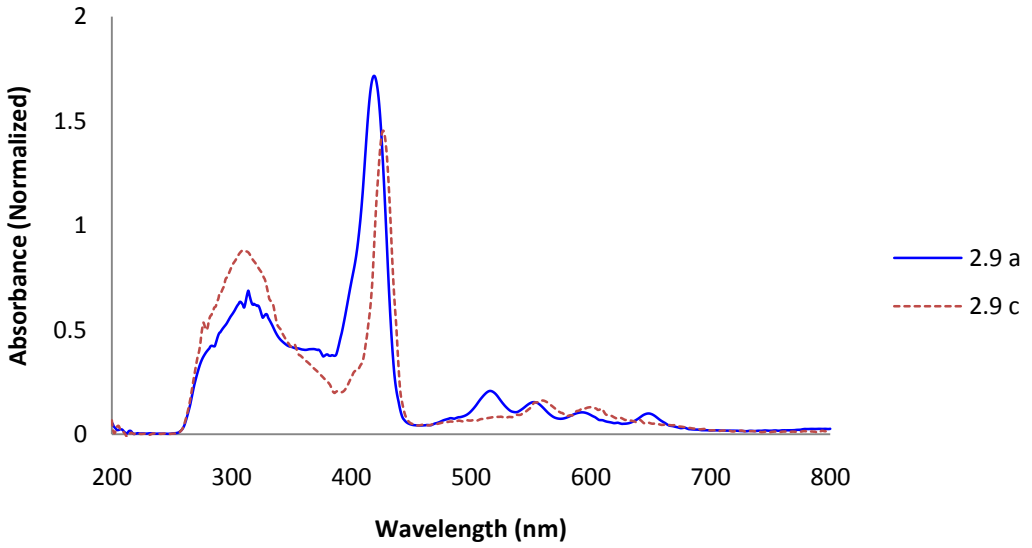

Figure 2-28: Absorption spectra of compounds 2.9a and 2.9c in DMF

Table 2-9: UV-visible data of compounds 2.9a and 2.9c in DMF (1.5 x 10^{-5} M)

Compounds	Absorption (λ_{max}/nm)				
	Soret band	Q band			
2.9 a	419	516	552	593	648
2.9 c	426	-	559	600	-

2.6.2 Fluorescence spectroscopy of free-base porphyrin dendrimer 2.9a and Zn-porphyrin dendrimer 2.9c

Due to the presence of 4-hydroxybenzyl alcohol moieties in free-base dendrimer **2.9a** and Zn-porphyrin dendrimer **2.9c**, the electron density in the porphyrin macrocycle increased, which lowered the energy for electron transition, and as a result, a red shift occurred in the fluorescence spectra compared to those of **2.4a** and **2.4c** (Table 2-8). The free-base porphyrin dendrimer **2.9a** was observed to fluoresce at 653 nm and 716 nm (Table 2-10, Figure 2-29). As expected, the fluorescence spectrum of zinc porphyrin dendrimer **2.9c** also demonstrated a slight red-shift by ~4 nm to fluoresce at 609 nm and 655 nm.

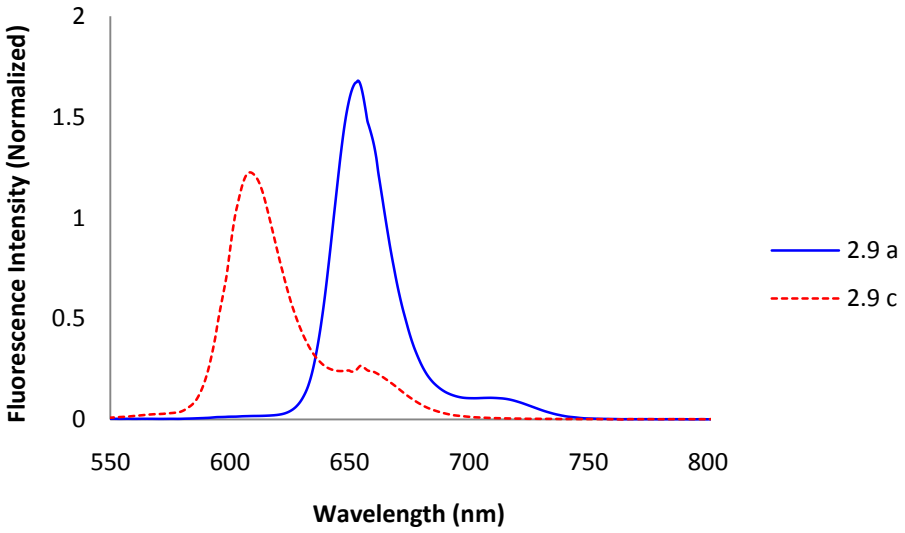

Figure 2-29: Fluorescence spectra of compounds 2.9a and 2.9c

Table 2-10: Fluorescence data of compounds 2.9a and 2.9c in DMF (1.5×10^{-5} M)

Compounds	Fluorescence (λ_{em}/nm)	
2.9 a	653	716
2.9 c	609	655

To study the effect of cyclopentadienyliron moieties on the fluorescence and absorption spectroscopy, solutions of dendrimer **2.9a** in CH_3CN were exposed to 300 nm light for 6 hours to give dendrimer **2.9d** without cationic cyclopentadienyliron moieties (Scheme 2-8).

As seen in the ^1H NMR spectrum of dendrimer **2.9d** (Figure 2-30), the resonance at 5.38 ppm due to the Cp moiety in previous dendrimer **2.9a** is completely removed, and the resonances indicating the complexed aromatics have dramatically shifted from 6.38 ppm and 6.64 ppm to overlap with the resonances of other aromatic environments.

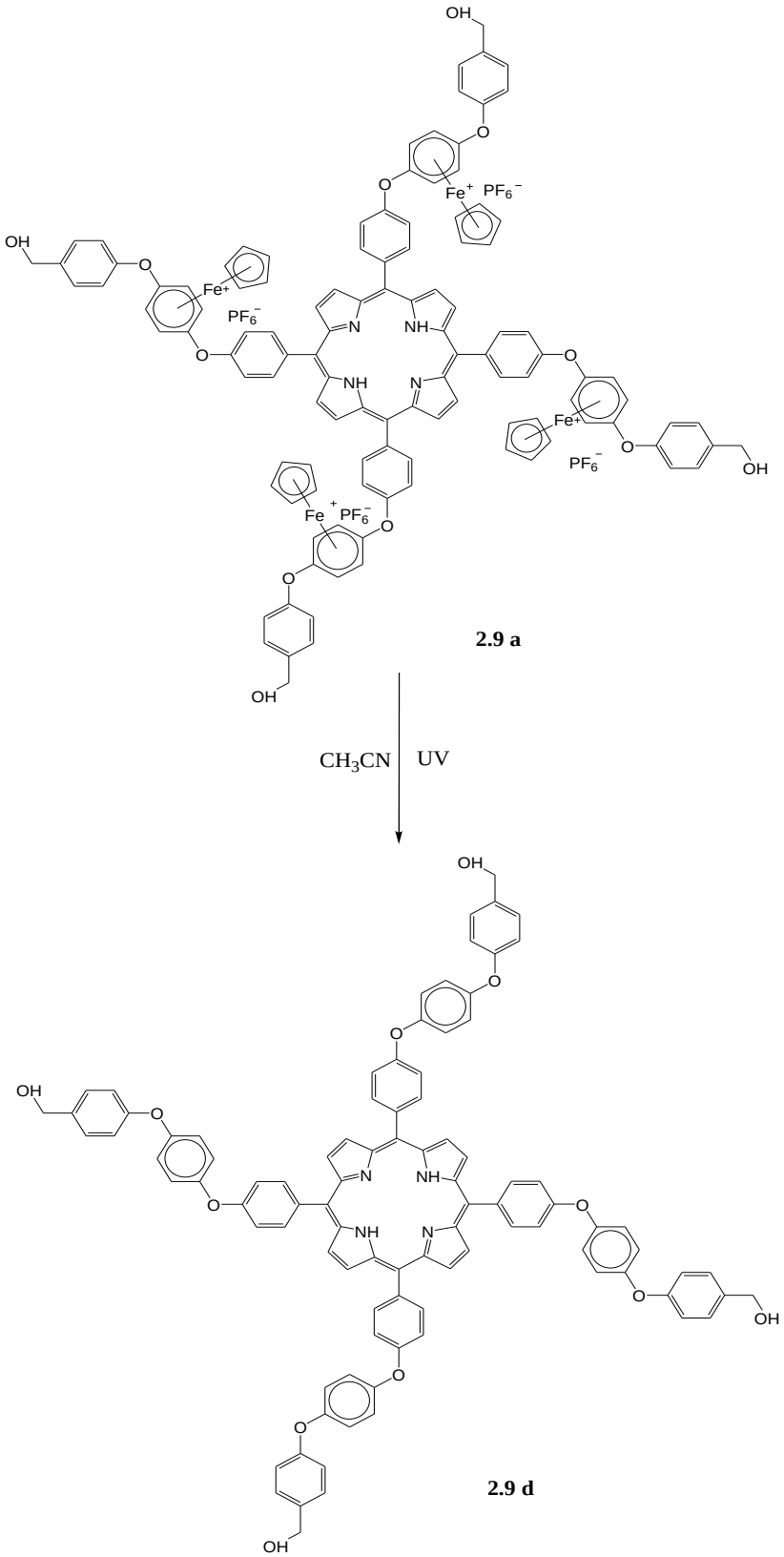

Scheme 2-8: Synthesis of free-base porphyrin dendrimer 2.9d

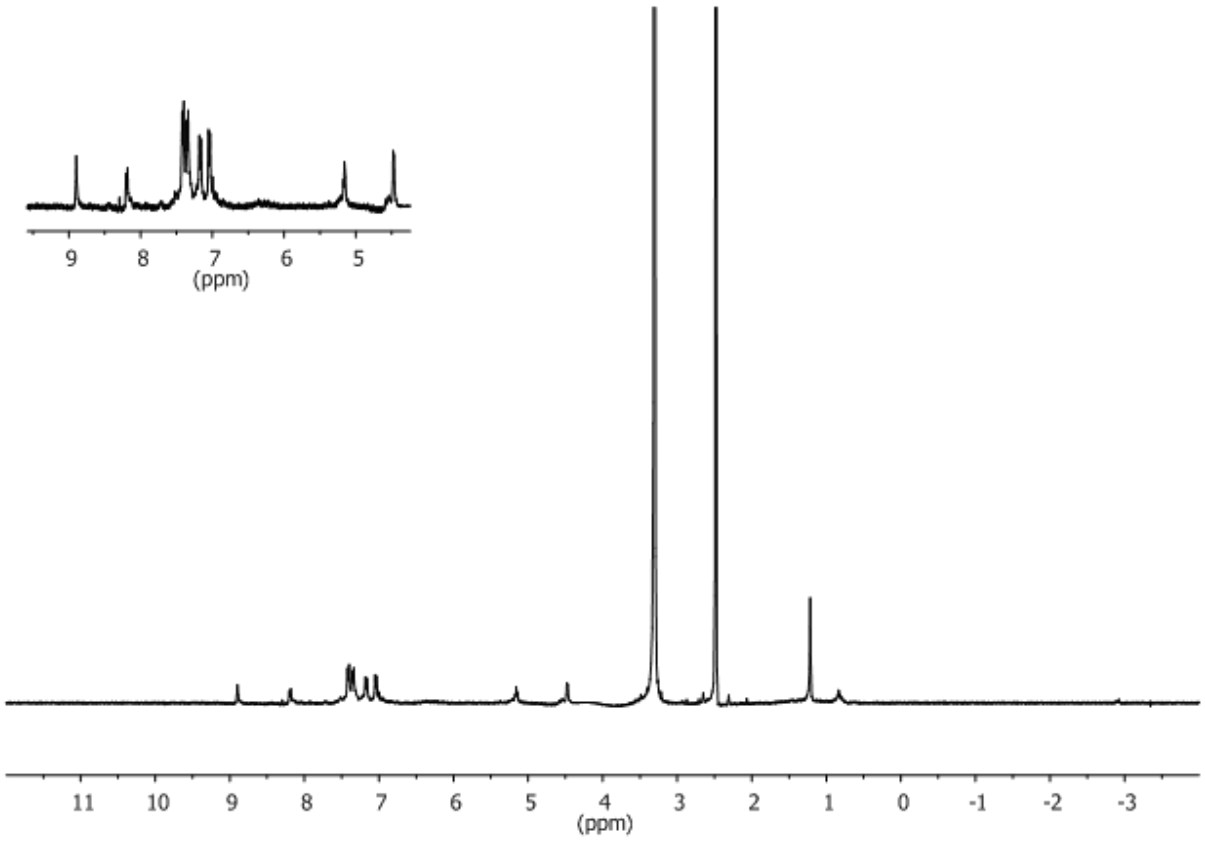

Figure 2-30: 400 MHz ^{1}H NMR spectrum of porphyrin 2.9d

To see the effect of cyclopentadienyliron moieties on the fluorescence and absorption spectroscopy, the fluorescence and absorption measurements of free-base porphyrin dendrimer **2.9d** were performed. Interestingly, the fluorescence and absorption spectra were exactly the same, suggesting that the electron transition energy of the porphyrin macrocycle is not affected by the demetallation process (Figures 2-31 and 2-32).

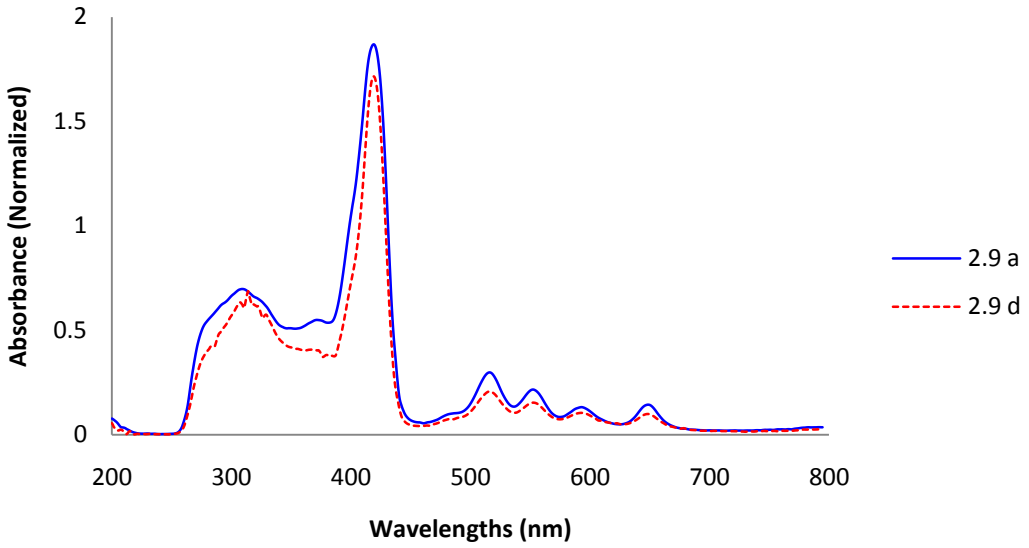

Figure 2-31: Absorption of 2.9a and demetalated porphyrin 2.9d in DMF

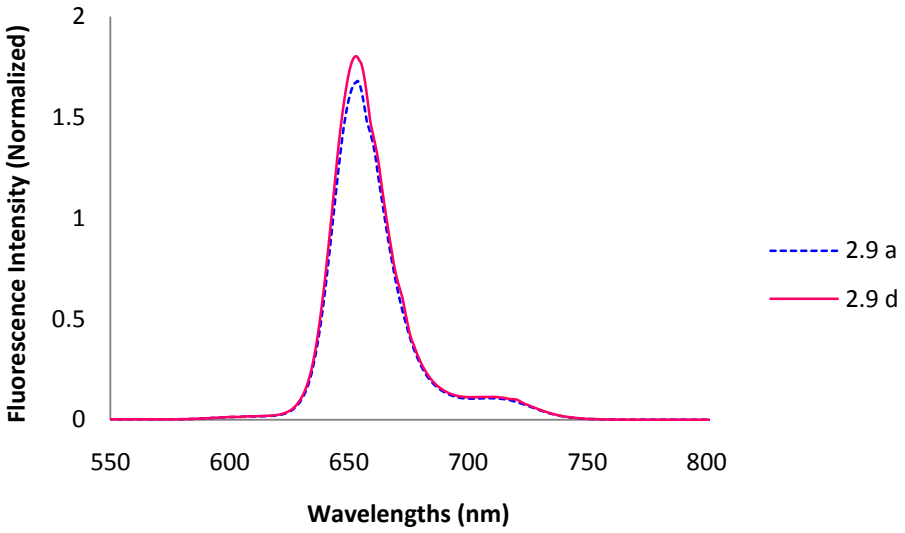

Figure 2-32: Fluorescence spectra of porphyrin dendrimers 2.9a and 2.9d

The terminal aliphatic alcohol groups of free-base porphyrin and metalloporphyrin dendrimers **2.9a-c** were esterified with ferrocene carboxylic acid. Carboxylic acid ferrocene is readily synthesized by Friedel-Crafts acetylation, followed by oxidation with iodine. The ease

of synthesis and affordability make it a valuable compound which allows for the incorporation of ferrocene into free-base porphyrins and metalloporphyrins alike.

The reaction of ferrocene carboxylic acid (**2.16**) with the terminal aliphatic alcohol groups of free-base porphyrin and metalloporphyrin dendrimers **2.9a-c** in the presence of DCC/DMAP gave the ferrocene-capped free-base porphyrin and metalloporphyrin dendrimers **2.10a-c** (Scheme 2-9).

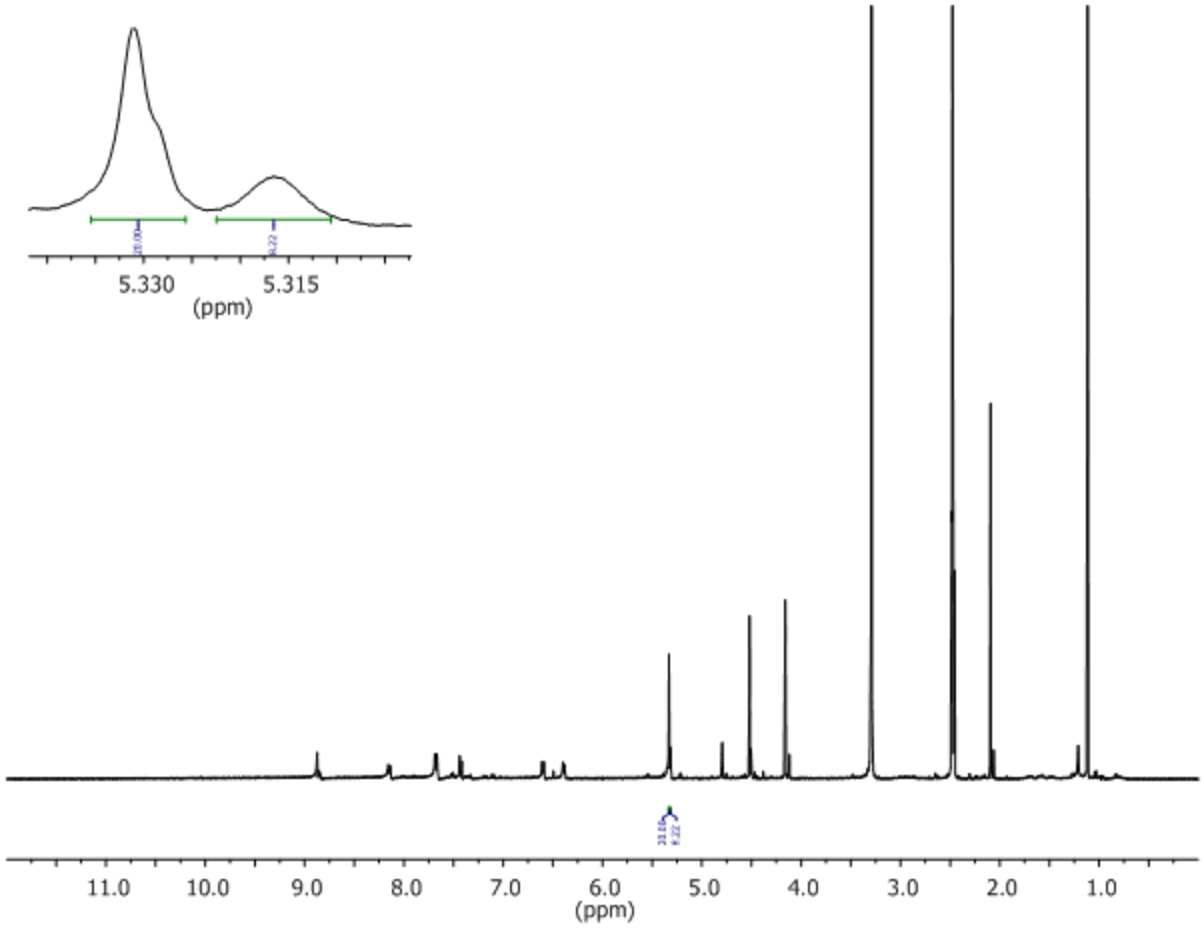

Figure 2-33: 400 MHz ^{1}H NMR spectrum of ferrocene-capped metalloporphyrin dendrimer 2.10c

The ^{1}H NMR spectrum of **2.10c** (Figure 2-33) confirmed the synthesis of ferrocene-capped metalloporphyrin dendrimer **2.10c** due to the presence of a new Cp resonance at 4.16 ppm of the non-functionalized Cp ring of ferrocene. There are also two resonances from the functionalized Cp ring at 4.79 ppm and 4.50 ppm. The benzylic CH_2 resonance also shifted very close to the cationic iron Cp at 5.32 ppm due to the increased electron-withdrawing nature of the ester, while the cationic iron Cp resonates at 5.34 ppm. Ferrocene-capped free-base porphyrins and metalloporphyrin dendrimers **2.10a-c** were orange in colour and were highly soluble in organic solvents due to the incorporation of the ferrocene moiety.

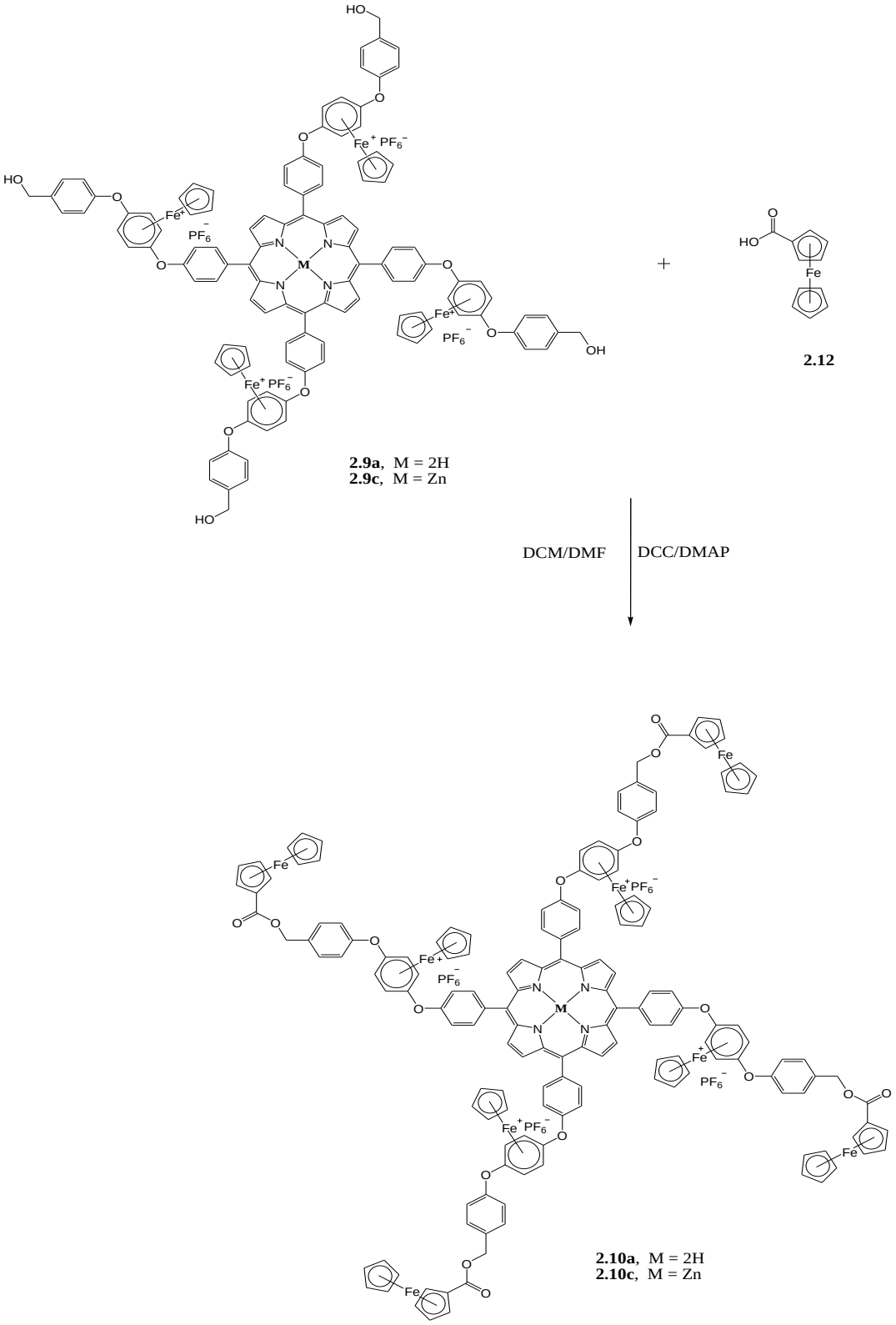

Scheme 2-9: Synthesis of ferrocene-capped free-base porphyrin and metalloporphyrin dendrimers 2.10a and 2.10c

A number of metallic moieties can be attachd to the dendritic porphyrins to increase the number of metal species in the molecule. As a result, free-base porphyrin and metalloporphyrin dendrimers **2.9a** and **2.9b** were reacted with four equivalents of the valeric bimetallic complex (**1.9**) to give free-base porphyrin dendrimer **2.11a** and metalloporphyrin dendrimer **2.11b** containing twelve metallic moieties (Scheme 2-10).

The ^{1}H NMR spectrum of porphyrin dendrimer **2.11a** is shown in Figure 2-34. The incorporation of the new metallic moieties is confirmed by a number of new resonances. For example, due to the formation of the ester, the resonance of the hydroxymethyl (CH_2OH) of the starting material has shifted from 4.58 ppm to 5.24 ppm, very close to the resonance of the cationic Cp of the second generation metallic species. Also, the formation of the second generation of the metallic unit was confirmed by the presence of two different Cp resonances which, when integrated, show a 2:1 ratio, as there are forty and twenty cyclopentadienyliron protons in two different electronic environments.

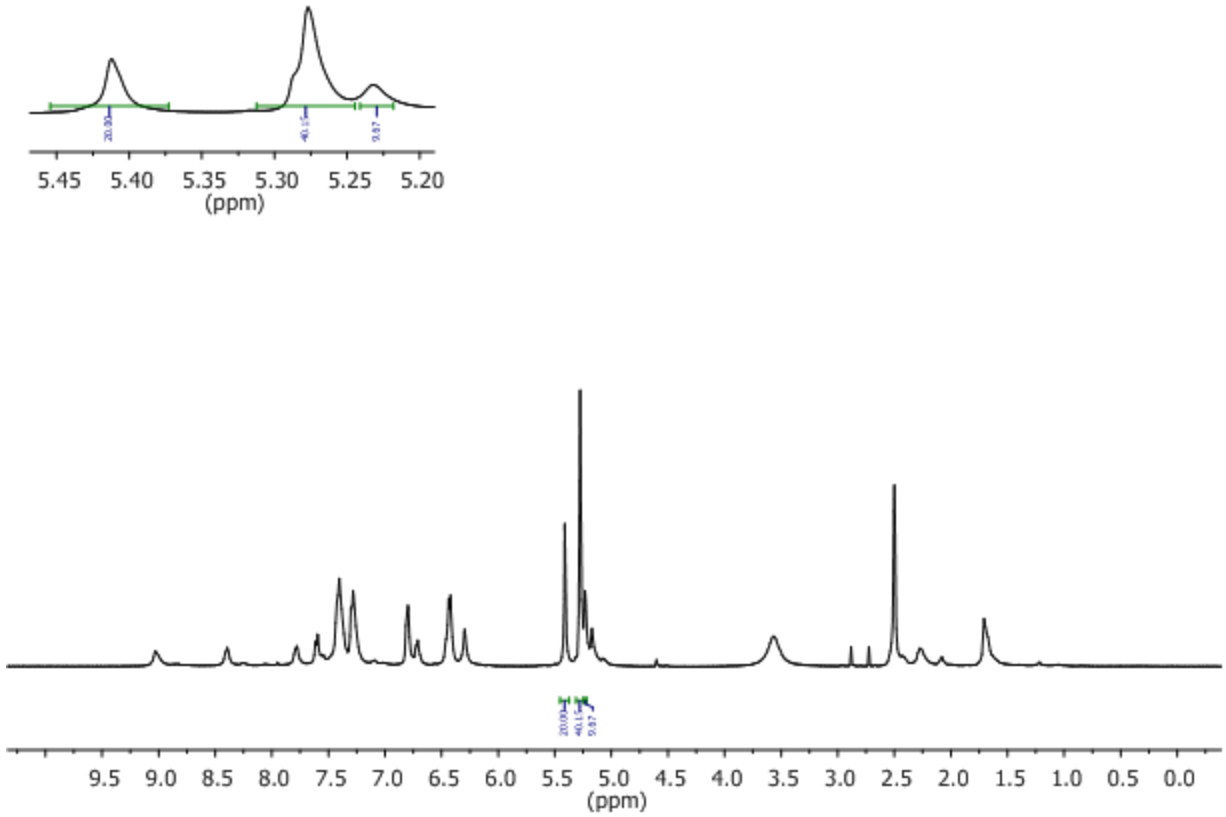

Figure 2-34: 400 MHz ^{1}H NMR spectrum of free-base porphyrin dendrimer 2.11a containing twelve metallic moieties

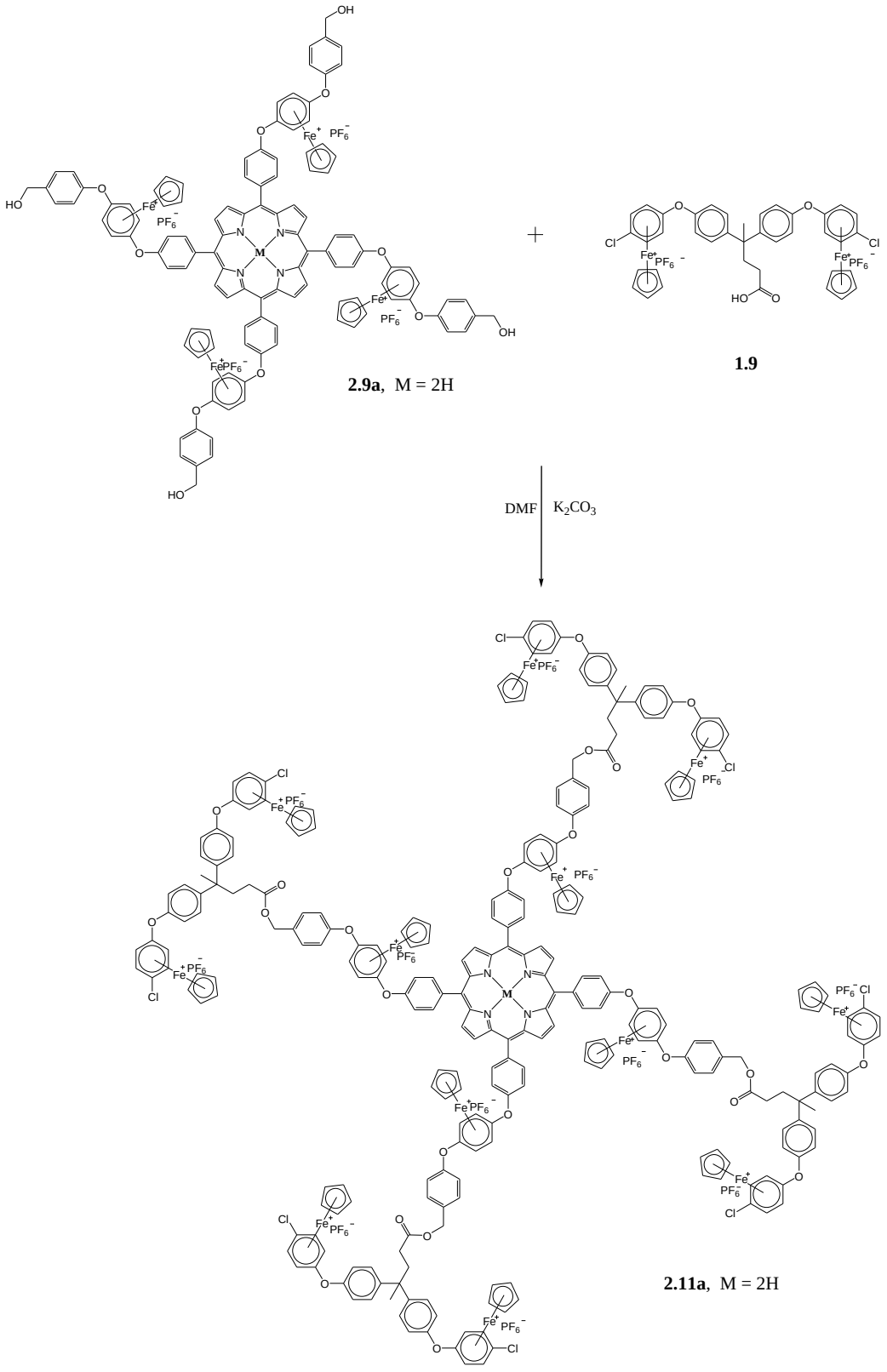

Scheme 2-10: Synthesis of free-base porphyrin dendrimer 2.11a with twelve metallic moieties

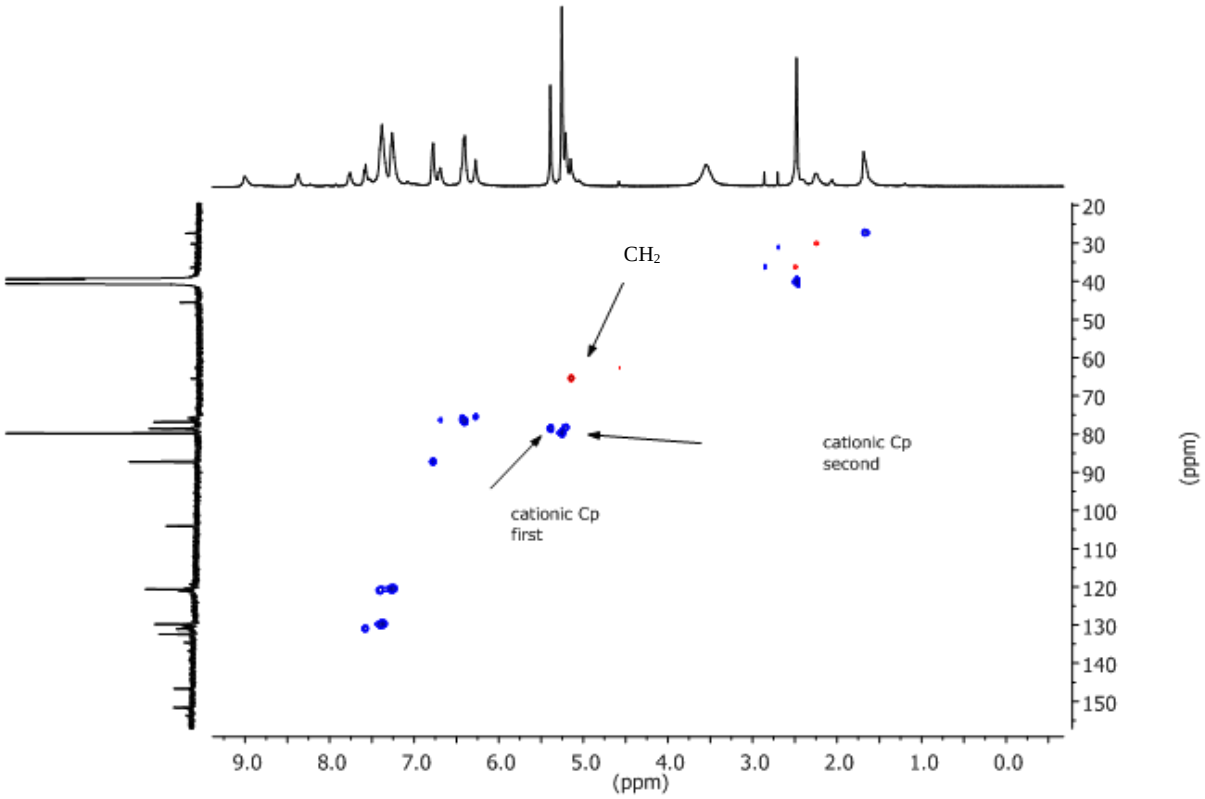

Figure 2-35: HSQC spectrum of metalloporphyrin dendrimer 2.11a

The HSQC spectrum (Figure 2-35) confirmed that the benzylic CH_2 proton resonance at 4.59 ppm correlates to a carbon at 63.90 ppm, which is again consistent with the structure of metalloporphyrin dendrimer **2.11a**. Also, the spectrum confirms that there are two different organoiron species that correlate to different carbons. The first generation Cp protons which resonate at 5.28 ppm correlate to carbons that resonate at 77.9 ppm while the second generation Cp protons resonate at 5.19 ppm and correlate to carbons that resonate at 79.3 ppm.

2.6.3 Absorption spectroscopy of porphyrin compounds 2.10a and 2.11a

The incorporation of valeric bimetallic complex **1.9** and carboxylic acid ferrocene into previously prepared porphyrin complex **2.9a** led to the isolated of free-base porphyrin

dendrimers **2.10a** and **2.11a** with no observable shift in the absorption spectrum (Table 2-11, Figure 2-36).

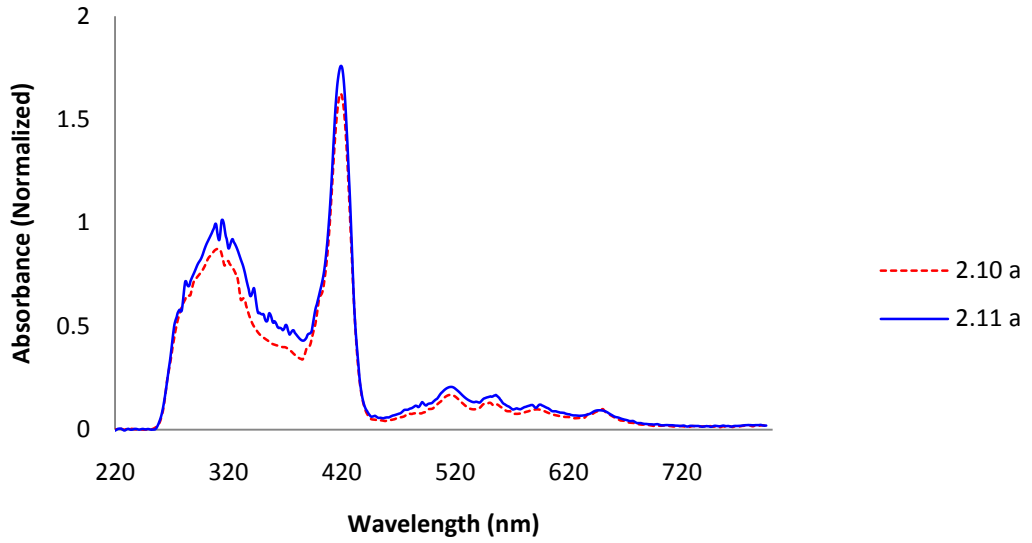

Figure 2-36: Absorption spectra of compounds 2.10a and 2.11a in DMF

Table 2-11: UV-visible data of compounds 2.10a and 2.11a in DMF (1.5 x 10^{-5} M)

Compounds	Absorption (λ_{max}/nm)				
	Soret band	Q band			
2.10 a	419	516	550	592	649
2.11 c	419	516	552	591	647

2.6.4 Fluorescence spectroscopy of free-base porphyrin dendrimers 2.10a and 2.11a

As expected, the fluorescence spectrum of porphyrin dendrimers **2.10a** and **2.11a** showed no shifts after the incorporation of valeric bimetallic complex **1.9** and carboxylic acid ferrocene (**2.16**) into previously prepared porphyrin compound **2.9a** (Table 2-12, Figure 2-37).

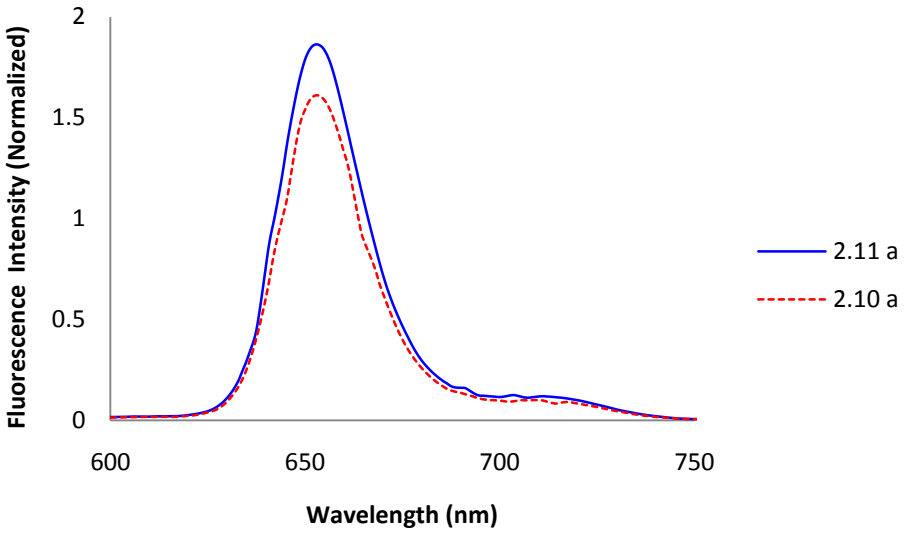

Figure 2-37: Fluorescence spectra of compounds 2.10a and 2.11a

Table 2-12: Fluorescence data of compounds 2.10a and 2.11a in DMF (1.5×10^{-5} M)

Compounds	Fluorescence (λ_{em}/nm)	
2.10 a	653	714
2.11 a	653	714

Chapter 3. Experimental

3.1 Materials

Compounds **1.5**, **1.4**, **1.7**, and **1.9** were prepared according to previously reported methodologies.[76,77,102] Pyrrole was distilled before use. All solvents were HPLC grade and purchased from Fisher Scientific. All reagents were purchased from Sigma-Aldrich and used without further purification. All reactions and complexes containing a η^6-dichlorobenzene-η^5-cyclopentadienyliron (II) hexafluorophosphate moiety were kept in the dark to prevent decomposition.

3.2 Characterization

^{1}H and ^{13}C NMR spectra were recorded at 400 MHz and 101 MHz, respectively, on a Varian Mercury Plus spectrometer equipped with a gradient field probe, with chemical shifts referenced to residual solvent peaks and coupling constants reported in Hertz. Infrared spectroscopy was performed on an IR Prestige-21 FTIR by Shimadzu with a MIRacle ATR by PIKE Technologies. A Varian Cary 100 Bio UV-visible spectrophotometer was used to conduct UV-visible measurement using a standard 1 cm^2 quartz cell.

3.3 Synthetic methodology

3.3.1 Synthesis of 5,10,15,20-tetrakis(4-hydroxyphenyl) porphyrin 2.1

p-Hydroxylbenzaldehyde (40 mmol) was dissolved in 250 mL propionic acid, stirred vigorously, and heated to reflux. To the solution, 30 mL nitrobenzene was added. Freshly distilled pyrrole (40 mmol) in 10 mL of propionic acid was slowly added dropwise, and the reaction mixture was heated to reflux for 30 min. The reaction mixture was left to cool and stirred overnight. The mixture was filtered and the solid product was washed repeatedly with a

mixture of ethanol and propionic acid (1:1 v/v), then with hot water until the rinsing solution was no longer dark. The product was air dried and then dried at 100°C to afford the purple crystalline product.

^{1}H NMR (400 MHz, DMSO-d_6) δ 9.96 (s, OH), 8.87 (s, 8H), 8.00 (d, J = 8.5 Hz, 8H), 7.21 (d, J = 8.5 Hz, 8H), -2.87 (s, N-H). ^{13}C NMR (101 MHz, DMSO-d_6) δ 157.65, 135.66, 132.38, 131.95, 120.44, 114.08.

3.3.2 Synthesis of T(P-OH)PPNi 2.2a and T(P-OH)PPZn 2.2b

T(P-OH)PPH$_2$ (0.1 mmol) was dissolved in 30 mL methanol and 10 mL $CHCl_3$ containing nickel(II) chloride or zinc(II) chloride (0.11 mmol). The reaction mixture was heated to reflux for 4 hours at 70°C, and then cooled to room temperature. Distilled water (60 mL) was added to the mixture, chloroform and methanol were evaporated under reduced pressure. The product was filtered to give either brownish-red crystals (**2.2a**) or purple crystals (**2.2b**).

2.2a: ^{1}H NMR (400 MHz, DMSO-d_6) δ 9.89 (br s, OH), 8.75 (s, 7H), 7.79 (d, J = 8.5 Hz, 8H), 7.13 (d, J = 8.5 Hz, 8H). ^{13}C NMR (101 MHz, DMSO-d_6) δ 168.0, 153.5, 145.2, 142.5, 142.4, 129.6, 124.5.

2.2b: ^{1}H NMR (400 MHz, DMSO-d_6) δ 9.82 (br s, OH), 8.80 (s, 8H), 7.95 (d, J = 8.5 Hz, 8H), 7.17 (d, J = 8.5 Hz, 8H). ^{13}C NMR (101 MHz, DMSO-d$_6$) δ 166.5, 151.2, 144.2, 14.4, 141.3, 129.2, 124.4.

3.3.3 Synthesis of 2.3a-c

Compound **2.1**, **2.2a**, or **2.2b** (0.1 mmol) was reacted with **1.4** (0.45 mmol) and K_2CO_3 (1.5 mmol) in 20 mL DMF at room temperature under N_2 in the dark for 72 h. The reaction mixture was precipitated into 250 mL 1.2 M HCl containing NH_4PF_6. The precipitate was

filtered, washed with water, and dried under reduced pressure. The product was further purified through a neutral alumina column eluting with DCM, then ethyl acetate. Yield: 82%.

2.3a: ^{1}H NMR (400 MHz, DMSO-d_6) δ -2.98 (br s, NH), 9.06 (s, 8H), 8.41 (d, J = 7.8 Hz, 8H), 7.80 (d, J = 7.8 Hz, 8H), 6.70 (d, J = 6.2 Hz, 8H), 6.45 (d, J = 6.2 Hz, 8H), 5.46 (s, 20H), 2.48 (s, under DMSO peak). ^{13}C NMR (101 MHz, DMSO-d_6) δ 153.6, 138.7, 136.3, 131.4, 135.1 (br), 119.1, 119.0, 100.6, 86.9, 78.9, 77.6, 76.8, 19.4.

2.3b: ^{1}H NMR (400 MHz, DMSO-d_6) δ 8.98 (s, 8H), 8.22 (d, J = 7.8 Hz, 8H), 7.74 (d, J = 7.8 Hz, 8H), 6.69 (d, J = 6.2 Hz, 8H), 6.44 (d, J = 6.2 Hz, 8H), 5.46 (s, 20H), 2.48 (s, under DMSO peak). ^{13}C NMR (101 MHz, DMSO-d_6) δ 153.4, 142.6, 138.7, 136.3, 131.4, 135.1, 133.4, 119.1, 119.0, 100.6, 86.9, 78.9, 77.6, 76.8, 19.4.

2.3c: ^{1}H NMR (400 MHz, , DMSO-d_6) δ= 9.00 (s, 8H), 8.26 (d, J = 7.8 Hz, 8H), 7.76 (d, J = 7.8 Hz, 8H), 6.69 (d, J = 6.2 Hz, 8H), 6.45 (d, J = 6.2 Hz, 8H), 5.46 (s, 20H), 2.48 (s, under DMSO peak).

3.3.4 Synthesis of 2.4a-c

Compound **2.1**, **2.2a** or **2.2b** (0.3 mmol) was reacted with **1.5** (1.40 mmol) and K_2CO_3 (3.5 mmol) in 45 mL DMF at room temperature under N_2 in the dark for 72 h. The reaction mixture was precipitated into 300 mL 1.2 M HCl containing NH_4PF_6. The precipitate was filtered, washed with water, and dried under reduced pressure. The product was further purified through a neutral alumina column eluting with DCM, then ethyl acetate. Yield: 78%.

2.4a: ^{1}H NMR (400 MHz, DMSO-d_6) δ 9.06 (s, 8H), 8.41 (d, J = 8.2 Hz, 8H), 7.82 (d, J = 8.2 Hz, 8H), 7.00 (d, J = 6.6 Hz, 8H), 6.86 (d, J = 6.6 Hz, 8H), 5.46 (s, 20H), -2.84 (br s, NH).

2.4b: ^{1}H NMR (400 MHz, DMSO-d_6) δ 8.94 (s, 8H), 8.20 (d, J = 8.4 Hz, 8H), 7.75 (d, J = 8.4 Hz, 8H), 6.96 (d, J = 6.8 Hz, 8H), 6.80 (d, J = 6.8 Hz, 8H), 5.43 (s, 20H).

2.4c: ^{1}H NMR (400 MHz, DMSO-d_6) δ 8.95 (s, 8H), 8.21 (d, *J* = 8.6 Hz, 8H), 7.75 (d, *J* = 8.6 Hz, 8H), 6.97 (d, *J* = 6.9 Hz, 8H), 6.81 (d, *J* = 6.9 Hz, 8H), 5.44 (s, 20H). ^{13}C NMR (101 MHz, DMSO-d_6) δ 153.3, 142.3, 137.8, 135.6, 132.9, 132.0, 119.4, 118.1, 103.9, 87.0, 79.5, 76.9.

3.3.5 Synthesis of 2.6a-c

Compound **2.4a**, **2.4b**, or **2.4c** (0.2 mmol) was reacted with **2.5** (0.88 mmol) and K_2CO_3 (2.5 mmol) in 45 ml DMF at room temperature, under N_2, in the dark for 72 h. The reaction mixture was precipitate into 10% HCl (300 ml) containing NH_4PF_6. The precipitate was filtered, washed with water, and dried under reduced pressure. The product was further purified through a neutral alumina column eluting with DCM containing 1-3% methanol. Yield 72%

2.6a: ^{1}H NMR (400 MHz, DMSO-d_6) δ 9.01 (s, 8H), 8.39 (d, *J* = 8.3 Hz, 8H), 8.19 (d, *J* = 8.9 Hz, 4H), 8.07 (d, *J* = 7.9 Hz, 4H), 8.03 (d, *J* = 7.7 Hz, 4H), 7.95 (d, *J* = 2.1 Hz, 4H), 7.79 (d, *J* = 8.3 Hz, 9H), 7.61 (m, 12H), 6.72 (d, *J* = 6.8 Hz, 8H), 6.54 (d, *J* = 6.8 Hz, 8H), 5.44 (s, 20H), -2.89 (br s, NH).

2.6b: ^{1}H NMR (400 MHz, DMSO-d_6) δ 8.87 (s, 8H), 8.34 (d, *J* = 8.3 Hz, 8H), 8.16 (d, *J* = 8.9 Hz, 4H), 8.04 (d, *J* = 7.9 Hz, 4H), 7.99 (d, *J* = 7.7 Hz, 4H), 7.90 (d, *J* = 2.1 Hz, 4H), 7.68 (d, *J* = 8.3 Hz, 9H), 7.60 (m, 12H), 6.72 (d, *J* = 6.8 Hz, 8H), 6.52 (d, *J* = 6.8 Hz, 8H), 5.42 (s, 20H).

2.6c: ^{1}H NMR (400 MHz, DMSO-d_6) δ 8.91 (s, 8H), 8.35 (d, *J* = 8.3 Hz, 8H), 8.17 (d, *J* = 8.9 Hz, 4H), 8.05 (d, *J* = 7.9 Hz, 4H), 8.00 (d, *J* = 7.7 Hz, 4H), 7.92 (d, *J* = 2.1 Hz, 4H), 7.72 (d, *J* = 8.3 Hz, 9H), 7.60 (m, 12H), 6.72 (d, *J* = 6.8 Hz, 8H), 6.53 (d, *J* = 6.8 Hz, 8H), 5.42 (s, 20H).

3.3.6 Synthesis of 2.7a and 2.7c

Compound **2.6a** or **2.6c** was placed in a 50 mL Pyrex tube and dissolved with acetonitrile. The Pyrex tube was purged with N_2 and placed in a photoreactor using a xenon

light source for 6 h. The resulting solution was extracted in $CHCl_3$, washed with water, and dried under $MgSO_4$. The $CHCl_3$ was removed *in vacuo* to collect the compounds.

2.7a: ^{1}H NMR (400 MHz, DMSO-d_6) δ 8.93 (s, 8H), 8.23 (d, *J* = 8.5 Hz, 8H), 8.01 (d, *J* = 8.9 Hz, 4H), 7.93 (d, *J* = 8.0 Hz, 4H), 7.86 (d, *J* = 8.0 Hz, 4H), 7.55 – 7.41 (m, 28H), 7.38 (dd, *J* = 8.9, 2.5 Hz, 4H), 7.30 (d, *J* = 9.0 Hz, 8H).

2.7c: ^{1}H NMR (400 MHz, acetone-d_6) δ 8.86 (m, 8H), 8.07 (d, J = 8.2 Hz, 8H), 7.99 (m, 8H), 7.92 (d, J = 8.1 Hz, 4H), 7.83 (d, J = 8.2 Hz, 4H), 7.50 (m, 4H), 7.39-7.45 (m, 16H), 7.36 (m, 4H), 7.28 (d, J = 8.1 Hz, 8H), 7.23 (m, 4H).

3.3.7 Synthesis of 2.9a-c

Compound **2.4a**, **2.4b**, or **2.4c** (0.3 mmol) was reacted with **2.8** (1.40 mmol) and K_2CO_3 (3.5 mmol) in 45 mL DMF at room temperature under N_2 in the dark for 72 h. The reaction mixture was precipitated into 300 mL 1.2 M HCl containing NH_4PF_6. The precipitate was filtered, washed with water, and dried under reduced pressure. The product was further purified through a neutral alumina column eluting with DCM, then ethyl acetate. Yield: 76%.

2.9a: ^{1}H NMR (400 MHz, DMSO-d_6) δ 9.01 (s, 8H), 8.37 (d, *J* = 7.0 Hz, 8H), 7.78 (d, *J* = 7.0 Hz, 8H), 7.55 (d, *J* = 7.6 Hz, 8H), 7.38 (d, *J* = 7.6 Hz, 8H), 6.70 (d, *J* = 5.9 Hz, 8H), 6.41 (d, *J* = 5.9 Hz, 8H), 5.41 (s, 20H), 4.60 (s, 8H), -2.90 (br s, NH).

2.9b: ^{1}H NMR (400 MHz, DMSO-d_6) δ 8.90 (s, 8H), 8.18 (d, *J* = 8.0 Hz, 8H), 7.71 (d, *J* = 8.4 Hz, 8H), 7.54 (d, *J* = 8.0 Hz, 8H), 7.36 (d, *J* = 8.4 Hz, 8H), 6.64 (d, *J* = 7.0 Hz, 8H), 6.38 (d, *J* = 7.0 Hz, 8H), 5.37 (s, 20H), 4.59 (d, *J* = 5.5 Hz, 8H). ^{13}C NMR (101 MHz, dmso) δ =153.93, 151.88, 142.27, 140.84, 137.42, 135.50, 132.77, 130.78, 129.83, 128.67, 120.37, 119.02, 118.08, 78.01, 75.79, 74.76, 62.18.

2.9c: ^{1}H NMR (400 MHz, DMSO-d_6) δ 8.95 (s, 8H), 8.21 (d, *J* = 8.0 Hz, 8H), 7.74 (d, *J* = 8.4 Hz, 8H), 7.54 (d, *J* = 8.0 Hz, 8H), 7.37 (d, *J* = 8.4 Hz, 8H), 6.66 (d, *J* = 7.0 Hz, 8H), 6.40 (d, *J* = 7.0 Hz, 8H), 5.39 (s, 20H), 4.59 (d, *J* = 5.5 Hz, 8H).

3.3.8 Synthesis of 2.9d

Compounds **2.9a** was placed in a 50 mL Pyrex tube and dissolved with acetonitrile. The Pyrex tube was purged with N_2 and placed in a photoreactor for 6 h. The resulting solution was extracted in $CHCl_3$, washed with water, and dried under $MgSO_4$. The $CHCl_3$ was removed *in vacuo* to collect the compounds.

^{1}H NMR (400 MHz, DMSO-d_6) δ=8.91 (s, 8H), 8.21 (d, *J* = 8.16 Hz, 8H), 7.43 (d, *J* = 8.81 Hz, 16H), 7.36 (d, *J* = 8.81 Hz, 8H), 7.18 (d, *J* = 8.54 Hz, 8H), 7.06 (d, *J* = 8.54 Hz, 8H), 4.49 (d, *J* = 5.5 Hz, 8H).

3.3.9 Synthesis of 2.10a and 2.10c

Compound **2.9a** or **2.9c** (0.3 mmol), carboxylic ferrocene (1.5 mmol), DCC (1.8 mmol), and DMAP (1.8 mmol) were stirred with 15 mL DCM and 5 mL DMF under N_2 for 24 h. The mixture was placed in a freezer to precipitate DCU. The reaction mixture was poured into 1.2 M HCl containing NH_4PF_6 and extracted into DCM. The organic layer was washed with water and dried over $MgSO_4$. The product was filtered and the solvent removed *in vacuo*. The product residue was dissolved in acetone and filtered to remove any remaining DCU. The product was precipitated into basic water to remove any excess carboxylic ferrocene. The precipitate was collected and dried under reduced pressure. Yield: 74%.

2.10a: ^{1}H NMR (400 MHz, DMSO-d_6) δ 8.96 (s, 8H), 8.33 (d, *J* = 8.1 Hz, 8H), 7.79 (m, 16H), 7.46 (d, *J* = 8.3 Hz, 8H), 6.64 (d, *J* = 6.6 Hz, 8H), 6.40 (d, *J* = 6.6 Hz, 7H), 5.31 (s, 20H), 4.79 (t, *J* = 2.0 Hz, 8H), 4.50 (t, *J* = 2.0 Hz, 5H), 4.16 (s, 20H).

2.10c: ^{1}H NMR (400 MHz, DMSO-d_6) δ 8.87 (s, 8H), 8.15 (d, J = 8.1 Hz, 8H), 7.68 (m, 16H), 7.43 (d, J = 8.3 Hz, 8H), 6.60 (d, J = 6.6 Hz, 8H), 6.39 (d, J = 6.6 Hz, 7H), 5.32 (s, 20H), 4.79 (t, J = 2.0 Hz, 8H), 4.50 (t, J = 2.0 Hz, 5H), 4.16 (s, 20H).

3.3.10 Synthesis of 2.11a

Compound **2.9a** (0.4 mmol), valeric bimetallic complex **1.9** (1.7 mmol), DCC (2.0 mmol), and DMAP (2.0 mmol) were stirred with 20 mL DCM and 10 mL DMF under N_2 for 24 h. The mixture was placed in a freezer to precipitate DCU. The reaction mixture was filtered and poured into 1.2 M HCl containing NH_4PF_6. The precipitated product was filtered and the residue was dissolved in acetone and filtered to remove any remaining DCU. The product was precipitated again into water, collected, and dried under reduced pressure. Yield: 72%.

^{1}H NMR (400 MHz, DMSO-d_6) δ 8.40 (br s, 8H), 7.78 (br m, 8H), 7.60 (br m, 8H), 7.43, (br m, 8H), 7.40 (br m, 24H), 7.28 (br m, 16H), 6.76(br m, 16H), 6.70 (br m, 8H), 6.43 (br m, 24H), 5.28 (br s, 20H), 5.19 (br s, 40H), 5.13 (br s, 8H), 2.51 (br m, 8H), 2.27 (br m, 8H), 1.71 (br s, 12H), -2.87 (br s, NH). ^{13}C NMR (101 MHz, DMSO-d_6) δ 26.9, 29.7, 35.9, 45.0, 64.9, 75.3, 75.9, 76.3, 77.9, 79.3, 86.8, 103.6, 118.7, 119.1, 119.9, 120.1, 120.5, 129.2, 129.3, 129.9, 130.2, 130.5, 131.9, 134.1, 136.3, 138.7, 146.0, 146.2, 151.1, 153.2.

Chapter 4. Conclusions and future work

The aim of this project was to synthesize a series of free-base porphyrins and their analogous metal-containing dendrimers via metal-mediated nucleophilic aromatic substitutions and ester condensation reactions, and to investigate their absorption and emission properties. As a result, novel free-base porphyrins and nickel and zinc porphyrin dendrimers containing cationic η^6-chlorobenzene-η^5-cyclopentadienyliron(II) complexes and cationic η^6-methylbenzene-η^5-cyclopentadienyliron(II) complexes functionalized with naphthalene and capped with ferrocene were synthesized. The incorporation of cationic η^6-dichloroarene-η^5-cyclopentadienyliron moieties enhance the solubility of the dendrimer and facilitate further nucleophilic aromatic substitution and addition reactions due to the intense electron-withdrawing ability of the iron center. Divergent approaches were employed to give highly symmetrical branched materials.

Photophysical studies of these dendrimers show that the incorporation of the terminal methyl group cyclopentadienyliron complex led to a blue shift in the absorption and fluorescence spectra by ~3 nm, while the incorporation of the terminal chloro group cyclopentadienyliron complex led to a blue shift in the absorption and fluorescence spectra by ~6 nm. This shift is most likely due to the incorporation of the iron complexes decreasing the electron density in the porphyrin macrocycle, which raises the energy of electron transition, leading to a blue shift in the absorption and fluorescence spectra. On the other hand, the presence of the electron-donating group, naphthalene, resulted in a red shift the absorption and fluorescence spectra because the naphthalene enables the strengthening of electron density on the phenyl ring, thus allowing the phenyl ring to become conjugated with the porphyrin macrocycle and reducing the electron transition energy of the porphyrin. Surprisingly, the

absorption and fluorescence spectra of the analogous organic porphyrin dendrimers after photolytic cleavage of the cationic cyclopentadienyliron moiety were found to be exactly the same as their iron complexes.

Much research can still be performed to further synthesize porphyrin-containing organometallic polymers and study their photophysical and electronic properties. Polymers containing assorted cationic iron complexes can be adapted to include porphyrins in either the polymer backbone or pendant from the main chain. Because porphyrins have both free-base and metallated forms, we can synthesize polymers containing two different transition metals. With the appropriate metal in the porphyrin coordination site, the polymer can cross-link through further reaction with a bidentate ligand, such as pyrazine or 4,4'-biphenyl. As the iron can be removed from the arene under mild conditions, we can also prepare a purely organic version of each polymer chain. Functional groups such as esters, amides, poly(ethylene oxide), and poly(phenylene ethynylene) can be used as spacers between iron complexes to alter the physical properties of the polymer. Chromophores or fluorophores such as azo dyes or triphenylene could also be included to tune the photophysical properties of the polymer.

References

[1] Wrobel, D.; Lukasiewicz, J.; Goc, J.; Waszkowiak, A.; Ion, R. *J. Mol. Struct*. **2000**, *555*, 407-417.

[2] Macdonald, I.J.; Dougherty, T.J. *J. Porphyrins Phthalocyanines.* **2001**, *5*, 105-129.

[3] Anderson, H.L.; Martin, S.J.; Bradley, D.D.C. *Angew. Chem. Int. Ed. Engl.* **1994**, *33*, 655-657.

[4] Li, Y.; Cao, L.; Tian, H. *J. Org. Chem.* **2006**, *71*, 8279-8282.

[5] Wagner, R.W.; Lindsey, J.S. *J. Am. Chem. Soc.* **1994**, *116*, 9759-9760.

[6] Abraham, R.J.; Medforth, C.J.; Mansfield, K.E.; Simpson, D.J.; Smith, K.M. *J. Chem. Soc. Perkin Trans*. *2*. **1988**, 1365.

[7] Zayats, V.Y.; Lobanov, V.V.; Pinchuk, V.M. *Theor. Exp. Chem*. **1988**, *24*, 328-331.

[8] Senge, M.O.; Smith, K.M. *Photchem. Photobiol.* **1991**, *54*, 841.

[9] Smith, K.M.; Unsworth, J.F. *Tetrahedron,* **1975**, *31*, 367.

[10] Scheidt.W.R. *Acc. Chem. Res.* **1977**, *10*, 339.

[11] Smith, K.M.; Goff, D.A.; Abraham, R.J. *J. Org. Magn. Reson*. **1984**, *22*, 779.

[12] Abraham, R.J.; Medforth, C.J.; Smith, K.M.; Goff, D.A.; Simpson, D.J. *J. Am. Chem. Soc.* **1987**, *109*, 4786.

[13] Medforth, C.J. In The Porphyrin Handbook; Kadish, K.M.; Smith, K.M.; Guilard, R., Eds.; Academic: New York, **2000**; Vol 5, Chapter 35.

[14] Asakawa, M.; Toi, H.; Aoyama, Y.; Ogoshi, H. *J. Org. Chem*. **1992**, *57*, 5796-5798.

[15] Storm, C.B.; Teklu, Y. *J. Am. Chem. Soc*. **1972**, *94*, 1745-1747.

[16] Eaton, S.S.; Eaton, G.R. *J. Am. Chem. Soc*. **1977**, *99*, 1601-1604.

[17] Hennig, J.; Limbach, H.-H. *J. Am. Chem. Soc*. **1984**, *106*, 292-298.

[18] Wehrle, B.; Limbach, H.-H.; Kocher, M.; Ermer, O.; Vogel, E. *Angew. Chem. Int. Ed. Engl*. **1987**, *26*, 934-936.

[19] Gouterman, M.; Wagniere, G.; Snyder, L.C. *J. Mol. Spectrosc.* **1963**, *11*, 108-127.

[20] Kuhn, H. *J. Chem. Phys.* **1949**, *17*, 1198-1212.

[21] Simpson, W.T. *J. Chem. Phys.* **1949**, *17*, 1218-1221.

[22] Milgrom, L.R. The Colours of Life: An Introduction to the Chemistry of Porphyrins and Related Compounds, OUP, Oxford, 1997; The Porphyrins, Ed. D. Dolphin, Academic Press, New York, **1978**.

[23] Dogutan, D.K.; Ptaszek, M.; Lindsey, J.S. *J. Org. Chem.* **2007**, *72*, 5008-5011.

[24] Baskin, J.S.; Yu, H.; Zewail, A. H. *J. Phys. Chem. A.* **2002**, *106*, 9837-9844.

[25] Yu, H.; Baskin, J.S.; Zewail, A. H. *J. Phys. Chem. A.* **2002**, *106*, 9845-9854.

[26] Meot-Ner, M.; Adler, A.D. *J. Am. Chem. Soc.* **1975**, *97*, 5107-5111.

[27] Kim, J.B.; Leonard, J.J.; Longo, F.R. *J. Am. Chem. Soc.* **1972**, *94*, 3986-3992

[28] Dudkowiak, A.; Teślak, E.; Habdas, J. *J. Mol. Struct*. **2006**, 792793, 93-98.

[29] Ashutosh, S; Stephen, G. Introduction to Fluorescence Spectroscopy. Wiley-Interscience, New York, **1999**.

[30] Rothemund, P. *J. Am. Chem. Soc.* **1935**, *57*, 2010-2011.

[31] Rothemund, P. *J. Am. Chem. Soc.* **1939**, *61*, 2912-2915.

[32] Adler, A.D.; Longo, F.R.; Shergalis, W. *J. Am. Chem. Soc.* **1964**, *86*, 3145-3149.

[33] Adler, A.D.; Sklar, L.; Longo, F.R.; Finarelli, J.D.; Finarelli, M.G. *J. Heterocycl. Chem.* **1968**, *5*, 669-678.

[34] Lindsey, J.S.; Hsu, H.C.; Schreiman, I.C. *Tetrahedron Lett.* **1986**, *27*, 4969-4970.

[35] Lindsey, J.S.; Schreiman, I. C.; Hsu, H.C.; Kearney, P.C.; Marguerettaz, A.M. *J. Org. Chem.* **1987**, *52*, 827-836.

[36] The Porphyrin Handbook; Kadish, K.M., Smith, K.M., Guilard, R., Eds.; Academic Press: San Diego, CA, **2003**; Vols. 1-20.

[37] Momenteau, M.; Reed, C.A. *Chem. Rev*. **1994**, *94*, 659-698.

[38] Karrasch, S.; Bullough, P.A.; Ghosh, R. *EMBO J*. **1995**, *14*, 631.

[39] Pullerits, T.; Sundström, V. *Acc. Chem. Res*. **1996**, *29*, 381.

[40] Jin, R.H.; Aida, T.; Inoue, S. *Chem. Commun.* **1993**, 1260.

[41] Dandliker, P.J.; Diederich, F.; Gross, M.; Knobler, C.B.; Louati, A.; Sanford, E.M. *Angew. Chem., Int. Ed. Engl.* **1994**, *33*, 1739.

[42] Bhyrappa, P.; Young, J.K.; Moore, J.S.; Suslick, K.S. *J. Am. Chem.Soc.* **1996**, *118*, 5708.

[43] Vinogradov, S. A.; Lo, L.-W.; Wilson, D. F. *Chem.-Eur. J*. **1999**, 5, 1338.

[44] Pollak, K.W.; Sanford, E.M.; Fréchet, J.M.J. *J. Mater. Chem*.**1998**, 8, 519.

[45] Finikova, O.; Galkin, A.; Rozhkov, V.; Cordero, M.; Ha¨gerha¨ll, C.; Vinogradov, S. J. *Am. Chem. Soc*. **2003**, *125*, 4882.

[46] Kimata, S.; Aida, T. *Tetrahedron Lett.* **2001**, *42*, 4187.

[47] Lahtinen, R.; Fermín, D.J., Kontturi, K., Girault, H.H. *Electroanal. Chem*. **2000**, *483*, 81-87.

[48] Konishi, T.; Ikeda, A.; Shinkai, S. *Tetrahedron*. **2005**, *61*, 4881-4899.

[49] Nalwa, H.S.; Watanabe, T.; Miyata, S. "Nonlinear Optics in Organic Molecular and Polymeric Materials", Nalwa, H.S.; Miyata, S. (Eds.) CRC Press: Boca Raton, FL, **1997**, 611-797.

[50] Nalwa, H.S. "Handbook of Organic Conductive Molecules and Polymers", Nalwa, H.S. (Ed.) John Wiley & Sons, Chichester, **1997**, Vol. 1-4, 261-363.

[51] Nalwa, H.S.; Shirk, J.S. "Phthalocyanines: Properties and Applications", Leznoff, C.C.; Lever, A.B.P. (Eds.) **1996**, Vol. 4, 79-118.

[52] Pearlstein, R.H. *New Compr. Biochem.* **1987**,*15*, 299.

[53] Fleming, G.R.; Martin, J.-L.; Breton, J. *Nature*. **1988**, *333*, 190.

[54] Paddock, M.L.; Rongey, S.H.; Feher, G.; Okamura, M.Y. *Proc. Natl. Acad. Sci., USA.* **1989**, *86*, 6602-6606.

[55] Baron, A.E.; Danielson, J.D.S.; Gouterrnan, M.; Wan, J.R.; Callis, J.B. *Rev. Sci. Instrum.* **1993**, *64*, 3394.

[56] Aida, T.; Inoue, S. *Acc. Chem. Res*. **1996**, *29*, 39.

[57] Shinmori, H.; Kajiwara, T.; Osuka, A. *Tetrahedron Lett.* **2001**, *42*, 3617-3620.

[58] Nathalie, S.; Regis; R.; Mathieu, W. *J. Porphyrins Phthalocyanines*. **2007**, *11*, 375-382.

[59] Nishiyama, N.; Jang, W.-D.; Kataoka, K. *New J. Chem*. **2007**, *31*, 1074.

[60] Jang, W.-D.; Nishiyama, N.; Kataoka, K. *Supramol. Chem*. **2007**, *19*, 309.

[61] MacDonald, I.J.; Dougherty, T.J. *J. Porphyrins Phthalocyanines*. **2001**, *5*, 105-129.

[62] Liotta, L.A. *Cancer Res*. **1986**, *46*, 1.

[63] Weinkauf, J.R.; Cooper, S.W.; Schweiger, A.; Wamser, C.C. *J. Phys. Chem. A.* **2003**, *107*, 3486-3496.

[64] Shelnutt, J.A.; Song, X.-Z.; Ma, J.-G.; Jia, S.-L.; Jentzen, W.; Medforth, C. *J. Chem. Soc. Rev*. **1998**, *27*, 31.

[65] Rose, E.; Quelquejeu, M.; Pandian, R.P.; Lecas-Nawrocka, A.; Vilar, A.; Ricart, G. *Polyhedron*. **2000**, *19*, 581-586.

[66] Li, Y.W.; Yao, J. H.; Liu, C.J.; Yang, J.W.; Yang, C.L. *Physics Letters A.* **2009**, *373*, 3974-3977.

[67] Yasuaki, K.; Masashi, O.; Kazuya, S.; Yasunori, T.; Satoshi, H.; Motoki, A.; Hajime, W.; Hiroshi, O.I.H. *J. Biol. Chem.* **2006**, *281*, 31729-31735.

[68] Zhu, L.-J.; Wang, J.; Reng, T.-G.; Li, C.-Y.; Guo, D.-C.; Guo, C.-C. *J. Phys. Org. Chem.* **2010**, *23*, 190-194.

[69] Baldo, M.A.; O'Brien, D.F.; You, Y.; Shoustikov, A.; Sibley, S.; Thompson, M.E.; Forrest, S.R. *Nature*. **1998**, *395*, 151.

[70] Sakakibara, Y. Okutsu, S.; Enokida, T.; Tani, T. *Appl. Phys. Lett*. **1999**, *74*, 2587.

[71] Virgili, T.; Lidxey, D.G.; Bradley, D.D.C. *Adv. Mater*. **2000**, *12*, 58.

[72] Burrows, P.E.; Forrest, S.R.; Sibley, S.P.; Thompson, M.E. *Appl. Phys. Lett*. **1996**, *69*, 2959.

[73] Yeh, H.C.; Yeh, S.J.; Chen, C.T. *Chem. Commun*. **2003**, 2632.

[74] Togni, A.; Hayashi, T. (Eds), *Ferrocenes: Homogeneous Catalysis, Organic Synthesis, Materials Science*, VCH, Weinheim, **1995**.

[75] Atkinson, R.C.J.; Gibson, V.C.; Long, N.J. *Chem. Soc. Rev.* **2004**, *33*, 313-328.

[76] Nesmeyanov, A.N.; Vol'Kenau, A.; Bolesova, I.N. *Dokl. Acad. Nauk SSSR*. **1963**, *149*, 615.

[77] Nesmeyanov, A.N.; Vol'Kenau, A.; Bolesova, I.N. *Tetrahedron Lett*. **1963**, 1725.

[78] King, R.B. In *Arene Complexes, The Organic Chemistry of Iron;* Academic Press: New York, **1981**, Vol. 2, pp 155-187.

[79] Astruc, D.; Dabard, R. *Tetrahedron Lett*. **1976**, *32*, 245-249.

[80] Kealy, T.J.; Pauson, P.L. *Nature*. **1951**, *168*, 1039-1040.

[81] Coffield, T.H.; Sandel, V.; Closson, R.D. *J. Am. Chem. Soc*. **1957**, *79*, 5826.

[82] Nicholls, B.; Whiting, M.C. *J. Chem. Soc*. **1959**, 551-556.

[83] J.R. Haman, J.Y. Saillard, A. Le Beuze, M.J. McGlinchey and D. Astruc *J. Am. Chem. Soc*. **1982**, 104 ,. 7549

[84] Astruc, D. *Tetrahedron Lett*. **1983**, *39*, 4027-4095.

[85] Sutherland, R.G.; Iqbal, M.; Piorko, A. *J. Organomet. Chem*. **1986**, *302*, 307-341.

[86] Muetterties, E.L.; Bleeke, J.R.; Wucherer, E.J.; Albright, T.A. *Chem. Rev*. **1982**, *82*, 499-525.

[87] Kane-Maguire, L.A.P.; Honig, E.D.; Sweigart, D.A. *Chem. Rev*. **1984**, *84*, 525-543.

[88] Pike, R.D.; Sweigart, D.A. *Coord. Chem. Rev*. **1999**, *187*, 183-222.

[89] Astruc, D. In *Organometallic Chemistry and Catalysis;* Springer-Verlag: New York, **2007**; p 608.

[90] Tsierkezos, N. *J. Solution Chem.* **2007**, *36*, 289-302.

[91] Bond, A.M.; Oldham, K.B.; Snook, G.A. *Anal. Chem.* **2000**, *72*, 3492-3496.

[92] Nesmeyanov, A.N.; Vol'kenau, N.A.; Petrovskii, P.V.; Kotova, L.S.; Petrakova, V.A.; Denisovich, L.T. *J. Organomet. Chem.* **1981**, *210*, 103-113.

[93] Abd-El-Aziz, A.S.; Winkler, K.; Baranski, A.S. *Inorg. Chim. Acta.* **1992**, *194*, 207-212.

[94] Nesmeyanov, A.N.; Vol'kenau, N.A.; Shilovtseva, L.S.; Petrokova, V.A. *J. Organomet. Chem*. **1973**, *61*, 329-335.

[95] Astruc, D.; Hamon, J.R.; Althoff, G.; Roman, E.; Batail, P.; Michaud, P.; Mariot, J.P.; Varret, F.; Cozak, D. *J. Am. Chem. Soc*. **1979**, *101*, 5445-5447.

[96] Darchen, A. *J. Chem. Soc. Chem. Commun*. **1983**, 768-769.

[97] Darchen, A. *J. Organomet. Chem*. **1986**, *302*, 389-402.

[98] Nesmeyanov, A.N.; Vol'kenau, N.A.; Shilovtseva, L.S. *Dokl. Akad. Nauk SSSR.* **1970**, *190*, 857-859.

[99] Schrenk, J.L.; Palazzotto, M.C.; Mann, K.R. *Inorg. Chem*. **1983**, *22*, 4047-4049.

[100] McNair, A.M.; Schrenk, J.L.; Mann, K.R. *Inorg. Chem*. **1984**, *23*, 2633-2640.

[101] Pearson, A.J.; Sun, L. *J. Polym. Sci. Part A: Polym. Chem*. **1997**, *35*, 447-453.

[102] Chrisope, D.R.; Park, K.M.; Schuster, G.B. *J. Am. Chem. Soc*. **1989**, *111*, 6195-6201.

[103] Abd-El-Aziz, A.S., Bernardin, S. *Coord. Chem. Rev*. **2000**, *203*, 219-267.